15 OCTOBER, 1983

UPDATE TO FERMILAB PROPOSAL 691

PHOTON PHYSICS WITH THE TEVATRON AT THE TAGGED PHOTON SPECTROMETER

THE TPS COLLABORATION

Carleton University
Fermilab
NRC Canada
UC Santa Barbara
University of Colorado
University of Toronto

1. Introduction

We propose an experiment with the Tagged Photon Spectrometer (TPS) to study charm photoproduction beyond the level of any existing experiment. In this update to P-691 we first describe the physics goals of the experiment. We then present the first E-516 results to illustrate the performance of the existing spectrometer, and follow this with the improvements and additions for the new experiment. The major addition is a vertex detector, constructed from silicon microstrip detectors (SMD), which will allow us to strongly suppress the non-charm background. Finally, we use our data from E-516, along with Monte Carlo studies of the improvements, to make estimates of the signals attainable by P-691.

2. Physics

The primary aim of this experiment is to study the properties of charmed particles and the mechanisms by which they are produced in high energy photoproduction. This physics is best achieved at the TPS with a two target scheme. We plan to use a 75 cm liquid hydrogen target followed by 3.5 cm of beryllium and the SMD vertex detector.

The spectroscopy will focus on F mesons, which cannot be studied easily at SPEAR. There now exist conflicting results on the F mass, and there is almost no information on branching ratios. (Are the final states with two kaons dominant, as expected for spectator-quark decay?). As we will show below we should see convincing signals in a number of decay modes for the

F. In addition, we will use the clean sample of D's and D*'s to look for excited charmed mesons.

The study of photoproduction mechanisms of heavy quarks is of fundamental importance. Perturbative QCD, with γ-gluon fusion as the elementary process, gives many specific predictions, most of which remain untested. With large signals of D^O's and D*'s we could address many of the unanswered questions. We will measure the ratio of the "diffractive" to "non-diffractive" parts of the charm cross section. Using clean recoil proton events we will measure the distributions of t (the 4-momentum transfer), the mass of the photon fragmentation system and the kinematical variables in its CMS. It may thus be possible to extract the gluon structure function of the proton. Measurement of ψ photoproduction on H_2 and Be targets in the same experiment will allow us to study the importance of nuclear target effects. Using clean signals obtained with the SMD's we will measure the charm production characteristics in regions where high backgrounds now obscure the charm signal. The clean, high statistics charm sample may allow us to measure charm particle lifetimes.

In addition to charm physics, the higher photon energy available with the Tevatron will enable us to extend our non-charm studies to new kinematical regions. The dynamics of particle production can be studied for forward masses up to 15 GeV, and for single particle p_T up to 6 GeV. For example, the study of the charge asymmetry at large p_T may isolate the QCD Compton diagram.

3. Results From E-516

The first results from E-516 demonstrate the versatility of the TPS and show that it is competitive with any apparatus that has contributed to fixed target studies of charm. For more details, and to put these results in the context of the present experimental situation, see Tom Nash's rapporteur talk from the Cornell conference, Fermilab-Conf-83/75-EXP.

The enclosed paper, "A Study of the Decay $D^0 \to K^-\pi^+\pi^0$ High Energy Photoproduction", which has been submitted for publication, contributes to a field in which few fixed target experiments have been active. Our result on the branching ratio of the D^0 to $K^-\rho^+$ resolves one inconsistency with the hypothesis that D^0 decay proceeds by the W-exchange diagram. It also establishes the existence of non-resonant $K^-\pi^+\pi^0$ decay at a rather high level. One factor which allowed us to do well compared to other experiments was a good efficiency for reconstructing π^0's.

The second enclosed paper, "Inelastic and Elastic Photoproduction of $J/\psi(3097)$" reports a cross section for elastic ψ photoproduction which agrees with that measured in muoproduction experiments. Our inelastic cross section is a factor of about three lower than the muoproduction results, but agrees with a second order perturbative QCD calculation by Berger and Jones. Working on hydrogen instead of iron allowed us to avoid problems associated with A-dependent corrections to the cross sections. The disagreement with the muon experiments might

be due to such effects. This analysis appeared in a thesis and is about to be submitted for publication.

A third topic, on which a paper is in draft form, is D^* production. We find that a large fraction of the D^*'s is produced with a clean recoil proton. We have also demonstrated that for these events, the forward state is not a low-mass $D^*\bar{D}$ or $D^*\bar{D}^*$ system, as commonly expected for diffractive charm production, but includes additional particles. The TPS is unique in combining a large acceptance forward spectrometer with a complete recoil system. Muon experiments which infer charm cross sections from dimuon events are unable to say much about the target fragmentation system; past photoproduction experiments have not been able to make conclusive statements about the entire forward state.

The other physics topics being actively pursued include: searches for other charm signals; a study of particle production at high P_T and in events with large forward mass; tests of scaling in x_F; and studies of inclusive production of ϕ, Λ and Ξ. Some of these results appeared in a thesis, and further publications will follow.

4. Improvements and Additions

In order to achieve the physics goals outlined above, we intend to use the TPS (see Fig. 1) with some modifications and upgrades. Improvements to the tracking and the Cerenkov counters, combined with the new silicon microstrip detectors downstream of a Be target and a new trigger will produce a very large increase in the size and cleanliness of charm peaks compared with those from E-516. Furthermore, the existence of a working reconstruction program will make it possible to analyze the data from this experiment expeditiously. We now proceed to a more detailed discussion of these points.

a. Trigger

The primary trigger in E-516 selected events consistent with the diffractive production of high mass forward states, using information on the incident tagged photon and the recoiling proton only. A high mass trigger, independent of the recoil system, will allow a more complete study of charm production mechanisms. We will implement such a trigger, based on cuts on the total transverse energy, E_T, of the photons, electrons and hadrons as measured by the forward calorimeters. The reduction in the hadronic interaction trigger rate for cuts on E_T was determined by studying events from E-516. The efficiency for charm events was determined by examining the events in the $(M_D{}^*-M_D)$ peak region. Our study indicates a 60% efficiency for these events with a reduction of the hadronic interaction trigger rate by a factor of 7. The trigger will therefore provide a substantial enrichment for charm events.

b. Tracking

The TPS has 29 drift chamber planes arranged in four groups: D1 (2 x UV XX') inside the gap of M1, the upstream magnet; D2 (3 x UXV) between M1 and M2; D3 (3 x UXV) downstream of M2; and D4 (UXV) downstream of the second Cerenkov counter. The efficiency for finding tracks was sensitive to the per plane chamber efficiency and was vulnerable to the loss of even one plane, especially in D2. We intend to provide more redundancy by adding a triplet of UXV planes to D2 and another to D3. This will dramatically increase our tracking efficiency from ~0.75 to >0.9. We also plan to move the 8 D1 planes to a position immediately upstream of M1. This requires only a new support structure for the chamber and allows a much better cabling scheme. We expect this change to increase the efficiency, decrease noise levels, and improve the chamber resolution by about 25%, while having practically no effect on the geometric acceptance. We estimate that this will also improve the momentum and angle resolution by 40% for the 35% of tracks which pass through M1 only.

A more significant improvement to the momentum resolution will be achieved by increasing the magnetic fields. We have used our E-516 Monte Carlo program which reproduces very well the characteristics of the observed charm signals, to determine that an increase by a factor of 1.3 for the M1 field and 2.5 for the M2 field results in a factor 2 improvement in the inclusive $D^0 \to K\pi$ and $K\pi\pi^0$ mass resolution, with no loss of signal.

c. <u>Cerenkov Counters</u>

There are two Cerenkov counters with twenty mirror cells each in the TPS. However, the maximum number of allowed cells is 28 in the upstream counter and 32 in the larger counter. We will instrument all 60 cells in this experiment. Our Monte Carlo program is being used to design the new mirror sizes to minimize the confusion due to overlapping tracks.

Sixty new Winston cones have been built with a reflective surface of aluminum coated with a protective cover of magnesium fluoride. The reflectivity of these new Winston cones has been measured to be far superior to that of our old ones, which have deteriorated due to the lack of protective coating. The new mirrors will be glass instead of plastic to improve their focussing properties and will also have magnesium fluoride protection.

d. <u>Silicon Microstrip Detectors (SMD)</u>

We plan to use a high resolution hodoscope of SMD's downstream of a Be target for tagging secondary vertices from charm decays. The hodoscope will consist of three stations each containing three closely spaced SMD planes measuring X,Y,and diagonal coordinates. The planes are 300 microns thick, have a 50 micron pitch, and range in size from 26×26 mm^2 to 46×46 mm^2. The hodoscope extends from 5 to 15 cm downstream of the target, and its acceptance is at least ± 100 mrad. There are 6500 channels in the system. We will use SMD's from Enertec (France) and hybrid preamplifiers from Laben (Italy). The preamp outputs

can be fed into a standard PWC readout system with only minor modifications.

To optimize the design of the hodoscope, we are carrying out Monte Carlo studies to determine the effect of the vertex detector on charm mass plots. Although these studies are not complete, the preliminary results for events with various types of charm decays indicate background reduction factors of 120 to 180 with efficiencies in the range 30% to 40%. These numbers result in signal to background enhancements in the range 36 to 72. Such impressive improvement is consistent with the results from CERN experiment NA11, where an SMD vertex hodoscope has achieved charm vertex efficiencies of 14% with a background reduction factor of 300, providing a signal to background enhancement of 43.

Test results from a prototype SMD station, and a more detailed description of the Monte Carlo studies are given in the appendix.

e. Offline Reconstruction and Analysis

In E-516, much effort went into the development of programs for calibration, reconstruction and data reduction. Although these will have to be revised for the new experiment, the scale of the effort will be much smaller. Moreover, virtually machine-independent versions of the reconstruction programs were written so that the reconstruction could be (and was) carried out at five different sites (on three different types of computers). The primary reconstruction program was also adapted for running

on six 168E's at the University of Toronto, thus greatly
increasing the total computing power available. All these
features will be important for rapid processing of the P-691
data. In addition, Fermilab's advanced computer program (ACP)
will produce a super processor aimed at the rapid reconstruction
of data from experiments such as P-691, and we hope to be among
the first to benefit from this system.

5. Signal Estimates

In Table 1 we list the signals and backgrounds we expect in a
few representative charm channels, based on the assumed cross
sections and the known efficiencies of the spectrometer. The
luminosity is calculated from the following assumptions:

- 1000 GeV protons
- 5×10^{12} protons per minute
- 6 months data-taking
- 20 days per month
- 20 hours per day
- 20% RL radiator
- 65% live-time

Integrated proton flux = 7×10^{17}

Integrated photon flux = 1.9×10^{12} (200 GeV e^-, $<E_\gamma> = 115$ GeV)

= 1.4×10^{12} (250 GeV e^-, $<E_\gamma> = 145$ GeV)

The charm cross section is rising rapidly over the lower part
of the photon spectrum, and the electron beam energy will be
chosen to balance this consideration with the requirement for
high luminosity. We assume 250 GeV.

As already discussed we will run with two targets simultaneously. We assume the following mix:

	Int. lengths	Rad. lengths	nbarn^{-1}
75 cm hydrogen	10 %	8.5 %	2600
3.5cm beryllium	8.5 %	10 %	2000
	18.5 %	18.5 %	4600

For these conditions, the instantaneous data-taking rate will be comparable to that in E-516.

To estimate the signals we use the values in Table 1 for the cross sections and branching fractions and determine efficiencies via our Monte Carlo simulation which includes all known sources of noise and inefficiency and reproduces in detail the E-516 charm signal. We have also included the effects of three detector changes: 1) better mass resolution from increased magnetic field, 2) higher reconstruction efficiency from the additional drift chambers, 3) a more efficient trigger using a computed forward mass. In addition a 35% efficiency for finding charm vertices and a background reduction factor of 150 are used for the SMD's. Not considered in our calculations are additional detector improvements that are also expected to strengthen our signals but are more difficult to quantify. For example, we have not included the the efficiency and resolution improvements expected from the SMD's and from moving D1 forward of the first magnet. The backgrounds are estimated from our measurements of the same channels in E-516 data.

We wish to emphasize that the numbers which are listed in Table 1 are based on our experience in E-516, namely the observation of a strong charm signal and a Monte Carlo program that reproduces this signal well.

6. Summary and Request

As we have shown above, the Tevatron run of the TPS will provide a dramatic advance in the study of charm photoproduction. Based on our detailed understanding of the TPS performance, we expect a large increase in the size of reconstructed charm signals and an improvement in the signal to background ratio of as much as two orders of magnitude. The new trigger will allow a more complete understanding of charm production mechanisms. The P-691 physics program can be accomplished with modest upgrades which can be completed by September 1984.

We request that P-691 be allotted the entire beam time available in P-East during the second Tevatron period. We expect that the first month will be devoted to commissioning the upgraded spectrometer. To fully exploit the physics potential of the TPS, we request a primary beam intensity of 5×10^{12} per spill. We need the immediate approval of the PAC and the continuing strong support of the laboratory for the success of this experiment.
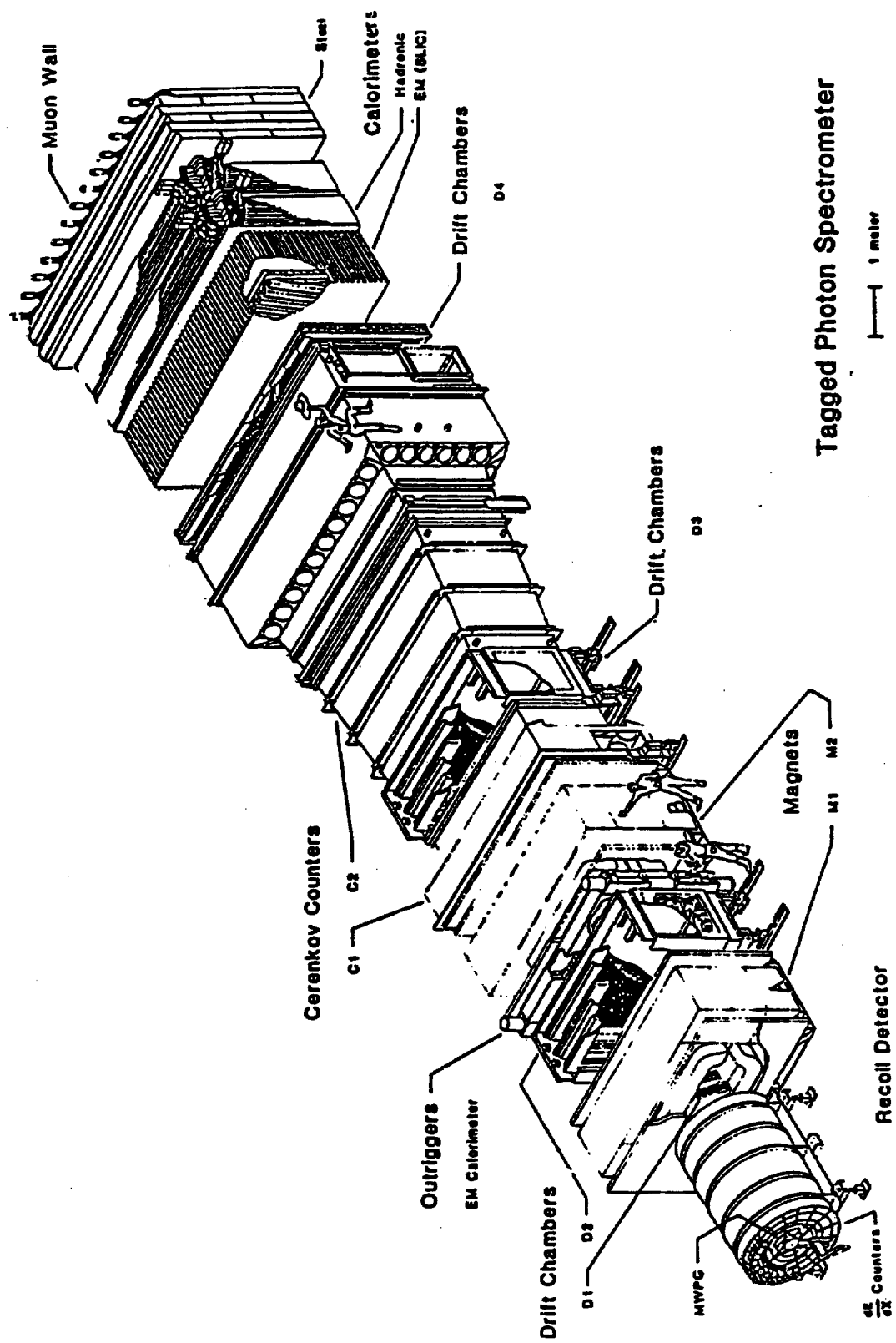
Tagged Photon Spectrometer

Figure 1

Table 1: Predicted Signals and Backgrounds

Channel [a]	$\sigma \times B$ (nb)	Target								
		Hydrogen			Beryllium			subsample Beryllium+SMD´s		
		S	B	$S/\sqrt{B}$	S	B	$S/\sqrt{B}$	S	B	$S/\sqrt{B}$
$D^{*+} \to D^°\pi^+ \to K^-\pi^+$	200x0.64 x0.024	2.1K	610	85	1.6K	465	75	570	3	320
$D^° \to K^-\pi^+$	440x0.024	8.8K	452K	13	7K	360K	12	2.5K	2.4K	50
$F^+ \to \phi\pi^+ \to K^+K^-$	100x0.03 x0.50	550	5K	8	420	4.1K	7	150	28	28
$F^+ \to K^°K^+ \to \pi^+\pi^-$	100x0.03 x0.33	410	2.7K	8	315	2.1K	7	b		

a. Includes charge-conjugate.

b. The efficiency of the SMD´s for one prong decays has not yet been studied.

APPENDIX

Development of Hardware and Software for the SMD Vertex Detector

Since 1981, members of the group have been working on ways of enriching the charm signal by observing the characteristic charm decay vertex. After some study of the many developing technologies, we decided that the one best suited to the high-rate environment of an electronic experiment is the silicon microstrip detector (SMD).
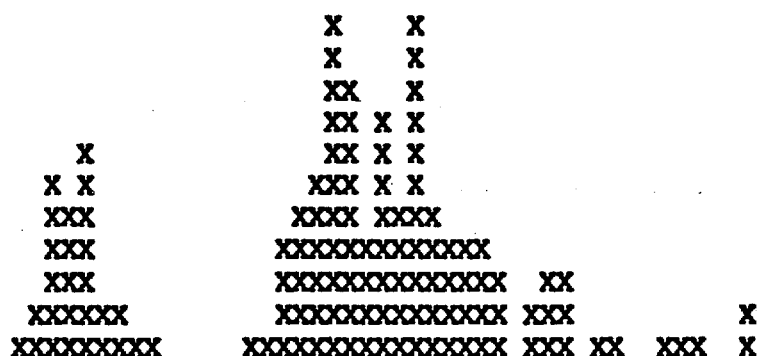
In 1982, additional funds were obtained to develop hardware for an SMD system. Two SMD planes were purchased from Enertec, the most successful and reliable commercial supplier. Each SMD plane has an active area of 1 cm x 3 cm and thickness 300 microns. There are 200 strips, with 50 micron spacing, and length 3 cm.

These planes were used to build a prototype SMD station with the planes closely spaced (6 mm) along the beam direction, and the strips of both detectors measuring the same transverse coordinate. Discrete component preamplifiers were built according to a CERN design, and mounted in close proximity to the detectors. Twisted pair ribbon cables carried the preamp outputs to NIM receiver modules providing, for each channel, a discriminated NIM level output suitable for input to a Camac latch, and an analog output suitable for a Camac ADC.

This apparatus was tested in a 10 GeV positron beam at SLAC during March, 1983. The trigger was such that the ADC output of a single downstream strip would be recorded when the

corresponding (same x-coordinate) upstream strip was above threshold, but neither of the adjacent downstream strips was above threshold. The resulting pulse height spectrum is shown in Figure A1. The positron spectrum is clearly separated from the noise pedestal spectrum. The ratio of the peak positron ADC value to the width of the noise pedestal is 9.6; a ratio quite sufficient for good signal to noise discrimination.

FIGURE A1

```
                            X   X
                            X   X
                            XX  X
                            XX X X
              X             XX X X
            X X             XXX X X
            XXX             XXXX XXXX
            XXX             XXXXXXXXXXXX
            XXX             XXXXXXXXXXXX  XX
           XXXXXX           XXXXXXXXXXXXX XXX                    X
         XXXXXXXXX     XXXXXXXXXXXXXXXXXX XXX XX   XXX   X
```

000001265722110000011456*9485*54443023301100111002

EVENTS PER ADC CHANNEL

In building and testing this prototype station, a great deal of experience was gained in the care and handling of SMD's. In addition, there has been extensive Monte Carlo work (described below) to study the performance of a full scale vertex detector and to study background sources which cause false charm decay vertices. All of this information has been used to design a vertex detector system which is selective and efficient for charm decays, can be constructed from commercially available components

with minimal development, and can be brought into operation in time for this experiment.

We plan to use the SMD's now available from Enertec which come with the silicon strips bonded to a printed circuit fanout built on a kapton sheet. The preamplifiers we have chosen were developed from the discrete circuit we have been using and are built by Laben. In tests with our prototype apparatus, we have found these hybrids to be comparable to our discrete version and they have signal to noise ratio more than twice that of the LeCroy integrated circuit version.

The SMD hodoscope we have designed for P-691 will be capable of resolving the spatial separation between a primary vertex and a charm decay vertex. In the lab frame, this separation has significance approximately c_τ/σ, were c_τ is the rest frame decay length of the charm particle, and σ is the spatial resolution of a single detector plane. This rule applies equally well to both the transverse and beam directions. The rule can be derived from a simple calculation and has been verified with Monte Carlo studies. Comparing the data book values for charm decay lengths (270, 140, and 66 microns for D^+, D^0, and F) with the expected spatial resolution (14 microns) of a 50 micron pitch SMD, it is clear that charm decay lengths can be easily detected with the SMD hodoscope.

Preliminary Monte Carlo studies of the SMD hodoscope include the effects of detector spatial resolution, multiple scattering in the target, and secondary interactions.

As an example, from a sample of generated events of the form

$$\gamma \ P \rightarrow \overline{D}^0 \ D^0 \ n(\pi)$$

where the mean pion multiplicity is about 6, and with the decays $D^0 \rightarrow K^- \pi^+$, $\overline{D^0} \rightarrow K^+ \pi^-$, we can define the charm efficiency, E_c, as

$$E_c = \frac{\text{(no. of charm K } \pi \text{ combinations seen in forward spectrometer and identified as originating from a secondary vertex)}}{\text{(no. of charm K } \pi \text{ combs seen in forward spectrometer)}}$$

From a generated sample of non-charm events with the same multiplicity distribution as the charm events, we can define the background reduction factor, R_b, as

$$R_b = \frac{\text{(no. of non-charm K } \pi \text{ combinations in D mass range accepted by forward spectrometer)}}{\text{(no. of non-charm K } \pi \text{ combs in D mass range accepted forward spectrometer and identified as originating from a secondary vertex)}}$$

Thus, the vertex detector provides an enhancement of the charm signal to background in a mass plot (K π in this example) by a factor $E_c * R_b$.

Fermilab

February 4, 1981

Norman Gelfand
Program Planning Office

Dear Norman:

We submit herewith 30 copies of our proposal to continue
our program of photoproduction into the Tevatron era. As you
know we are very busy running E516 and it has been difficult to
prepare a proposal. We intend to submit addenda to this
proposal as we gain more experience from our present run.

Very truly yours,

Thomas Nash

TN:mjb
enc.
cc: J.A. Appel
    G. J. Luste
    J. F. Martin
    R. J. Morrison
    U. Nauenberg

Proposal to Do Photon Physics with the Tevatron
at the Tagged Photon Spectrometer

Submitted by the TPS Collaboration

J. Elliott[1], P. Mantsch[2], R.J. Morrison[3]**, J. Spalding[4], J. Bronstein[2],
K. Stanfield[2], S.E. Willis[2], J. Biel[2], S. Bracker[4], J. Pinfold[5],
G. Luste[4], R. Kennett[3], P. Estabrooks[5], D. Blodgett[4], S. Yellin[3],
R. Kumar[4], K. Shahbazian[4], C. Zorn[4], D. Bintinger[2], J. Martin[4]**,
M. Robertson[7], G. Hartner[4], T. Nash[2]*, G. Kalbfleisch[7],
B. Denby[3], M. Losty[6], U. Nauenberg[1]**, V. Bharadwaj[3], D. Summers[3],
J.A. Appel[2]**, A. Duncan[1], A. Lu[3], D.O. Caldwell[3], S. Bhadra[1]

[1] University of Colorado, Boulder, Colorado 80302

[2] Fermi National Accelerator Laboratory

[3] University of California, Santa Barbara, California 93106

[4] University of Toronto, Toronto, Ontario, Canada M5S 1A7

[5] Carleton University, Ottawa, Canada K1S 5B6

[6] National Research Council, Ottawa, Canada K1S 5B6

[7] University of Oklahoma, Norman, Oklahoma 73019

*Spokesperson

**Deputy Spokespersons

Proposal To Do Photon Physics with the Tevatron

at the Tagged Photon Spectrometer

Introduction

We propose to use the existing Tagged Photon Spectrometer (TPS) to do high energy photon physics at a very early stage of Tevatron operation. The Tagged Photon Spectrometer was built over the last few years by our group following the design defined in the TPS Design Report, which is attached. It is a very large acceptance, high resolution magnetic spectrometer with electro-magnetic and hadronic calorimetry, Cerenkov particle identification and a sophisticated recoil detector surrounding the target. The spectrometer was conceived from the beginning with the Tevatron in mind, and represents at this time we believe, the first operational Tevatron detector. (See the two letters to L. Lederman, November 6, 1978 and April 25, 1980, regarding Tevatron physics with photons, which are attached.) The spectrometer sits in the Tagged Photon Beam which we presently operate at ~ 140 GeV electron energy with 400 GeV protons. Without change this beam is capable of 300 GeV electron energy which is the ideal energy to run with 1000 GeV Tevatron protons.

At this writing we are running experiment 516 with the TPS. This experiment uses an elastic recoil proton, missing mass, trigger to explore diffractive charm, psi, and QCD physics at large masses. Before the Tevatron comes to Proton East we are intending (appropriate letters will follow) to continue to exploit the

spectrometer with experiments focussed on physics complementary to the diffractive approach of the present run. This will include the use of forward mass and $P_\perp$ triggers, emphasizing non-diffractive photoproduction, and/or the use of active solid state target decay detectors.

The Tagged Photon Tevatron detector is already built and running. Therefore it is not necessary for us to justify a major expenditure for a large Tevatron facility to do photoproduction physics. Furthermore we are presently using a very powerful trigger processor in association wih the recoil detector, and this processor can be readily reconfigured for a wide variety of triggering purposes. These considerations afford us the flexibility of deciding on a specific trigger and experimental configuration at a later date in order to optimize the study of physics which will be interesting at the time Tevatron energy beams are available. The precise physics direction which we will want to take will be determined by three factors:

a) Our experience over the pre Tevatron years in exploring the complementary photon physics areas noted above will teach us the capabilities of the spectrometer and the associated analysis software. This will allow us to select the best match of Tevatron physics to the detector.

b) The relevance of different physics directions will be better understood closer to the time of the first Tevatron photon run than now.

c) In addition, actual knowledge of the integrated luminosity and energy to be available from the doubler/saver must play a major role in the final choice of physics.

Subject to these determining factors we expect to select our first Tevatron physics from one of the areas outlined in the following.

QCD Physics

The photon is an ideal probe for the study of QCD and jet physics. For example, in the region of large $P_\perp$ we believe it possible to isolate the basic sub-processes often referred to as QCD Compton and photon-gluon fusion.
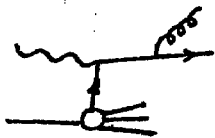
a) QCD Compton
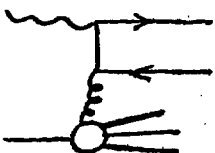
b) Photon Gluon Fusion

In both processes we expect to observe two high $p_\perp$ jets, corresponding to the interesting sub-processes, and a soft target jet. It is interesting to compare photoproduction of three jet processes with hadron-hadron jet experiments and with hadroproduction of direct photons. The three jet photoproduction events are clearly cleaner than hadron-hadron jet events, both

theoretically and experimentally. For example, hadron beams necessarily have a soft jet from the beam fragment, which, in a fixed-target experiment, tends to overlap kinematically in the detector with the hard constituent scattering jets. The photon 3-jet interactions have no beam fragments. This is illustrated in the following figures.
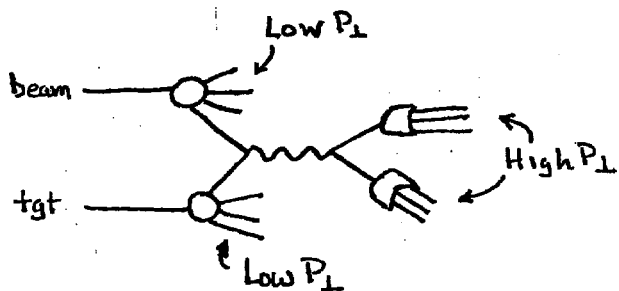

4 JET hadron - hadron scattering
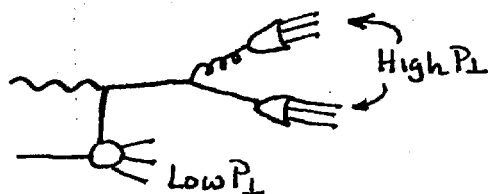
3 JET photon - hadron scattering

In addition, since the photon has a pointlike coupling to quarks, all of the incident photon energy is available for the basic subprocess. In a hadron beam the energy is shared among more than one constituent. Therefore, a 300 GeV photon, for example, can deliver the same amount of effective energy to the fundamental constituent interaction as a 600 GeV meson or a 900 GeV baryon. As a result high $p_\perp$ jets are a larger part of the cross section in photoproduction than in hadroproduction. Furthermore, from the theoretical point of view the photon structure function should be calculable from basic principles.

Direct photon production in hadron hadron scattering experiments is intended to probe the same constituent sub-processes. The experimental problem in those experiments is the extraction of the single photon signal from the large $\pi^0 \to \gamma\gamma$ and $\omega \to \pi^0\gamma$ background in the final state.

E516 data presently being collected contains a sample of jet events. Our experience analyzing these events will lead to an understanding of our ability to isolate and measure photon initiated jets at Tevatron energies.

In the present run, as noted earlier, our data is triggered by a single recoil proton. This should result in a sample of unbiased two jet events which might be called Bethe-Heitler quark production.

Proton
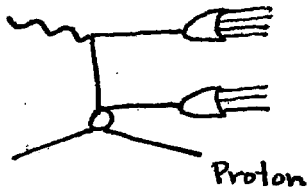
c)

We also have a trigger, based on the outer regions of our electromagnetic calorimeter which should give us a sample of QED Compton events.
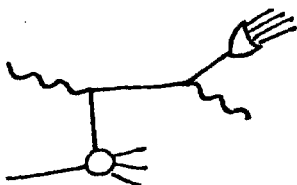
d)

In this case we should see a high $p_\perp$ jet recoiling against the high $_\perp$ photon. Experience gained from the present and future runs with the 400 GeV machine should prove invaluable for doing an excellent Tevatron QCD experiment.

A significant test of QCD can be carried out without identifying jets by comparing the $p_\perp$ dependence of inclusive π^+ and π^- production at high $p_\perp$.[3,4,5] A difference of ~ 1 nb/GeV^2 at a $p_\perp$ of 2 GeV/c is predicted because of the presence of gluon bremstrahlung. Quark-antiquark jets cannot contribute to a $\pi^+\pi^-$ production cross section difference, so a measurement of this difference would be a clear test of QCD theory. It is important to note that this difference is of the order of 50% of the inclusive π^+ cross section at high $p_\perp$ (see Figures 3 and 4 of Ref. 4).

The Tagged Photon Spectrometer is ideally suited for the study of QCD physics. The spectrometer can use all of the flux which the tagged photon beam is likely to deliver. The large acceptance and fine segmentation (which can be easily improved further for the Cerenkov and SLIC systems) should be ideal for the isolation of jets. Rate estimates indicate total cross sections for processes a and b to be ~ 0.2 μbarns each, for a jet $p_\perp \geq 2$ GeV and $\sim 10^{-2}$ μb for $p_\perp > 4$ GeV. With the minimum standard Tevatron luminosity described later this would mean 3000 events in 1000 hours for each process for $p_\perp > 4$ GeV, and $\sim 60,000$ events for $p_\perp > 2$ GeV.

Charm-Bottom Studies

It is obvious that the rate of charm and bottom production is orders of magnitude higher in fixed target experiments than in e^+e^- annihilation. This fact, along with the relatively high ~ 1% charm component in photon induced reactions, is the motivation for the present Experiment 516. In E516 we have used a recoil proton trigger to select clean charmed events. In a Tevatron experiment we would extend the present charm study to higher mass, energy and $|t|$ regions and possibly also to rarer decays. We would use both a recoil and a forward trigger which would accept non-diffractive charmed events as well.

A continuing interest at the Tagged Photon Spectrometer is the study of charmed meson and baryon decays. Rare charm decays will provide a wealth of information about the structure of the charged weak currents.[7] An obvious case is a measurement of the branching fractions of the Cabibbo-suppressed decays $D^0 \rightarrow K^+K^-$ and $D^0 \rightarrow \pi^+\pi^-$. A low statistics measurement of these decays has indicated a factor of three difference between the two rates.[8] This can be understood by the presence of heavier quarks in the weak currents. A systematic study of the Cabibbo-suppressed two body decays of D^0, $D^{\pm}$, $F^{\pm}$ will have implications for the weak couplings of heavier quarks. Additionally, measurements of Cabibbo-suppressed semi-leptonic modes of charmed mesons will provide useful information about the Cabibbo angle associated with charm decays. Also measurement of rarer Cabibbo-favored decays will help in the

understanding of the $\Delta I = 1/2$ rule as it is extended to heavier quark decays. Cabibbo-suppressed decays generally will have branching ratios of 10^{-3}. For a total D^O cross section of 500 nb this means cross sections of 0.5 nb for Cabibbo-suppressed decays. With the integrated luminosities we can expect in standard Tevatron running (300 events/nb as discussed later) we can expect a reasonable number of these decays. Experience may justify a maximum luminosity run which is also discussed in a later section. The most important factor for a successful long range program of charm physics is, however, a systematic study with continuity through the years before and after 1000 GeV protons.

One additional way of identifying charm events with very low background would involve the use of a high resolution vertex detector. We are thinking here in terms of solid state detector developments or the high pressure – high resolution gaseous hydrogen drift chamber described in the Appendix. Developmental efforts on a high pressure chamber will start soon at UCSB.

Another possible goal is the study of bottom states. We anticipate that bottom studies will be very difficult due to the low cross section, which is expected to be $\sim 1/30$ of the charm cross section in photon reactions, and to the anticipated relatively large number of high multiplicity decay modes.

We do not claim that the isolation of bottom events will be easy. However, we can make the following observations:

a) Bottom is expected to decay predominantly to charm. Very recent results from CESR appear to confirm this.[10]

b) A sample of clean charm events with a total forward mass of $\geq$ 10 GeV will therefore be enriched in bottom.

c) Since combinatorial backgrounds go up very rapidly with multiplicity, bottom particles with unambiguously reconstructed charmed particles will be the cleanest candidates for bottom events.

d) Bottom events should be much more spherical than most events with high foward masses. The large acceptance of our spectrometer will be very valuable for this physics.

We anticipate having a clean sample of $\gtrsim$ 100,000 charm events with $\sim$ 1,000 - 3,000 of these containing bottom. From experience with the E516 data we hope we will learn how to add up various decay modes in mass plots. This approach would lead to a good bottom signal.

Beam Requirements and Costs

What kind of luminosities will this experiment require? We have given an indication in the discussions above of the cross sections involved for the different physics. Present experience is that one can expect about 1500-2500 events per nb per 1000 hours at

5×10^{12} 400 GeV protons, average 12 second rep rate, 30% dead time, 50 GeV electrons. Scaling this conservatively to 800 GeV protons, 300 GeV electrons, 60 second rep rate, one can expect at least 300 events per nanobarn per 1000 hours at 5×10^{12}. (Use of the high pressure H_2 active target described in the Appendix would reduce this by 10.) This represents a reasonable luminosity to carry out most of the physics outlined in this proposal.

Certain classes of physics, the rare decays of charm, for example, may be able to benefit from increased luminosity at lower γ energy. With the Tevatron, a factor of three increase in luminosity is possible at an electron beam energy of 140 GeV. A factor of 10 in electron yield is gained from the 1 TeV protons compared to 400 GeV. Considering 10^{13} protons on target in the improved drawers (vs 5×10^{12} at present) and a rep-rate of once per minute (one sixth the current rep-rate) a factor of three increase in luminosity (compared to present running) to $\lesssim 8000$ events/nb in 1000 hours can be obtained. A long 20 second Tevatron spill would allow the instantaneous rates in the drift chambers to be equal to the instantaneous rates of the present run even at these high luminosities.

What costs and expenditures will be required? Very, very little. We expect to be carrying out a steady program of relatively modest improvements over the next several years. This will include additional tubes and Winston cones on the Cerenkov counters, forward backward segmentation of the SLIC readout, improvements in the tagging system, adding redundancy in the recoil detector, and muon counters, trigger change capabilities, etc. Costs of the order of $100,000 per year will be handled routinely by support

funds of the various university and Fermilab physics departments groups. Specific to the Tevatron is the need to cater the data acquisition capabilities of the on line computer to the twenty second spill expected by increasing the buffer bulk memory. It can also be expected that a major upgrade of the online computer system will be carried out because the present PDP11 system is a serious limitation for a facility of this magnitude. (The support for this upgrade will be shared between the Fermilab computing department and the Fermilab and University Physics Departments in a manner which will be determined after discussion and negotiation).

We emphasize that no changes are required in the electron beam or tagging system for Tevatron physics at the TPS. Both are capable of 300 GeV operation without change. This is the maximum electron energy for which there will be sufficient flux to carry out any conceivable program of photon physics (other than a total cross section measurement). As is the case for other experimental areas muon hardening may have to be implemented. However, the 20 times longer flattop will go a long way toward mitigating any difficulties with ambient muons. To bring Tevatron protons to Proton East at the early stage we are requesting will, of course, also require the right bend construction work to be complete by the time the energy doubler is operational.

Conclusion

Our understanding of the present Fermilab approval system is that Stage 1 approval refers to the proposed physics program and Stage 2 is for major expenditure for construction of the experiment. In our case the experimental spectrometer is already constructed and waiting. The experiment specific expenditures will be relatively minor. Furthermore some form of approval for this proposal this year is extremely important to us because of planning, funding contract, and personnel considerations. We request that Stage 1 approval be granted now for the general plans for physics that have been outlined in this proposal. Stage 2 approval and the agreement would apply to the specific choice of physics and what will be, we believe, the most sensitive issue in the early Tevatron era, intensity and scheduling.

In conclusion, we would like to emphasize that we are proposing a very early Tevatron experiment. The argument for this is based on the fact that at the time the Tevatron turns on this Tevatron detector will be thoroughly seasoned by several experiments. Our group will be experienced in its use and the analysis of its data. Reconstruction and other offline software packages will be in routine operation. This proposal to do photo-production at the Tagged Photon Spectrometer offers the laboratory an assured and inexpensive access to significant Tevatron physics as soon as energy doubler protons are available in Proton East.

References

1. J. F. Owens, Phys. Rev. D $\underline{21}$, 54 (1980).

2. D. W. Duke, J. F. Owens preprint FSU-HEP-800709.

   S.F. King, A. Donnachie and J. Randa, Nuclear Physics $\underline{B157}$,1980 pp.98-?

3. M. Fontannaz, A. Mantrach, B. Pire and D. Schiff, Phys. Lett. $\underline{89B}$, 263 (1980).

4. M. Fontannaz _et al_., LPTHE 80/12 (preprint).

5. M. Fontannaz _et al_., LPTHE 80/21 (preprint).

6. H. Fritzsch and P. Minkowski, Phys. Lett., $\underline{69B}$, 316 (1977).

7. Charmed Meson Decays and the Structure of the Charged Weak Current, C. Quigg, Fermilab Pub-79/62-THY, August 1979.

8. Observation of Cabibbo-Suppressed Decay $D^O \rightarrow \pi^-\pi^+$, and $D^O \rightarrow K^- K^+$, G. S. Abrams, et. al., PRL $\underline{43}$, August 1979.

9. Proton Department, private communication.

10. Felix Sannes, Invited talk at N.Y. APS meeting, January 29, 1981.

APPENDIX I   Possibility of Using High Pressure H_2 Gas as a Charm

Vertex Detector

1. Basic considerations of vertex detection

2. Some important properties of H_2 gas drift chambers

3. Limits on resolution

4. Basic design of the detector

5. Analysis of a possible experiment

1. Basic considerations of vertex detection

There are two basic approaches to detection of downstream vertices in charm decay. The first, track count detection, uses ionization measurements to give a signal indicating that the number of charged particles has changed at some location downstream of the primary vertex. This method works best at high charm particle lab energy, taking advantage of the time dilation effect to give large separations between the primary and decay vertices. Here we concentrate on the second method, vertex reconstruction, which is potentially more general and provides more information. In particular, the tracks which emanate from the decay vertex can be associated with those found in the forward spectrometer, greatly reducing combinatorial backgrounds.

Vertex reconstruction techniques require a track resolution which is independent of the charm particle energy. To see this consider the following schematic picture:

$$\delta \sim c\tau \frac{E}{m} \cdot \frac{m}{E} = c\tau$$
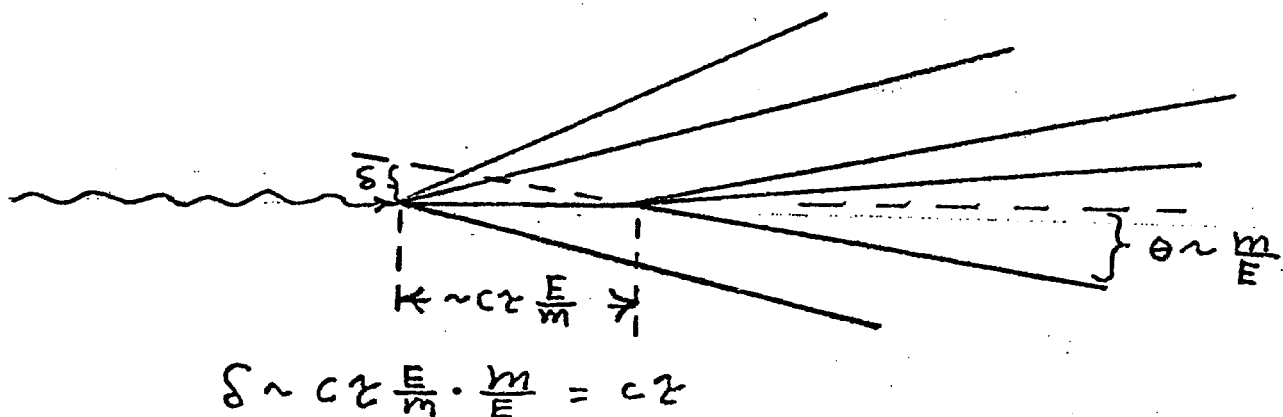
The time dilation effect, which leads to increasing vertex separation with increasing energy, is compensated by the vertex resolution which is proportional to the lab decay angles, which in turn decrease with increasing energy. The conclusion is that transverse track coordinates need to be measured with

a precision of $\sim c\tau$. These values range from $\sim$ 30 microns for D^o's to 300 microns for charged D's, with F's and Λ_c's probably closer to 30 microns. To select D^o, F and Λ_c events with this technique will require resolutions of better than $\sim$ 30 microns. Charged D's are relatively easy.

2. Some important properties of H_2 gas drift chambers[i]

We consider the use of a 100 Atmospheric H_2 gas drift chamber as an active target in a high energy beam. H_2 has the obvious advantages of low z, which is important in photon beams, and a theoretically nice target particle. The density of 100 Atmospheres is approximately 1/10 that of liquid hydrogen.

What is perhaps less obvious is the possibility of very high resolution obtainable with H_2. This is due to two considerations. The first is the fact that under reasonable drift field conditions the drift speed is about an order of magnitude slower than standard drift chamber conditions. This means that with normal timing electronics we can do an order of magnitude better in position resolution. The second consideration is the low thermal diffusion of hydrogen. These considerations are explained more thoroughly in the next section.

The drift speed, w, in H_2 gas scales approximately as $1.15 \, (E/P)^{.56}$ cm/μsec where E is the electric field in volts/cm and P is the pressure in Torr. This corresponds to 6 microns/nsec at 100 Atmospheres with an electric field of 25 KV/cm.

3. Limits on resolution

The position resolution is ultimately limited by diffusion of the drifting electrons and by fluctuations in the ionization processes. In addition to these fundamental limits there will be geometrical and instrumental effects.

First we consider the fundamental limitations.

A. Diffusion

The rms deviation of an electron in a drifting swarm is $\sigma_x = \sqrt{2Dt}$

where D is the diffusion constant and t is the time of drift. For electrons

the diffusion in the direction of the field is given by D_L which is usually

smaller than D_T, the transverse diffusion.

It is true that the quantities $\frac{D}{\mu}$, $\frac{D_L}{\mu}$ and w are functions of E/N where E

is the electric field, N is the particle density, μ is the mobility, and w

is the drift velocity. The value of E/N is often expressed in the units Td

(Townsend) which is 10^{-17} volts/cm^2. At 293°K we can convert to E/P units

where P is the pressure in Torr (1 Atmosphere = 760 Torr).

$$E/N \text{ in Td } = 3.03 \ (E/P) \text{ in } \frac{V}{cm \ Torr}$$

At 100 Atmospheres $E/P = 1.3 \ 10^{-5}$ E(volts/cm) and E/N = 4 10^{-5} (E volts/cm).

We then express σ_x in terms of the measured quantity $\frac{D_L}{\mu}$

$$\sigma_x = \sqrt{2 \frac{D_L}{\mu} \mu t} = \sqrt{2 \frac{D_L}{\mu} \frac{x}{E}}$$

where we have used the definition $\mu \equiv \frac{w}{E}$ and x = wt. A plot of $\frac{D_L}{\mu}$ is shown

in Fig.A1.[2] The range of likely values for E lie between 10 and 25 kv/cm.

The values of σ_x, after 1 cm of drift, then lie between 26 and 19 microns,

respectively.

We can count on a measured resolution significantly better than σ_x.

In principal, one could measure the mean of the swarm to a precision of $\frac{\sigma_x}{\sqrt{N}}$

where N is the number of electrons in the swarm. For 1 mm sample of H_2

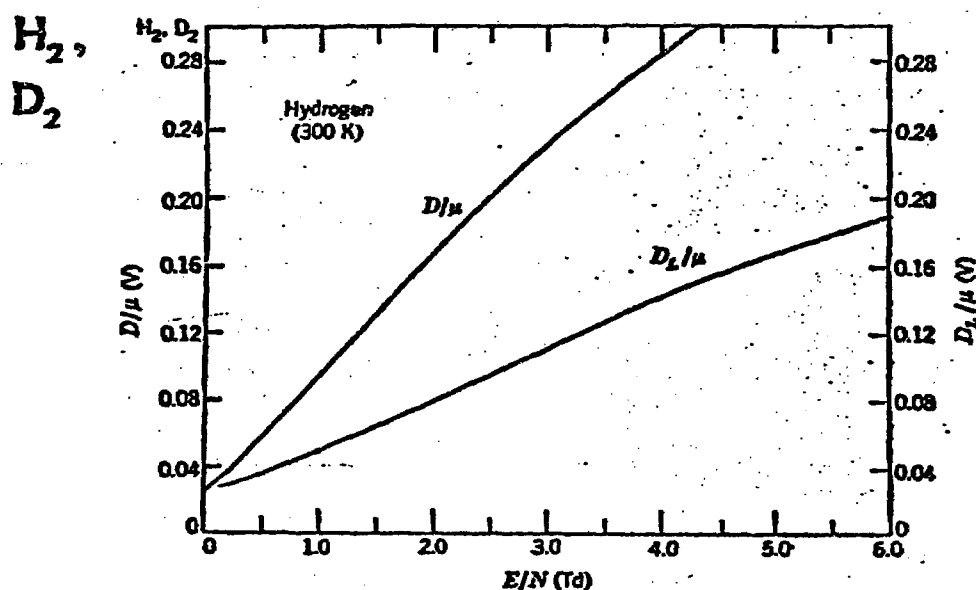at 100 atmospheres N is $\sim$ 100, so the theoretical limits are 2.6 and 1.9

Fig. AI

microns respectively. If one triggers the timing electronics on the first electron to arrive, Gaussian statistics gives a resolution of

$$\sigma = \frac{\pi}{2\sqrt{3}\ell nN}\sigma_x \sim .4 \; \sigma_x$$

i.e. $\sim$ 10 microns.

B. Resolution Due to Fluctuations in the Primary Ionization

In the ionization process most of the electrons have only a few tens of eV of energy and lose all of their energy very close to the ionizing particle's path. Due to Landau fluctuations one can expect a few electrons to have more energy, and a larger range, leading to a smearing of the ionized electron from the ideal perfect straight line. We can make estimates which indicate that this effect is in general not serious.

The spectrum of larger energy transfers is

$$\frac{dN}{dT} = \frac{.153 \ (\rho \ dx)}{T^2} \ \text{MeV}$$

where $\rho \ dx$ is the matter thickness in gms/cm^2 penetrated by the beam and T is the ionized electron kinetic energy. The number of electrons with energy T_o or greater is

$$N_o = \frac{.152 \ (\rho \ dx)}{T_o} \ .$$

For 1 mm of H_2 at 100 atmospheres $\rho \ dx$ is $9 \ 10^{-4} \ \text{gm/cm}^2$. Typically we then have a 1 electron of energy > 140 eV per mm, and a 14% chance of having an electron of energy > 1 keV.

These electrons will multiple scatter in an almost isotropic manner with an effective range $R = .71 \ T^{1.72}$[3] gm/cm^2 where T is in MeV. The range for a 1 keV electron is about 5 microns. We conclude that the primary ionization process will not seriously degrade our resolution.

C. Geometrical Effects

We expect our tracks to slope at angles $\sim .05$ to $.1$ milliradians. This leads to a transverse distance spread of < 100 microns per 1 mm of track length or a $\sigma \sim \frac{.05}{\sqrt{3}} = 30$ microns. This is comparable to the diffusion spread.

D. Timing Resolution

A serious contribution to current drift chamber resolution is time reso-lution, time stability, etc. In careful experiments[4] it has been shown that the observed resolution is accounted for by the combination of elec-tronic resolution and by diffusion. Even with $\sim 50 - 60$ micron resolution,

the electronics is still important. For our case we have drift speeds be-
tween .4 cm/sec - .6 cm/sec (depending upon the drift voltage), which are an
order of magnitude slower than most drift gases. For our case 6 microns is
about 1 nsec so we are less sensitive to timing problems.

E. Miscellaneous

A resolution of 5 or 10 microns is quite an achievement and we can ex-
pect numerous troubles in achieving this. They don't, however, appear to
be fundamental.

4. The Basic Design of the Detector

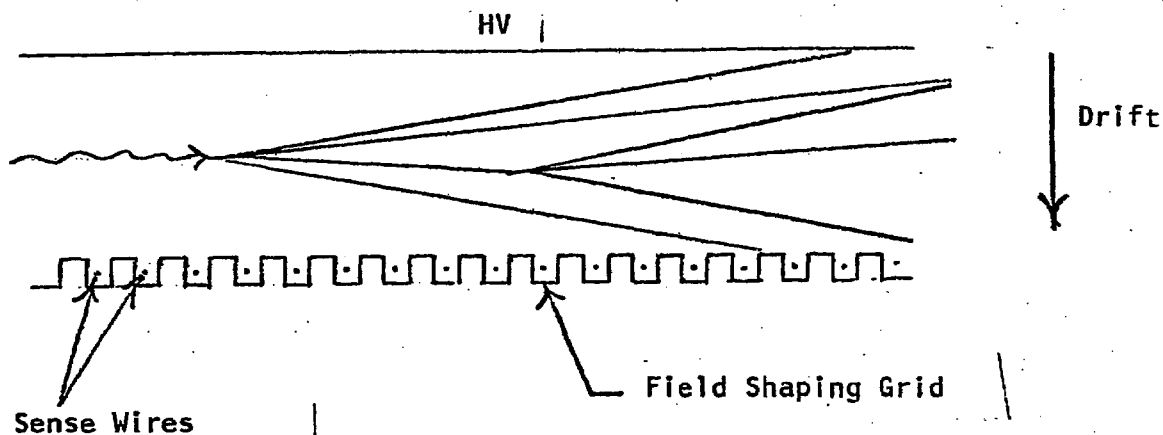We have in mind a detector geometry something like that shown in Fig. A2.

Fig. A2

The incident photon interacts with the hydrogen nucleus in the active region
on constant drift field. The electron swarms, corresponding to the event
tracks, drift toward the multiple parallel sense wires which lie in a plane
which is parallel to the incident photon direction. To maintain the necessary
high resolution properties, the sense wires will need to be surrounded by an

aperature limiting and field shaping grid, shown schematically in Fig. A2. The sense wires feed multi-hit TDC's so that each sense wire gives the location of all of the charged tracks in one dimension transverse to the beam direction. The electron swarms have a width of a few nsec and are separated by typically 150 nsec at a distance 5 cm downstream of the primary vertex. A typical track, produced at an angle of .1 radian, will leave the sensitive region of the detector which we have in mind, after travelling 10 cm. With sense wires every 2 mm this would give a highly redundant series of $\sim$ 50 measurements per track in the one projection. If these measurements are each accurate to a precision of $\sim$ 15 microns we should be able to identify the presence of downstream vertices due to D^O's, F's, Λ_c's, and charged D's unless the decays are unfavorably oriented. This precision may be optimistic but in any case charged D's should be easy.

5. Analysis of a Possible Experiment

The design of an experiment using such a detector is very constrained by the necessity of minimizing background rates. In a photon beam the main backgrounds come from photon-pair conversions in the H_2 gas and upstream window, and by Compton scatters of very low energy photons from the infrared part of the bremsstrahlung spectrum and from synchrotron radiation. The slow drift speed of the electrons in H_2, which is an advantage for position resolution, is then a disadvantage as far as sensitivity to background is concerned.

It is important to keep the size of the beam, in the bend plane, small. This allows for tight collimation just upstream of the detector which will reduce synchrotron radiation. A small beam size also means that the drift region of the detector can be kept small, reducing the sensitive time. A small beam size also means that the upstream window can be made smaller and therefore thinner.

The photon beam can be made ∿ 1 cm in width by means of beam tuning, up-
stream collimation, and proper choice of radiator size, without a large loss
of beam flux. We then choose a drift distance of 2 cm, which means that most
tracks will go at least 10 cm before exiting the drift region. With an elec-
tric field of 25 kv/cm at 100 atmospheres we have a drift speed of 0.6 cm/μsec.
The average time of drift of a pair background track is then 1.7 μsec.

Now we try to estimate the incident photon flux which can be used with
this detector. We assume that the limit will be a desire to have a small
probability of having an accidental pair or Compton track in the region of
the event, rather than problems in the functioning of the chamber. It seems
quite likely that most accidental tracks could be identified without causing
problems, but we adopt the criterion that we would like the accidental prob-
ability to be less than 30%.

Now we estimate the pair and Compton rates per incident tagged photon.
We assume that the target length is 1.5 meters as in E516. The target is then
1.35 gm/cm^2 which gives a 1.7% chance per photon for pair conversions. We
assume an upstream Be window which is 1 cm wide by .5 cm thick, which adds
another 1.1%. The center of the detector then has a flux of pairs which is
2.3% per incident photon. A 30% accidental rate due to pairs corresponds to
1.5 10^5 pairs/sec or 6 10^6 photon/sec.

Pairs above 200 meV traverse the entire detector without multiple scat-
tering out of the drift region. The number of photons with sufficient energy
to cause such pairs is approximately

$$N_\gamma = T N_e \int_{.2Gev}^{300Gev} \frac{dk}{k} = T N_e \ln(1500)$$

where T is the radiator thickness in radiation lengths and N_e is the number
of incident electrons. The number of tagged photons is approximately

$$N_\gamma^{tagged} = T N_e \int_{150Gev}^{300Gev} \frac{dk}{k} = T N_e \ln 2$$

so that $T N_e = \dfrac{N_\gamma^{tagged}}{\ln 2}$. The number of tagged photons allowed is then

$$N_\gamma^{tagged} = \frac{6 \cdot 10^6 \ln 2}{\ln(1500)} = 6 \cdot 10^5/sec$$

This is about 1/4 the flux being used in E516.

We need to show that the accidentals due to Comptons are not worse than those due to pairs. In the energy region from .2 to 10Mev the Compton cross section on hydrogen is large compared with the pair cross section. This is also a region where absorption hardening of the photon beam is difficult. The bremsstrahlung part of the flux is

$$dN_B = \frac{N_\gamma^{tagged}}{\ln 2} \frac{dk}{k} = 1.4 \, N_\gamma^{tagged} \frac{dk}{k}$$

The synchrotron flux is, for each incident electron, very approximately

$$dN_s = \frac{\alpha \left(\frac{E}{mc^2}\right)}{k} \times \frac{.15 \cdot 10^{-3}}{2\pi} \, dk$$

for $k < E_c$ where E_c is the critical energy, E is the electron beam energy, $.15 \cdot 10^{-3}$ is the angular acceptance of the beam defining collinator with respect to the last bend in the beam transport, and α is the fine structure constant. The critical energy is always above the region of interest so the equation can be used for our present purposes. We must multiply by a factor of two to take into account the tagging bend as well as the last bend in the electron beam transport. We then find, using $T = .2$,

$$dN_s = 2.9 \, N_\gamma^{tag} \frac{dk}{k}$$

The probability of an accidental Compton in the 10 cm fiducial region of an event is then

$$N^{comp} = 1.35 \text{ gm/cm}^2 \times \frac{10 \text{cm}}{150 \text{cm}} \times (1.4+2.9) N_\gamma^{tag} \int\limits_{.2 \text{Mev}}^{10 \text{Mev}} \frac{dk}{k} \frac{\mu}{\rho}(k) \frac{\text{cm}^2}{\text{gm}}$$

Values of the absorption coefficient, $\frac{\mu}{\rho}$ (k) vary from 0.2 cm^2/gm to 0.03 cm^2/gm, in the region of interest. A rough value for the integral is 0.41. The accidental Compton probability is then 0.16. We conclude that Compton backgrounds are less than or are comparable to those from pairs.

We conclude that a flux as high as 6 x 10^5 tagged photons/sec can be handled readily by this detector. The standard Tevatron luminosity referred to in the text of this proposal corresponds to ~ 2 10^6 tagged photons in 20 seconds or ~ 1 x 10^5/sec. At the maximum luminosity, 140 GeV, condition referred to in the text we would have ~ 2 10^7 tagged photons in 20 seconds or ~ 1 x 10^6 per second which is somewhat more than 6 x 10^5 but probably tolerable. In using this detector at high luminosity we will, of course, be able to adjust the photon flux if necessary by changing to higher beam energy to the point where the accidental levels are determined to be acceptable.

We would like to thank Professor Sebastian White for numerous useful discussions concerning the properties of hydrogen drift chambers.

REFERENCES

1. These important properties of hydrogen gas are described in the Diffusion and Drift of Electrons in Gases, L.G.H. Huxley and R.W. Crompton, John Wiley and Sons.

2. This plot is taken from Reference 1, page 622.

3. E.J. Kobetich and R. Katz, Phys. Rev. 170, 391 (1968).

4. Nina A. Filatova, et al., Nucl. Inst. & Methods 143, 17-28 (1977).

November 6, 1978

To: Leon Lederman

From: Tom Nash

Subject: Photon Physics with the Minimal Tevatron

Photon physics is presently undertaken in the Broad Band and Tagged Photon
Beams in Enclosures EE-4 and the Tagged Photon Laboratory respectively. At
Tevatron energies it is unlikely that the μ flux in EE-4 will allow viable
experimenting. One will thus be limited to use of the Tagged beam (perhaps
modified after first generation Tevatron experiments) and the possibility of
a new high intensity, large momentum bite electron to photon beam going into
a new area just east of the TPL. (This assumes that P-West is saturated with
non-photon physics and that funding is "minimal" so that the much needed re-
building of Proton targetting does not happen at first.)

It is my opinion that construction of a new photon beam is not warranted at
Tevatron startup since a) the new Tagged Photon Spectrometer was designed
specifically with Tevatron photons in mind (see following discussion); b) its
use can be shared by two alternating groups with different physics goals thus
making efficient use of P-East; and c) as far as I can see from the physics
perspective of 1978 the present facilities will not be beam intensity limited
and will be able to make a good start at Tevatron photon physics. Over the
next few years as the physics horizon develops (before and after initial Teva-
tron results) it will become far clearer whether, and how, to build an alternate
photon facility. I will therefore limit the following discussion to experiments
in the Tagged Photon Spectrometer using the existing beam with a "minimal" Teva-
tron.

The Tagged Photon Beam can transport up to 300 GeV. With the present accelerator,
electron yields are not sufficient to do physics above about 140-170 GeV (with
the exception of the total cross section which went up to 200 GeV). With the
minimal Tevatron this translates to an upper limit on e^- energy of $\sim$ 300 GeV
which matches exactly the existing capability of the transport. With 150 GeV
electrons (75-145 GeV photons) the spectrometer acceptance approaches 100% for
charm-like masses in the 3-6 GeV range. $\left| t_{min} \right|$ effects in photoproduction start
to become a limitation to physics around 10 GeV. With 300 GeV electrons (150-290
GeV photons) and no geometrical change in the spectrometer there will be full
acceptance in the 6-12 GeV mass range and $\left| t_{min} \right|$ limitations setting in at $\sim$ 20 GeV.

(Although basic detector positions would remain unchanged the bending power of the magnets would have to be scaled by a factor of two to maintain resolution. The magnets are capable of providing the additional field required.) The higher energy will not only extend the useful mass range it will help certain energy dependent processes at lower masses. In particular as discussed later Primakoff production (of the η_c , for example) is somewhat dependent on energy.

An alternative approach to doing photon physics with the Tevatron is to use the higher proton energy to increase the e^-/γ beam intensity at lower energies. Doubling the proton energy will increase the e/γ intensity by approximately a factor of 10 at 150 GeV. This additional intensity will be extremely useful but it will require some tagging system modification (more channels) if tagging is required and it is not likely that the spectrometer drift chambers (in particular) will be able to stand the higher rates. A change to the new Charpak gated drift chambers will very possibly be appropriate for the chambers nearest the target. Other spectrometer changes will probably also be required for very high intensity. For this reason, as well as the reduced intensity of the initial minimal Tevatron, I expect a push to higher photon energies will tend to proceed a push to higher intensity.

Maximum luminosity is now $\sim$ 20 events/nb hr with 150 GeV e^-, 5×10^{11} p/sec. With a minimal Tevatron this translates to roughly 4 events/nb hr at 300 GeV and 40 events/nb hr at 150 GeV.

Listed below are some specific examples of experiments. For any particular experiment there is an optimal electron energy (and corresponding maximum intensity) given the capability of the detectors and the accelerator at the time.

New Quark Physics: Obviously the extended mass range opens up important physics involving the new b quark states and, imaginably, the t quark. There are difficulties, of course, but they do not appear insurmountable. First is the matter of rates. Whereas the total charm photoproduction cross section is thought to be 1-3 μb, the total bottom cross section is estimated at 25-50 nb. With a 300 GeV minimal Tevatron e^- beam this would still produce some hundreds of bare bottom states/hour. Second are the higher multiplicities and lower branching ratios making it harder to find signals. However, large multiplicities are the strong point of a spectrometer with a fixed target compared to a colliding beam. I would not be surprised if the colliding beams have an even harder time finding bottom states than they had with charm.

The cross section for $\gamma p \to \Upsilon$ with 300 GeV e^- will be the order of $\frac{1}{2}$ nbarn compared to 35 nbarns for ψ. With the minimum Tevatron one should get a total of 2Υ/hour. Although a recoil missing mass trigger will be very useful for this channel one will have to cope with small branching ratios. A 1000 hour minimal Tevatron run would yield $\sim$ 40 each $\Upsilon \to e^+e^-$, $\mu^+\mu^-$ and most interestingly $\tau^+\tau^-$. The latter can be definitely identified by looking for a peak at the Υ mass in the missing mass spectrum for events with $\tau^+\tau^-$ signatures (μe, $\mu\mu$, $\mu\tau$, etc.). This is a definitive test of the point like leptonic nature of the τ since the rates $\Upsilon \to e^+e^-$ and $\Upsilon \to \tau^+\tau^-$ should agree within a few percent. The Υ resonance strongly enhances τ production over Bethe Heitler in the 9.5 GeV mass region.

Jets: It has been a common belief that real photons because they have $q^2 = 0$ cannot be used to kick quark or gluon jets out of a nucleon. John Ellis recently pointed out that QCD specialists have realized this is not true. In fact it is just as good for the virtual quark or gluon to be off its mass shell as for the photon. Kinematically this corresponds to large forward mass ($M_F \geq 8$ GeV) which can be identified in the spectrometer. At Tevatron energies, jets will be better collimated by a very helpful factor of 2. This and the clean photoproduction environment will allow a good study of jet phenomena including, perhaps, identification of gluon jets.
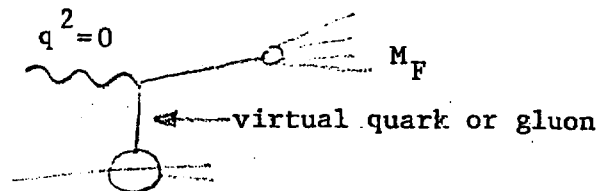
Primakoff production of 0^+ states: An optimist would insist that Primakoff production of $\eta_c(2.8-3.1$ GeV) is feasible with the present accelerator. Total event rates have been estimated at $\sim$ 4/hr at maximum luminosity ($\Gamma_{\gamma\gamma}=20$KeV In reality the number of final states, most in principle detectable, and their backgrounds make this a difficult undertaking. The extra energy at 300 GeV increases the cross section by maybe as much as a factor of 3. Note that this gain is lost by the factor of 5 reduced minimal Tevatron intensity so that η_c may best be dealt with at $\sim$ 150 GeV. At a mass of 3.5 GeV (η_c') rates are lower by $\sim$ 3 at 150 GeV and the Tevatron factor of 2 would bring this up to the borderline of feasibility. The reason Primakoff production is important enough to worry about factors of 2 is that it is a calculable process with one parameter, $\Gamma_{\gamma\gamma}$. Thus an experiment can set a strict limit on the existence of η_c at a given mass and $\Gamma_{\gamma\gamma}$.

Heavy Lepton Bethe Heitler Production: Coherent pair production of 2 GeV leptons on Be increases from about 1/hr with a 150 GeV e^- beam to about 5/hr at 300 GeV (5×10^{11} p/sec). The gain is lost with minimal Tevatron intensities. Here again a marginal but important experiment becomes somewhat less marginal. With a Pb target an increase due to energy of 10 can be expected giving only $\sim$ 1 ev/hr for a target $.2X_0$ thick.

One is very tempted to consider the Primakoff and Bethe Heitler experiments in particular with a new broad band electron to photon beam bringing maybe 50X more photons to either the TPL or a new enclosure. However a large (full) acceptance spectrometer is, in my view, essential to exploit properly this physics and the use of such a spectrometer at super high luminosities is a very difficult problem which will take time to solve. In fact, the tendency for cross sections to fall with mass and for multiplicities to increase will force us to deal with very high luminosity in large acceptance spectrometers in order to be able to take full advantage of the broad array of new physics available with the Tevatron. This is clearly one of the major challenges for the next few years.

TN:plm

cc: C. T. Murphy
      J. Peoples

Fermilab

April 25, 1980

To: L. Lederman

From: T. Nash

Subject: Heavy Quarks at the Tagged Photon Spectrometer:

     Considerations for the Woods Hole Panel

From our earliest design discussions, it has been almost intuitively obvious to many of us at the Tagged Photon Spectrometer that we are building the first Tevatron detector. At this time we are working hard bringing the system up to take data. The aim is to get successful data and results from either this run or the one coming in the fall. So successful, we would hope, that it will then also be intuitively obvious to the world outside our private discussions that the TPS will be ideal for 1000 GeV physics. However, right now we are religiously keeping our blinders on and concentrating on bringing up the system to look at diffractive charm production in its first run. I can therefore not provide the latest predicted rates for bottom production, etc., but rather only an outline of what are the future prospects for the spectrometer.

The spectrometer is now set up in an optimized match of rate and acceptance to look at charm and QCD physics (quark masses ~2 GeV, forward masses 4-6 GeV) with tagged photons from 70-140 GeV (e⁻ beam energy 150 GeV; proton energy 400-450 GeV). The optimization was done based on the idea (not yet proved or disproved) that the best (perhaps, only) way to study heavy quark states which dominantly decay into many particles is to struggle for maximum acceptance (both geometric and particle type) of all final state particles. Exclusive measurements, constraining both charmed and anti-charmed masses, should have signal to noise far higher than those seen in the inclusive measurements made to date; and these require full acceptance in order not to lose rate. QCD studies require full acceptance to avoid trigger and analysis biases. For the masses and beam energies indicated above, the spectrometer has >90% geometrical acceptance (see Tagged Photon Magnetic Spectrometer Design Report, Table IV, attached).

At these energies the Tagged Photon Beam provides $\gtrsim 10^6$ tagged photons/pulse which is turning out to be (as we planned) near the limit of rate for a large acceptance spectrometer.

The required spectrometer acceptance was determined from two parallel types of considerations. Table III from the 1977 TPS Design Report shows Lorentz transformed SPEAR data at 4 GeV. Figure 8 shows the range of lab momentum and angle for a cascade decay of a 3 GeV particle at 100 GeV. (Similarly for

$$(M = 4.4) \rightarrow (M = 1.85) + (M = 1.85)$$

$$\rightarrow (M = 0.14) + (M = 0.14)$$

this type of analysis gives $\theta_{max} \approx 150$ mrad.) The approximate detector acceptance is shown on the figure showing how the 2 magnet low p/high p charged particle detection system matches the required acceptance.

So, the system is ideally matched for charmed study for 400 GeV protons, 150 GeV electrons. The intuitively obvious statement is that because of the Intuitively Obvious Scaling Parameter (IOSP), m_q/E_γ^{LAB}, the detector acceptance is also ideally matched for 5 GeV quarks with 1000 GeV protons and 300 GeV electrons. (IOSP is obvious because angles scale as

$$\frac{P_\perp}{P_\parallel} \sim \frac{m_{q\bar{q}}}{E_{q\bar{q}}} \sim \frac{m_q}{\text{Lorentz Factor } (\gamma)} \sim \frac{m_q}{E_\gamma^{LAB}} \cdot)$$

The spectrometer's magnets can be powered to more than twice the field we require for the initial 150 GeV experiment and thus will be ready for 300 GeV without change. With no changes at all the e^- beam and tagging system can go to 300 GeV. (They were designed to go to those energies for the σ_{T} experiments.) Thus it almc appears that all that is needed for this first Tevatron experiment are 1000 GeV protons on the P-East target.

Nothing in the world can be that perfect. First of all, the fact is we are, as said earlier, just bringing up the system and have a lot to learn about how to do this kind of physics: how to trigger, how to reconstruct, how to cope with the complexities of the system and the highest possible rates. From all this learning will come a better understanding of what -- presumably modest -- modifications ought to be proposed to do physics with the Tevatron and exactly what that physics ought to be. The second catch is that bottom physics, scaling considerations aside, is harder than charm because a) rates will be ~10X lower and b) multiplicities will be ~30% higher. The hope is that the increase of experience from doing this kind of physics with charm will scale with the added complications of bottom.

Another intuitively obvious area of discussion has to do with why this physics can't be done better at colliding machines. We were frequently asked in 1977 why we were undertaking our effort when SPEAR was going to do it all. The fact is (and was) that SPEAR couldn't do it all because sitting in the center of mass they would have had to cover 4π in the lab to cover 4π in the CM. With a fixed target we will cover (nearly) 4π of the Lorentz

transformed photon fragmentation by covering ±~200 mrad in the lab. This allows one to use a long strung-out detector (see Fig. 1) in which measurement and identification of different particles can be dealt with in a systematic and serial fashion. There is thus hope that π^0, μ, $\pi^\pm$, K and nucleons can all be detected and identified over essentially 4π in the center of mass.

Decay lifetimes of charm and bottom also become more thinkable as subjects of study because of the Lorentz boost (particularly at 1000 GeV) compared to colliding detectors. Some of my colleagues have been thinking seriously about triggers based upon lifetimes of heavy quark states that become particularly attractive with Tevatron energies and are, of course, impossible with colliders.

One stated objective of our program of physics is to understand the production of heavy quark pairs from photons in the presence of a nucleon. This should lead to information on heavy quark interactions with conventional quarks and nucleons that probably cannot be obtained in any other interactions, manifestly not e^+e^- collisions.

In sum we are talking of a whole area of physics which can only be done with the Tevatron. It would be irresponsible not to pursue these subjects and to bang on with no more than 5 or 6 identical experiments around the world each time a new interaction region energy is reached. That would be much too limited as I cannot imagine that anyone believes that all possible surprises have been predicted and that these are only to be "discovered" at low luminosity and extreme energy.

The trouble is that we are struggling on with ridiculously low levels of funding, high levels of bureaucratic regulations, low repetition rates and proton energies, long shutdowns, etc. that are making it very difficult for us to compete with Europe. In our experiment, the on-line computer, just to name one area of difficulty, is 1/4 the size of what a similar sized experiment at CERN has and 1/2 what is minimally needed. Engineering support for electronics is so limited that we are forced to use commercial equipment of unspeakably low quality. We need engineering support to develop off-line processing systems to cope with the huge amounts of analysis that will be required.

As lumbering and slow as is the general pace at CERN, they now appear to be able to mount large experiments faster than we can. One can only hope that our large experiments, like the TPS, are either aimed better or are more flexible than those at CERN, because there is little hope of funding new systems faster than the Europeans.

TN:mef

Attachments

Scientific Spokesperson:

T. Nash
Fermilab

FTS number: 370-3795
Commercial: (312) 840-3795

The Tagged Photon Magnetic Spectrometer:
Facility Design Report

May 1, 1977

J. Appel, D. Bartlett, S. Bracker, W. Ford, G. Hartner, G. Kalbfleisch,
 G. Luste, P. Mantsch, J. Martin, R. Morrison, T. Nash, U. Nauenberg,
    D. Ritchie, J. Smith, K. Stanfield, and S. Yellin

Fermi National Accelerator Laboratory, Batavia, Il.*
University of California at Santa Barbara*
University of Colorado, Boulder*
University of Toronto†

Table of Contents

I. Introduction

This report describes the design of a magnetic spectrometer facility to be built in the Tagged Photon Lab. The design has been developed by a collaboration of physicists from Fermilab, The University of California at Santa Barbara, The University of Colorado and The University of Toronto. This group was formed to build the facility and to carry out the experiment described in Proposal 516,[1] which is a study of photoproduced states (including charm and hidden charm) with a forward mass > 2.5 GeV. Although the design of the facility is developed from that outlined in P-516, much thought has gone into making the facility versatile enough to be used for a continuing program of physics by different groups. In addition to the 100 GeV photon physics of P-516, this facility is designed to be useful for experiments like the following: pion production experiments, hadron jet experiments,≳ 300 GeV and very high intensity photon physics with the energy doubler including searches for and studies of heavy leptons.

A detailed layout of the spectrometer is shown in Fig. 1. In Table I may be found the sizes and locations of the detectors. These are the locations expected for the startup of the facility with photon energies in the range 70 < k < 140 GeV. However, much of the spectrometer will be mounted on a rail system. This will allow, for example, the spectrometer to be stretched out for future use at higher energies.

The following is a brief overview of the system prior to the

detailed discussions in the remainder of the report. The recoil

system surrounding the target identifies recoil protons and measures

their angles and kinetic energy (see Fig. 3 & 4 in Section II).

This information can be used to determine the missing mass of

the forward going system of particles that recoiled off the proton.

Angles are measured by three cylindrical wire chambers (PWC1, PWC2,

PWC3). Energy is measured by total absorption and range in a four-

tiered cylindrical liquid scintillator detector (A_i, B_i, C_i, D_i).

Pions and protons are distinguished by the dE/dX information.

The forward spectrometer is a two magnet system (M_1, M_2) consisting

of a low momentum, high acceptance spectrometer combined with a

lower acceptance spectrometer for higher momentum particles. There

are five banks of drift chambers $(D_1, D_2, D_3, D_4, D_5)$ to measure

momenta and angles of charged tracks. Two atmosphere pressure

Cerenkov counters $(\check{C}_1, \check{C}_2)$ will be used for K, π, p particle

identification. A segmented liquid scintillator shower counter

(SLIC) will measure energy and angles of electromagnetic particles

$(e^{\pm}, \pi^o, \gamma)$. A segmented hadrometer will be used to detect neutral

hadrons (K_L^o, n) and will be used in triggers. It will also be

essential to possible hadron jet experiments. Table II summarizes

broadly the capabilities of the facility, including acceptances,

resolutions, etc.

In the following sections of this report we will first

discuss the design considerations and constraints that have lead

to the present design of the recoil system and the forward spectrom-

eter. We will describe the approach to triggering that we are

planning and the reconstruction of multitrack events. This will

Table I

Locations, Sizes and Acceptance of Detectors

	Location (m) on beam line	Size (m) [2] Hor.	Vert.	Acceptance [1] P_{min} (GeV)	$\Delta\theta_x$ (mrad)	$\Delta\theta_y$ (mrad)
tgt center	0	–	–	–	–	–
D1XUV	1.68	.67	.56	1	±199	±167
D2XUV1	2.18	.85	.65	1	±182	±149
D2XUV2	2.21	.85	.65	1	±180	±147
D2XUV3	2.24	.85	.65	1	±178	±145
M1	2.2±.6	~2	.76	–	~±350	±136
D3XUV1	3.41	1.75	1.20	1	±176	±176
D3XUV2	3.71	1.75	1.20	1	±162	±162
D3XUV3	4.01	1.75	1.20	1	±150	±150
M2	4.7±.6	~2	.76	–	~±170	± 72
C1 upstr	4.2	1.40	.64	5	±148	± 74
C1 dnstr	7.45	2.51	1.14	5	±135	± 77
D4XUV1	7.51	2.10	1.25	10	±120	± 79
D4XUV2	7.97	2.10	1.25	10	±120	± 78
D4XUV3	8.12	2.10	1.25	10	±120	± 77
C2 upstr	8.2	2.1	1.25	10	±120	± 77
C2 dnstr	15.1	4.33	2.50	10	±120	± 82
D5X12	15.2	4.33	2.50	10	±120	± 82
Control Shower Ctr (C) upstr	15.3	.064	.064	accepts γ beam only		
SLIC dnstr	16.4	4.14	2.64	neutrals	±127	± 82
Hadrom. dnstr	18.15	4.90	2.95	10	±110	± 81

Notes:

1) Acceptance for rays from target center. Magnet bends at 5 kG-m, same polarity

2) Sizes specified as follows: Only magnet apertures to limit vertical rays from either end of target. Horizontal acceptance ± 120 mrad for P_{min} rays from upstream end of target for low P system and from target center for high P system (± 110 mr for hadrometer).

Table II

Overview of Spectrometer Capabilities
(for electron beam energy = 140 GeV)

Recoil:

$.1 < |t| < .6$ GeV^2

$30° \lesssim \theta \lesssim 90°$

acceptance $\simeq 50\%$ for $e^{-\lambda|t|}$,

  $2 < \lambda < 15$ GeV^{-2}

$\frac{\delta T}{T} \simeq \pm .1$ $\delta\theta = \pm 6$ mr

$\delta M_x < \pm 350$ MeV for $M_x > 2$ GeV

$\pi\pm$ vs p identification range $|t| \leq .6$ GeV^2

π° identification efficiency $\sim .72$

n identification efficiency $\sim .45$

Forward charged spectrometer:

Low momentum system

  $1 < P < 10$ GeV

    $\theta_{horiz} < \pm 150$ mr

    $\theta_{vert} < \pm 135$ mr

$\frac{\delta P}{P} = \pm 8.6 \; 10^{-4} P$ $\delta\theta = \pm .1$ mr

High momentum system

  $10 < P < 120$ GeV

    $\theta_{horiz} < \pm 120$ mr

    $\theta_{vert} < \pm 72$ mr

$\frac{\delta P}{P} = \pm 2.2 \; 10^{-4} P$ $\delta\theta = \pm .05$ mr

Particle Identification - π vs (K or p): $5.5 < P \lesssim 50$ GeV

π vs K vs p: $21 < P \lesssim 50$ GeV

Neutrals:

    $\theta_{horiz} < \pm 120$ mr

    $\theta_{vert} < \pm 82$ mr* $\frac{\delta E}{E} \lesssim \pm .1 \; E^{-\frac{1}{2}}$ $\delta\theta = \pm .3$ mr

---

Luminosity: ~ 1 event/nb/10^{15} protons

*(± 120 mr with upstream shower counters)

MUON COUNTERS

STEEL ABSORBER

HADROMETER

CENTRAL SHOWER COUNTER

SLIC

$\check{C}_2$

$\check{C}_1$

DRIFT CHAMBERS

MAGNET-2

SHOWER DETECTOR

MAGNET-1

RECOIL SPECTROMETER

TARGET

PLAN VIEW

D_5

D_4

D_3

D_1

D_2
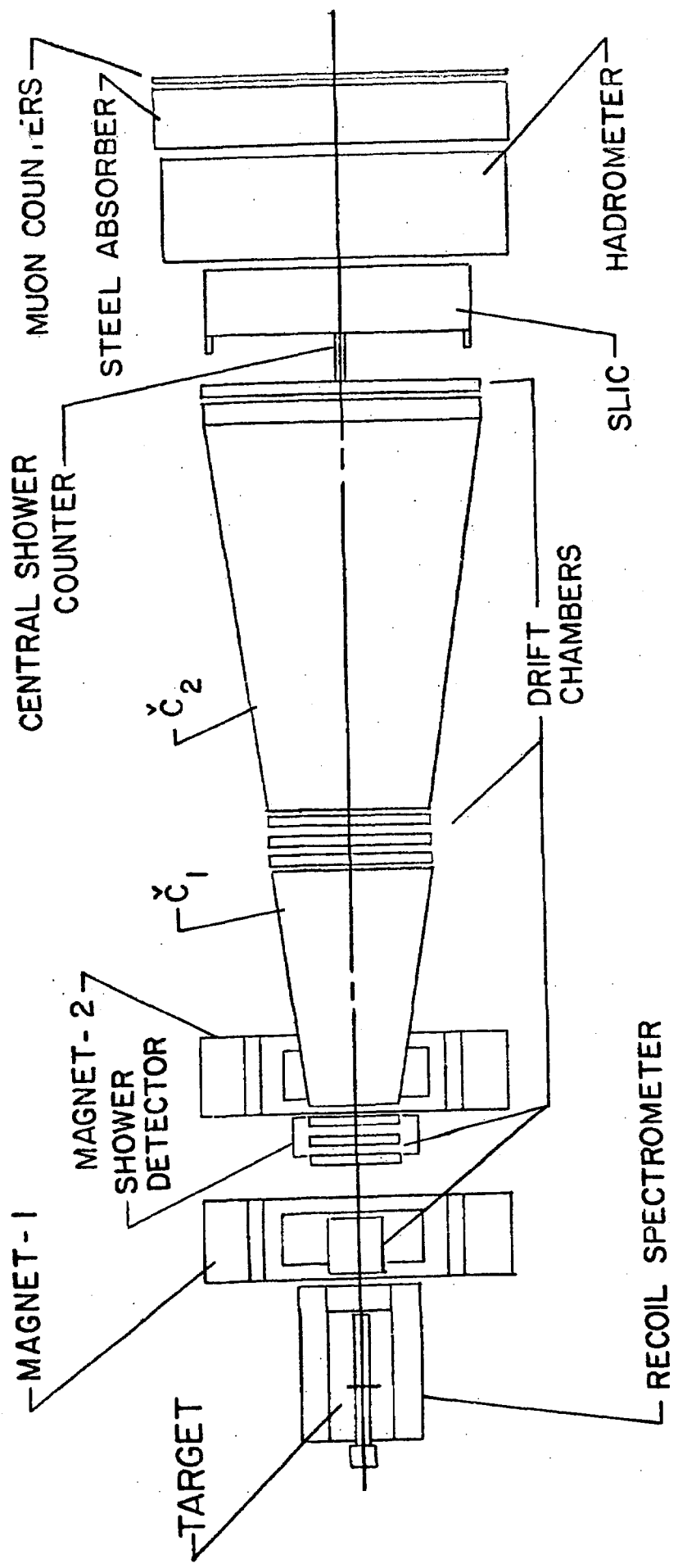
ELEVATION

1 meter
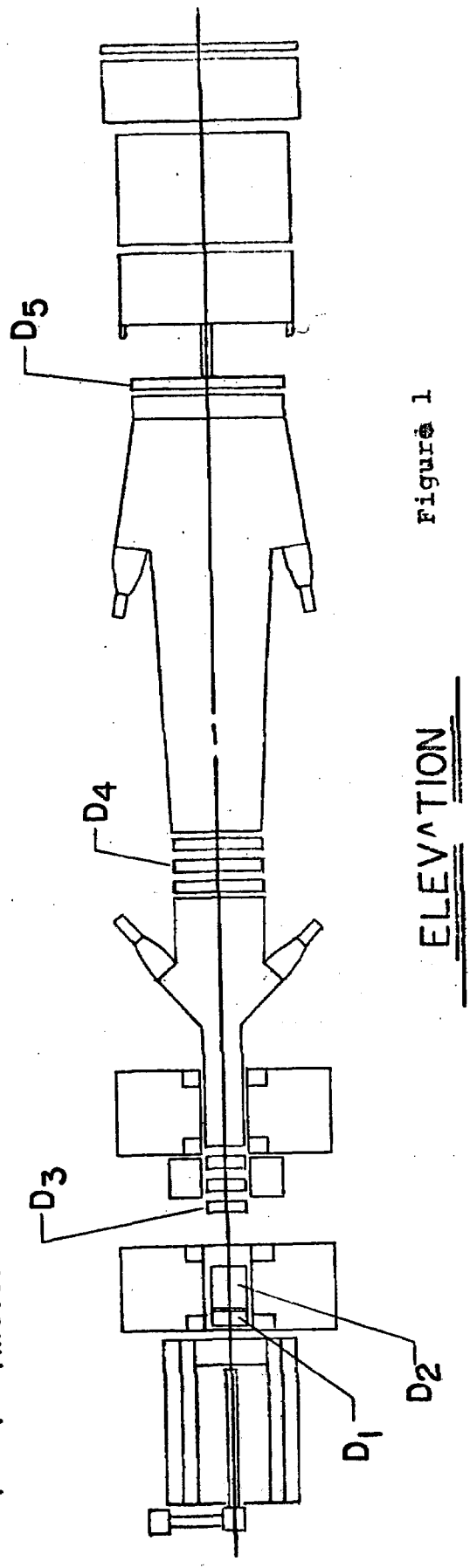
Figure 1

be followed by a detailed description of the various detectors
and experimental equipment that will be built. We will leave to
the last, appropriately next to the acknowledgements, an outline
of costs and scheduling.

II. Design Considerations of the Recoil System

The purpose of the recoil system is to measure the four
vectors of particles recoiling from the 2m long hydrogen target.
It must do this in less than ~ 1μsec so that a missing mass can
be calculated and used in the trigger. Since the associated
photoproduction of charmed states will require missing mass in
excess of 2 times 1.80 GeV, the missing mass threshold can be
safely set at 2.5 GeV in the trigger. As discussed in Section
IV, this will reject most of the γp cross section including all
the low mass neutral vector mesons $(\rho^o, \omega^o, \phi^o, \rho^{o'}$, etc.) and
will enrich the data with charm events.

A. Acceptance

We consider the reaction

$$\gamma p \rightarrow M_x p'$$
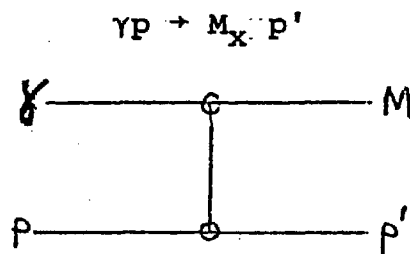
where particle M_x is the forward going system predominately
detected in the two magnet spectometer. Figure 2 shows the
simple two body kinematics curves for this reaction at
several energies. It is clear that the polar angle θ for the

Fig. 2

END VIEW OF

RECOIL DETECTOR

Fig. 3   Scale 1:10

RECOIL DETECTOR

ELEVATION
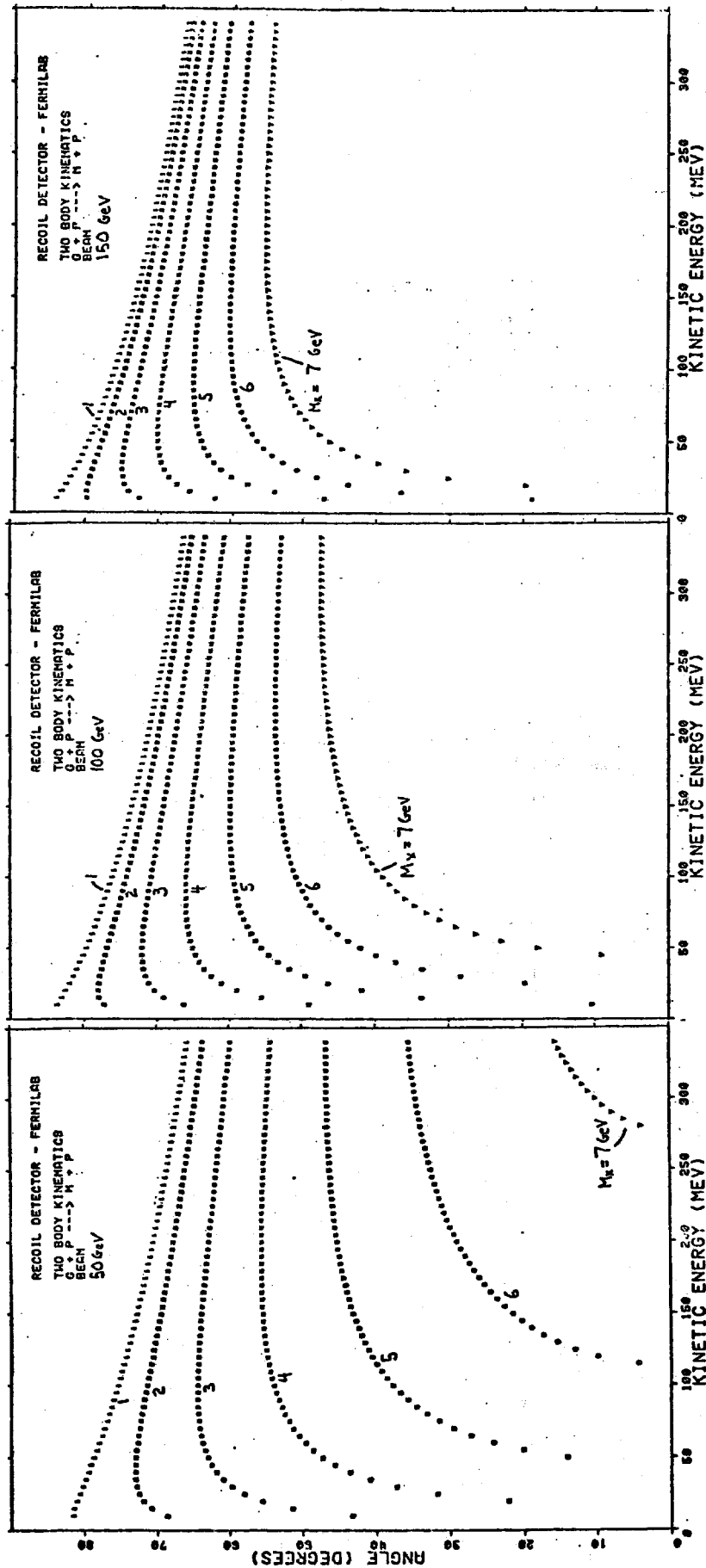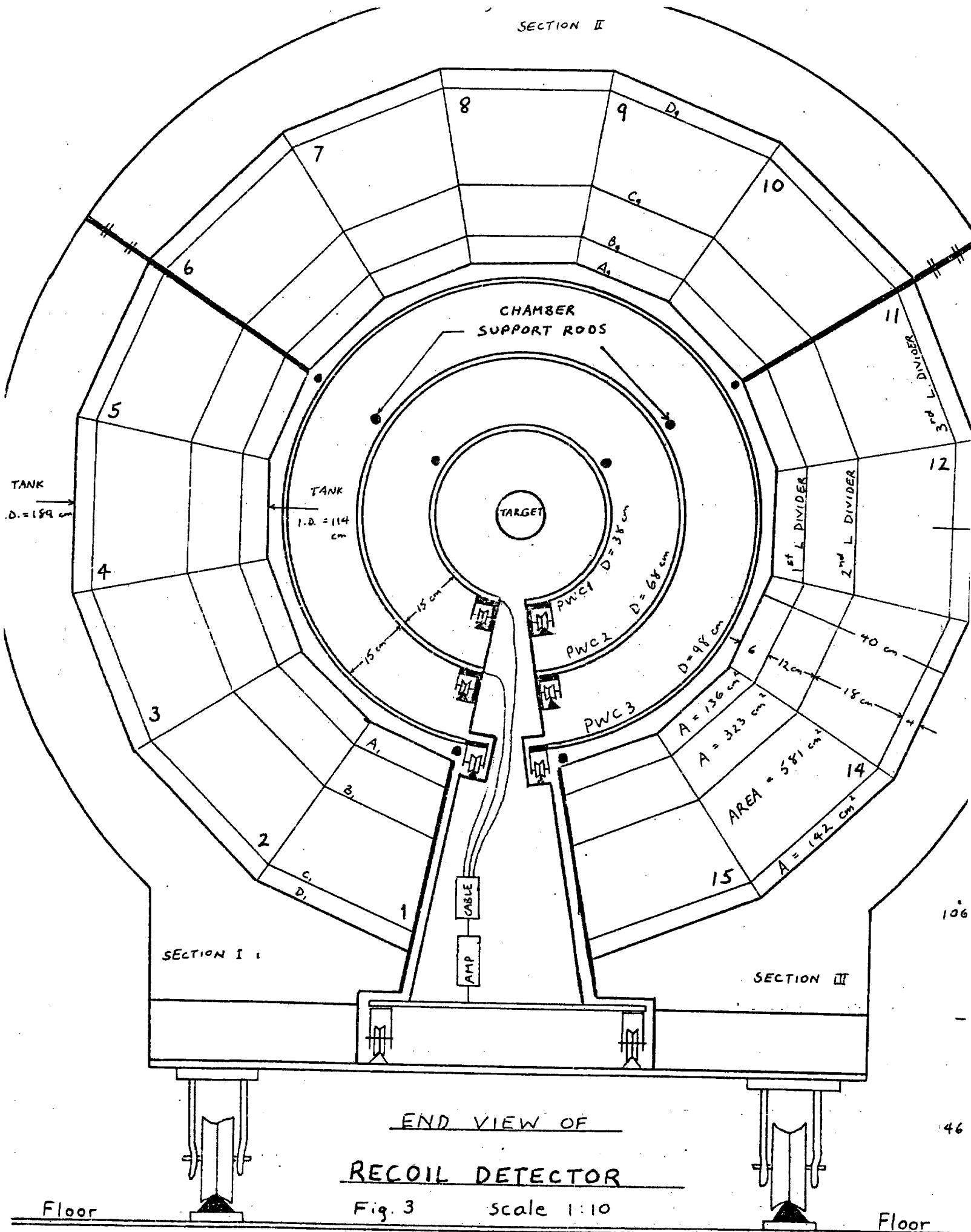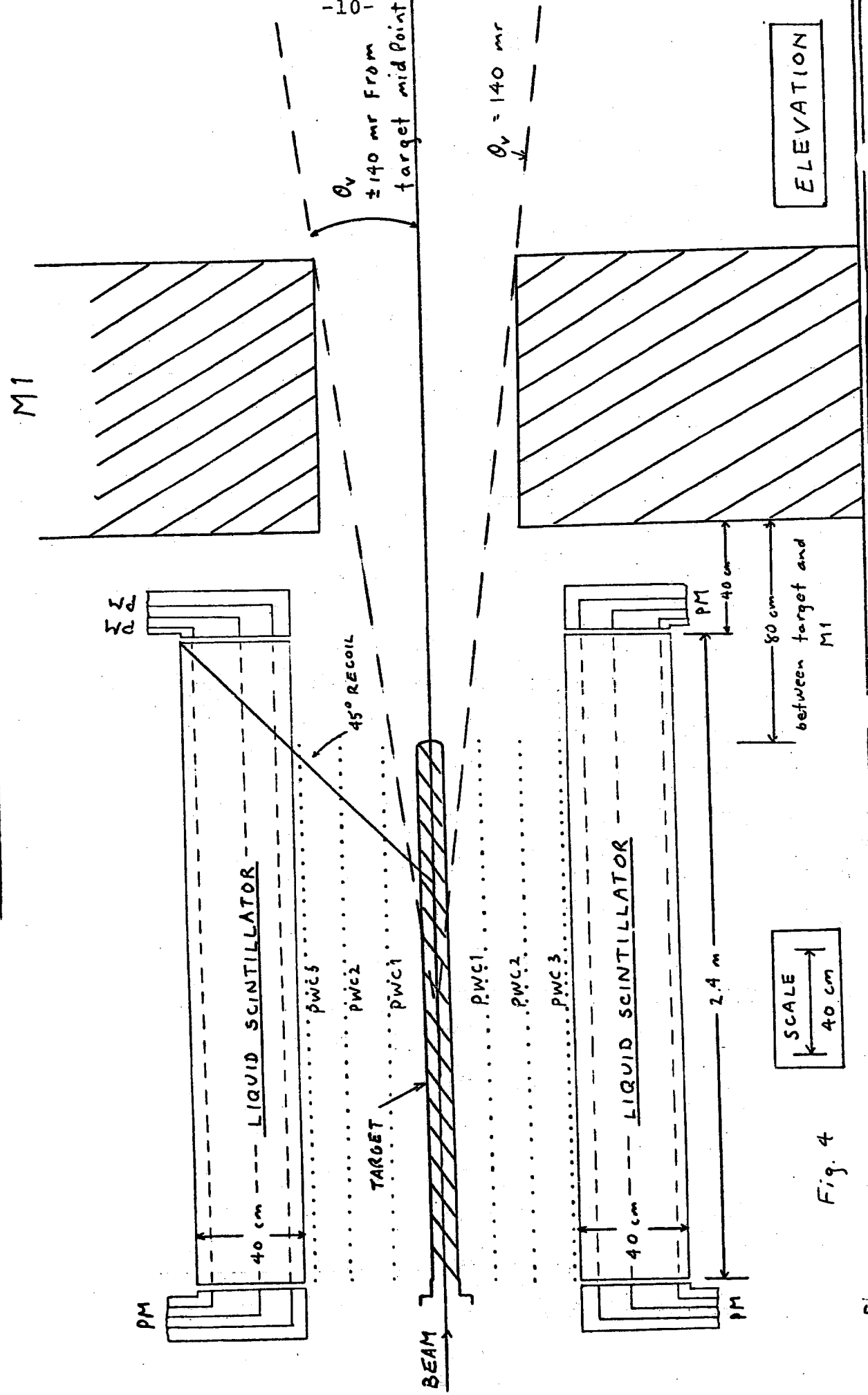
Fig. 4

p' recoil mainly lies between 30° and 80° for the M_x range

of 2 to 6 GeV. Only near values of $|t|_{min}$ is the angle less

than 30°. Thus the recoil system is designed to have high

acceptance for $\theta \gtrsim 45^O$. Only in the downstream one-half

meter of a 2.0 m long hydrogen target is there any accep-

tance loss for $\theta \lesssim 45^O$. Figures 3 and 4 show a side and

frontal view of the recoil system and illustrate how the

detector encloses the target.

The azimuthal angle acceptance is almost 337.5^O. This

is 94% of the full 2π. As shown in Fig. 3, a segment in θ

is removed to provide structural support for the access to

the three cylindrical PWC's.

We define momentum acceptance of the recoil proton as

that percentage which stop inside the liquid scintillator

range detector. This of course depends on the t distribution

of the recoil particle, and its recoil angle θ. The recoil

angle θ determines how much material the proton must traverse

(in the target and PWC's) before it reaches the scintillator.

It defines a minimum momentum. The effective scintillator

thickness increases as θ decreases and defines a maximum

momentum. A reasonable estimate is that the acceptance will

be in the range of 45% to 55%. This assumes a recoil slope

of $\lambda \simeq 4$ GeV^{-2}, which is the value suggested by the high

energy ψ photoproduction experiments. Figure 5 shows how

the proton recoil acceptance varies with the $e^{\lambda t}$ recoil slope

λ and for three different ranges of t measurement. The

expected range is $0.1 < |t| < 0.6$ GeV^2. It is clear that

RECOIL PROTON ACCEPTANCE
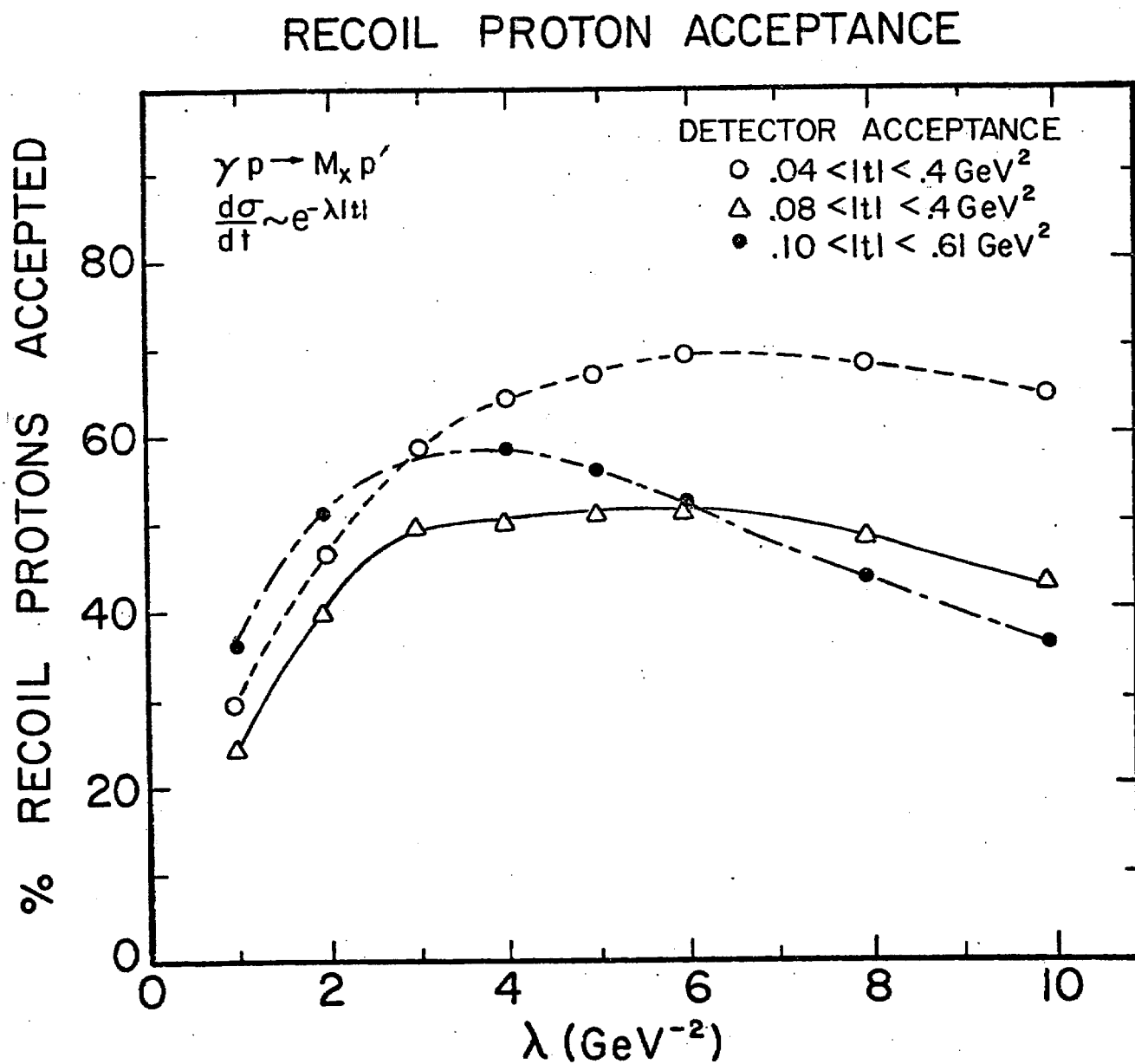
Figure 5

building a detector to measure much lower and/or higher t,

which would greatly increase the complexity and expense,

would not provide a commensurate gain in acceptance.

B. Resolution

The equation for missing mass is $M_x^2 = 2kp'\cos\theta - 2kT$

$-2mT$ where k is the beam energy, T and p' are the recoil

proton kinetic energy and momentum, θ is the recoil proton

angle relative to the beam and m is the proton mass. The

error contributions then vary as

$$\delta M_k = \frac{1}{M} (p' \cos\theta - T)\delta k$$

$$\delta M_T = \frac{1}{M} (\frac{k \cos\theta}{\beta} - (k+m))\delta T$$

$$\delta M_\theta = \frac{1}{M} k p' \sin\theta \, \delta\theta$$

and the total missing mass resolution is

$$\delta M_x = \sqrt{\delta M_k^2 + \delta M_T^2 + \delta M_\theta^2}$$

The variation of the δM_i curves with T and different

values for M, k, δk, δT, and $\delta\theta$, representing extremes, are

shown in Figs. 6a-d. The T interval from about 30 to 300 MeV

represents the typical acceptance of the liquid scintillator.

At very low T, multiple scattering dominates $\delta\theta$ which, in turn,

dominates δM. These low T protons are also the recoils

which will not make it through the hydrogen, the target walls
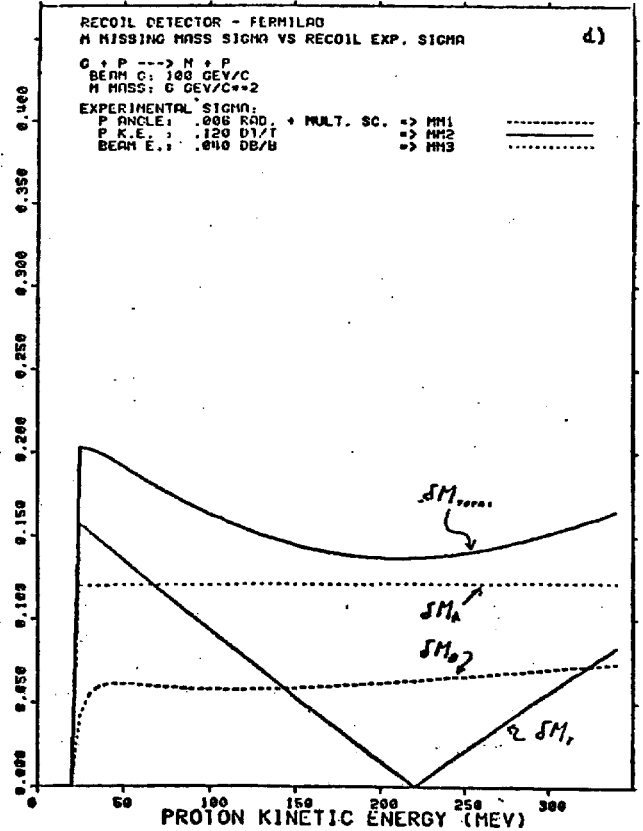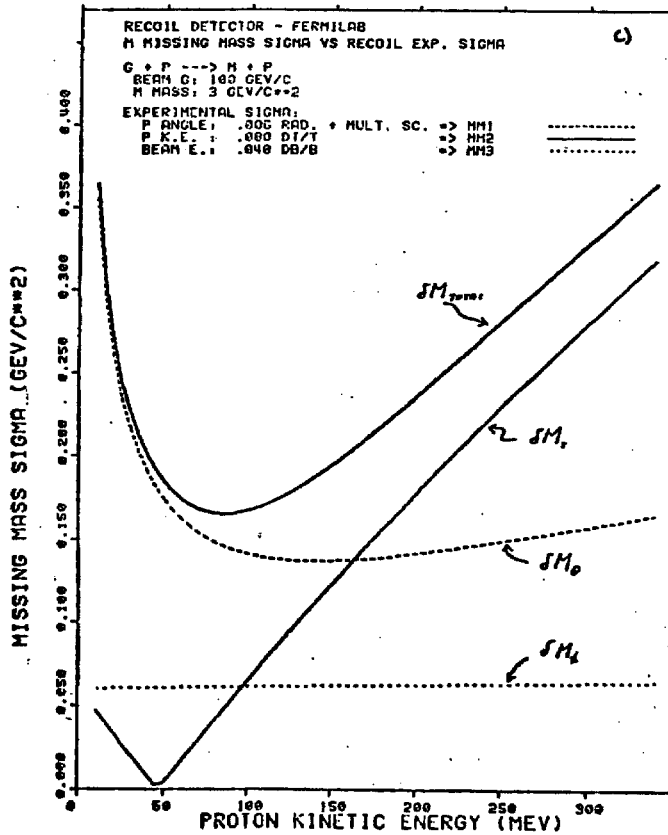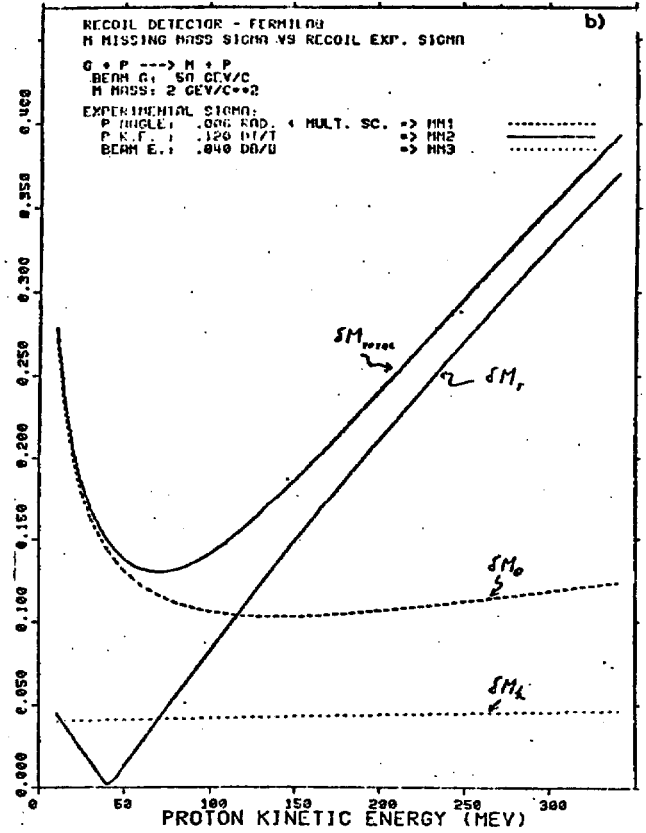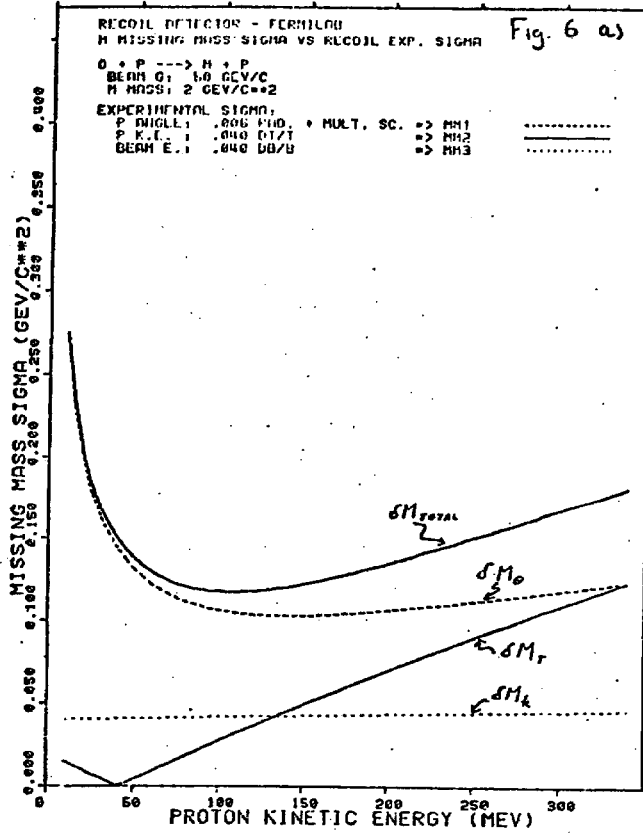
Fig. 6 a)

and the chambers into the liquid scintillator.

In Fig. 6a, at T = 300 MeV the error contributions from δM_T and δM_θ are equal when $\delta T/T = \pm 4\%$ and $\delta\theta = \pm 6$ milliradians. The resulting $\delta M_{total} = \pm 175$ MeV at M = 2 GeV, k = 50 GeV. This guides our choice of wire spacing in the cylindrical PWC's to measure $\delta\theta$ to ± 6 mrad. A pessimistic case of $\delta T/T = \pm 12\%$ gives $\delta M_{total} = \pm 350$ MeV for the difficult case of low mass (2 GeV) and γ energy (50 GeV), as shown in Fig. 6b. Even here the missing mass resolution is acceptable. For very high missing mass the resolution is dominated by the beam momentum uncertainty $\delta k/k \simeq \pm 4\%$. This is illustrated in Fig. 6d.

In conclusion, the recoil system is designed to measure recoil protons in the t range 0.1 to 0.6 GeV^2 and to calculate the missing mass to within ± 350 MeV/c^2 for $M_x > 2$ GeV.

C. π, P Identification

Pions and protons (T < 300 MeV) can be separated by relative dE/dx signals in liquid scintillator compartments A_i, B_i, C_i, and D_i. The relative pulse heights in each compartment are shown in Fig. 7a for recoil angle $\theta = 90°$ and in Fig. 7b for recoil angle $\theta = 30°$. For example, in Fig. 7b, a 230 MeV proton could not be mistaken for a pion of any energy because of its large pulse height in segment B and zero pulse height in segment C. A more ambiguous case is a ~ 470 MeV proton, which perhaps could be interpreted as a 200 MeV pion.

ENERGY ABSORBED IN SCINTILLATOR CHAMBERS
AS A FUNCTION OF INCIDENT KINETIC ENERGY
PROTONS ———— PIONS .....

Figure 7
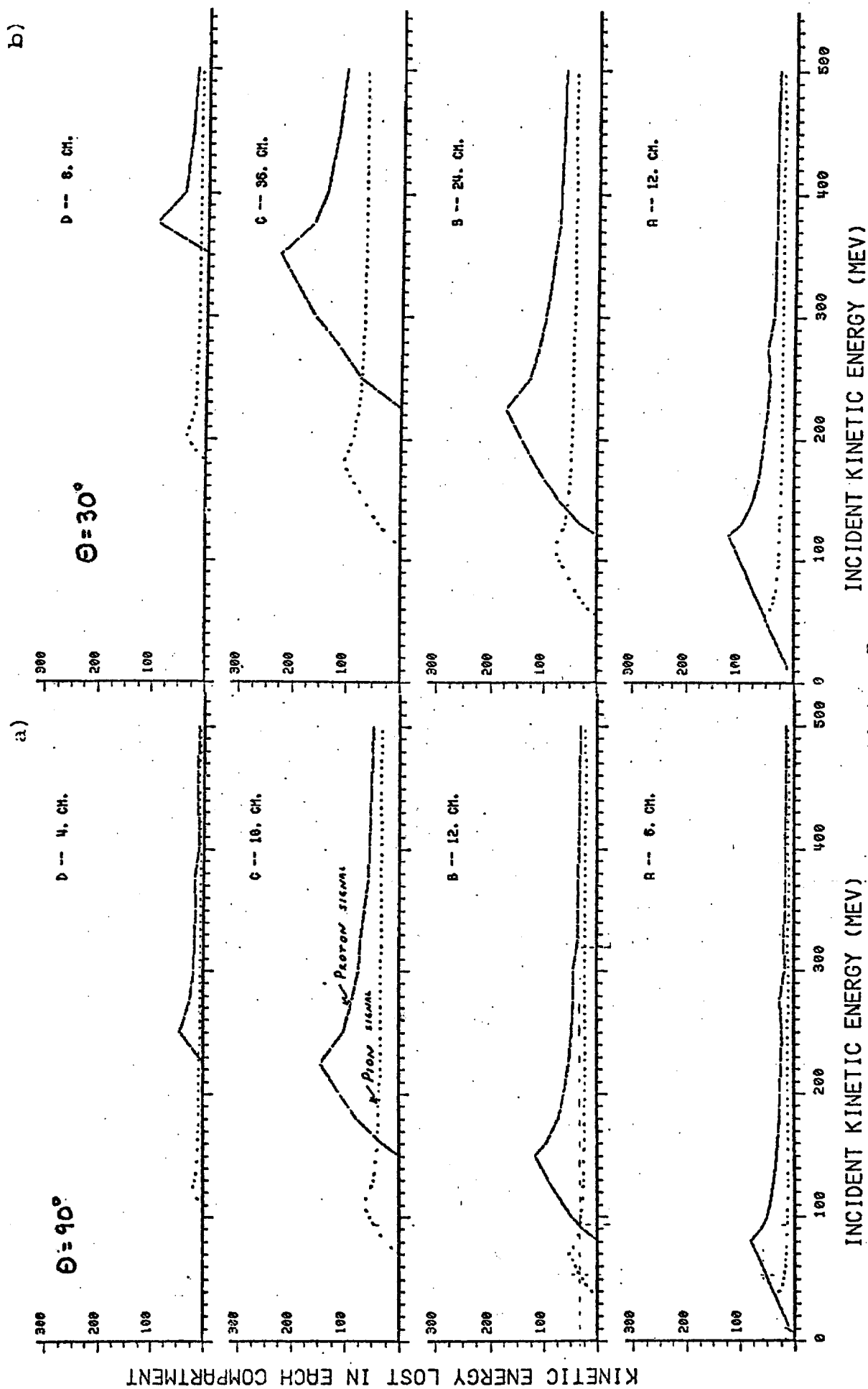
The exact energy range over which this particle identification is useful will depend upon the precise energy loss dependence and the resolution of the energy measurement in each compartment. If no special mapping or correction calculations are required, it may be possible to have this information on-line. Otherwise it will be available off-line, after the resolution has been fine tuned.

III. Design Considerations for the Forward Spectrometer System

A. Acceptance

High mass states tend to decay into a high multiplicity of particles. In order to be able to reconstruct the masses and decays of these states it is essential to have very good single particle acceptance. For experiments involving electromagnetic production of η_c or heavy leptons, cross sections are extremely low and one cannot afford to lose any acceptance. Nature has apparently been more generous with charm photo-production cross sections, but not so generous as to allow experiments that skimp on acceptance. For these reasons we have studied carefully the acceptance requirements and have designed the spectrometer to meet these requirements.

A first guide to the acceptance requirements for the forward detector comes from Lorentz transforming to the lab the x dependence of e^+e^- colliding beam data at 4 GeV as measured in the SPEAR magnetic detector.[2] Table III shows the results of integrating these distributions. The Table

Table III

Typical Angular Acceptance Requirements for Multi Hadron Final States

(Lorentz transformed from SPEAR inclusive data.)

$M_x = 4$ $n_{ch} \simeq 4$ $n = 6$

Angles that include 95%, 98% and 99% of secondaries

k GeV	p_{GeV}	$\theta(95\%)$ rad	$\theta(98\%)$ rad	$\theta(99\%)$ rad
100	1	.262	.300	.326
	5	.110	.127	.139
	10	.076	.088	.096
	15	.062	.072	.079
	20	.054	.062	.068
	30	.045	.053	.058
	40	.040	.046	.051
75	1	.300	.345	.377
	5	.126	.145	.160
	10	.088	.101	.111
	15	.072	.083	.091
	20	.064	.074	.080
	30	.053	.062	.067
	40	.047	.054	.059

gives angles that include 95%, 98% and 99% of all secondaries above a given momentum. From these numbers we see that magnet acceptance of ± 120 mrad will include almost all secondaries down to 5 GeV and most of those below 5 GeV. Above 10-15 GeV only about ± 75 mrad is required. The two magnet system matches these requirements by providing more bending power at smaller angles for the higher momentum particles and large acceptance at low momentum. A more graphic approach which also demonstrates the reason for a two magnet system is shown in Fig. 8. Here, as an example, the solid curve shows the dependence of angle on momentum for a pair of 500 MeV particles decaying from a 3 GeV state produced at 100 GeV. These in turn decay into a pair of 140 MeV particles for which θ and p are allowed to fall within the dashed curves. The spectrometer acceptance is roughly shown on the figure. For this particular case $\theta_{max} \simeq 170$ mrad. As another example, the cascade

$$(M = 4.4) \rightarrow (M = 1.85) + (M = 1.85)$$
$$\quad\quad\quad \longrightarrow (M = .5) + (M = .5)$$
$$\quad\quad\quad\quad\quad\quad \longrightarrow (M = .139) + (M = .139)$$

has $\theta_{max} \simeq 150$ mrad and will also have good acceptance. For M = 6 GeV instead of M = 4.4 the same cascade will have $\theta_{max} \simeq 300$ mrad indicating a beginning of the fall-off in acceptance at 6 GeV for k = 100 GeV.

Considerations like those outlined above have been used as a guide in designing the acceptance of the spectrometer.

100 GeV

$(M=3) \longrightarrow (M=.5) + (M=.5)$

$\longrightarrow (M=.14) + (M=.14)$

θ_{max}

HORIZONTAL ACCEPTANCE

VERTICAL ACCEPTANCE

θ (mrad)

p(GeV)

Figure 8

We have also checked the acceptance of the design in detail using a Monte Carlo program. Several different production models were used including

1) Assuming the photon to be excited to a 4 GeV intermediate state and then decaying with the characteristic multiplicity and spectrum measured in e^+e^- interactions at SPEAR as described above.

2) Assuming the photon to be a hadron, interacting with a proton, and producing hadrons with the characteristic spectrum measured in πp and pp interactions:

$$\frac{d\sigma}{dP_\perp dX} = P_\perp\, e^{-6P_\perp}\, (1 - x)^4$$

3) Assuming the photon is diffractively excited into a $D\bar{D}$ state with each charm particle decaying into a $K\pi\pi$ final state.

As can be seen from Table IV, the results are similar for the different models with the acceptance falling below 98% of secondaries only for pairs of particles with masses over 6 GeV.

B. Resolution

Given realistic limitations on drift chamber resolution and magnet power consumption, there is a tradeoff between mass resolution (derived from angle and momentum resolution) and acceptance. From the standpoint of charm spectroscopy one can get an idea of mass resolution requirements by noting that theoretical predictions[3] for meson and baryon states of

Table IV

Monte Carlo Calculation of Spectrometer Acceptance

Model (see text)	n_{ch}	K (GeV)	Mass (GeV)	Acceptance Per Particle	Per Event
1. Lorentz transformed SPEAR e^+e^- data	~4	75	4	.988	.95
		100		.998	.99
		140		.999	.997
2. Hadronic	6	75		.995	.97
	7	100		.999	.992
	7	140		.999	.999
3. Charm Pair	6	75	4 (2+2)	.984	.90
			5 (2½+2½)	.96	.80
			6 (3+3)	.93	.73
			7 (3½+3½)	.91	.57
	6	100	4	.995	.964
			5	.984	.90
			6	.97	.83
			7	.95	.73
			9	.90	.52
	6	140	4	.999	.994
			5	.995	.97
			6	.982	.93
			7	.975	.865

2-3 GeV suggest level spacing of 40-90 MeV and higher. Widths are either extremely narrow (low lying mesons) or when cascades are involved (baryons) widths are expected to be at least 30 MeV and usually over 100 MeV.[4] Taking into consideration these numbers and the good signal to noise we expect for these channels we feel that it will be appropriate to start with $\delta M \lesssim 25$-50 MeV and maximum acceptance. If at some point it becomes desirable to improve resolution (at higher mass, for example) to study a particular channel at a cost of reduced acceptance, it will be a straightforward matter to increase magnet current or to stretch out the spectrometer. There is plenty of space at the back of the experiment in the Tagged Photon Lab.

The mass resolution for an n particle system with mass M is

$$\frac{\delta M}{M} = \frac{1}{M^2} \ \Sigma\Sigma^{\text{Quadrature}} \ \frac{1}{2} P_i P_j \theta_{ij}^2 \left[\left(\frac{\delta P_j}{P_j}\right)^2 + \left(\frac{\delta\theta_{ij}}{\theta_{ij}}\right)^2 \right]^{1/2}$$

$$\approx \left[\left(\frac{\delta P_j}{P_j}\right)^2 + \left(\frac{\delta\theta_{ij}}{\theta_{ij}}\right)^2 \right]^{1/2}$$

in the approximation that each $\frac{1}{2}P_i P_j \theta_{ij}^2 = \langle\frac{1}{2}P_i P_j \theta_{ij}^2\rangle = \frac{M^2}{n(n-1)}$. Since $\langle\theta_{ij}\rangle \approx \sqrt{2}\,\frac{M}{k}$ and $\delta\theta_i \approx \frac{1}{\sqrt{2}}\delta\theta_{ij}$

$$\frac{\delta M}{M} \approx \left[\left(\frac{\delta P_i}{P_j}\right)^2 + \left(\frac{k}{M}\,\frac{\delta\theta_i}{\theta_i}\right)^2 \right]^{1/2}$$

where k is the photon energy. Generally it is easy to have $\delta\theta$ make a smaller contribution to δM than does δP. It is clear then that the requirement on δP is $\frac{\delta P}{P} \lesssim \frac{\delta M}{M}$. So for 25 MeV resolution at 2 GeV, $\frac{\delta\theta}{\theta}$ and $\frac{\delta P}{P}$ should be $\lesssim$ 1% for average momenta. It may be noted in Table VI which will be discussed later that the ~1% requirement has been met for charged particles in this spectrometer. For photons detected by the SLIC, one will not be able to reach the 1% level particularly at low energies since at best, $\frac{\delta E}{E} \simeq \frac{8}{\sqrt{E}} \simeq 1.7\%$ at 22 GeV. Thus, final states with π°'s will have somewhat worse mass resolution. Table V gives examples of δM for a variety of conditions. The resolutions in the Table are given for the case where there is either a recoil particle or one can project several forward particles to a vertex and substantially improve δP, $\delta\theta$ and therefore δM. When no vertex is available δM is a factor of 1.5 to 2 times worse.

C. Particle Identification and the Overall Length of the Spectrometer

The length of the forward spectrometer is primarily determined by the need to measure the momenta and identify the masses of the secondaries. For momenta of interest the only known technique for mass identification is to use gas Cerenkov counters in conjunction with the magnetic spectrometer. Ideally we would like full particle (π,K,p) identification from the lowest energies to the highest. Below about 5.5 GeV it is impossible at the present time to do this without using gas pressures over 1 atmosphere. In photoproduction experiments

Table V

Monte Carlo Calculation of Forward Mass Resolution

Model (see text)	n_{ch}	K (GeV)	Mass (GeV)	$\frac{\delta M}{M} \times 10^{-4}$	δM (MeV)
1. Lorentz transformed SPEAR e^+e^- data	~4	75	4	.50	20 (34)[*]
		100		59	24 (39)[*]
		140		71	28 (47)[*]
2. Hadronic	6	75	–	56	–
	7	100		64	–
	7	140		80	–
3. Charm Pair	6	75	4 (2+2)	46	9 + 9
			5 (2½+2½)	46	12 + 12
			6 (3+3)	46	14 + 14
			7 (3½+3½)	45	16 + 16
	6	100	4 (2+2)	52	10 + 10
			5 (2½+2½)	52	13 + 13
			6 (3+3)	52	16 + 16
			7 (3½+3½)	52	18 + 18
			9 (4½+4½)	50	23 + 23
	6	140	4 (2+2)	67	13 + 13
			5 (2½+2½)	66	17 + 17
			6 (3+3)	65	20 + 20
			7 (3½+3½)	64	22 + 22

*Examples of resolution for states of 60% charged, 40% neutral are given in parenthesis. This fraction of neutrals causes ~ 70% increase in δM.

it is necessary to keep material in the path of the beam at a minimum. This prohibits use of a pressure vessel. To achieve full π, K, p separation above 5.5 GeV would require three Cerenkov counters. In order to keep the overall spectrometer length under control we have limited to two Cerenkov counters so that K,p separation is in effect only above ~20 GeV.

The number of photoelectrons/cm $\simeq \alpha \sin^2\theta_c$ where α is, in practice, a figure of merit including phototube, window, reflection and gas effects. As described later, α may be as high as 170 for the counters, not including reflections. Since this assumes ideal conditions we have chosen the lengths assuming a more conservative $\alpha = 120$ and have required at least 12 photoelectrons for an ultra-relativisitic particle. The resulting lengths are 3.25 meters and 7 meters for C1 and C2, respectively. This design yields sufficient numbers of photoelectrons that it may be possible to differentiate particles near threshold from those having higher momenta. The counters will be built in a modular fashion so that the lengths may be extended for higher energy (low index of refraction gasses) or shortened if the designed lengths prove to be more conservative than necessary.

D. Spectrometer Layout

The last three subsections of this report have described the requirements that acceptance, resolution and particle identification make on the spectrometer. One of the strongest

motivations for the two magnet design comes from the typical
secondary particle distribution shown in Fig. 8. Low momentum
secondaries, tending to come out at large angles, require a
large acceptance. This forces the location of the first
magnet to be as close to the target and recoil system as
possible. It also requires that the length of this first
magnet be kept as short as possible in order to keep the
vertical acceptance high without opening the magnet gap
prohibitively wide. The second magnet adds the additional
bending power necessary to get good momentum resolution for
higher momentum particles that do not require as much
acceptance. The position of the second magnet is chosen to
optimize the momentum resolution of high momentum tracks
without compromising their acceptance. Low momentum par-
ticles need not be detected following the full magnetic
bend required for the high momentum particles. As a result,
detector sizes are reduced in the two magnet design. In
addition the two magnet approach lowers power consumption and
makes it possible to install the first drift chamber (D1)
in the fringe field of the first magnet, thereby protecting
it from the problem causing low energy electron soup that
spills out of the target.

The first Cerenkov counter (C1) is located as far up-
stream as possible so it will accept particles down to 5 GeV.
Since there is not enough room for C1 between the magnets,
it is located in and following M2. Sufficient space is left

for reflectors and phototubes between the end of M2 and the
end of C1. The upstream part of C1 protudes through M2 to
meet the length requirement outlined earlier. C2 immediately
follows a small gap for drift chambers after C1.

Drift chambers are used to measure track positions
because their good resolution allows the use of relatively
low magnet bending power. This in turn permits us to use
the large acceptance magnets we require without making un-
reasonable electrical power demands. As will be discussed
in a separate section below, the drift chamber locations
are motivated primarily by requirements on tracking multi-
particle states.

With the magnet and chamber location of this design
(Table I) the momentum resolution requirements described
earlier can be met with bends of +5kG-m in each magnet.
Table VI lists $\frac{\delta P}{P^2}$ and $\delta\theta$ for this and several other magnet
conditions. The calculations of resolution assume δx =
.0015 m except for D5, the largest chamber, where δx = .0003 m.
Table V gives estimates of the forward mass resolution for
various final state masses, energies and multiplicities.
Both magnets are assumed to have a bend of +5kG-m and the
resolution for photons is assumed to be $\delta E = \pm \frac{8}{\sqrt{E}}$ %,
$\delta x \simeq .5$ cm ($\delta\theta \simeq .3$ mrad) as discussed in the later section
on the SLIC. Shown in Table VI are resolutions both
for the case where no vertex information is available and
for the case where there is at least one other high momentum
charged track so that a vertex fit can be made. The latter

Table VI

Momentum and Angular Resolution for Charged Tracks

Magnet Settings (kG-m)		$\frac{\delta P}{P^2}$ (x10^{-4}GeV^{-1})		$\delta\theta_x$ (mrad)		$\delta\theta_y$ (mrad)	
M1	M2	Hi P	Lo P	Hi P	LoP	Hi P	Lo P
		No vertex used in Fit					
5	5	2.8	20.8	.064	.26	.059	.21
	-5	3.7		.024			
	+10	1.5		.048			
		Vertex used in Fit					
5	5	2.2	8.6	.051	.098	.046	.10
	-5	3.7		.024			
	+10	1.3		.041			

has significantly improved resolution.

As can be seen from Table VI, there is a good deal of flexibility in the choice of magnet conditions. In particular, one can choose between operating the magnets at the same or opposite polarities. Magnets at the same polarity give better momentum resolution. When the magnets are set at opposite polarity, trajectories following the second magnet preserve the original production angle. This reduces ray crossing in the Cerenkov counters and the resulting confusion (see below). It also means that for a fixed hadrometer size the acceptance is larger. Another option is to run M2 at 10 kG-m for improved resolution at a cost of a factor $2\frac{1}{2}$ more power and a loss of some acceptance particularly in the hadrometer. This will be a useful option when experiments require the ultimate in mass resolution. The magnet setting options demonstrate the flexibility of this facility.

E. Magnet Requirements

In order to be specific in this design report, we have assumed except in this subsection, that SCM105 magnets will be used for M1 and M2. In Table VII we outline the minimum dimensional and field requirements for magnets in this spectrometer. These specifications will be used in selecting the magnets to be built or obtained for actual use in the facility. The specifications follow from the resolution and acceptance requirements described in the previous sections

Table VII

Magnet Requirements

	M1	M2
Bending Power	$\gtrsim$ 12 kG-m	$\gtrsim$ 12 kG-m
Gap - vertical	$\geq$ 30"	$\gtrsim$ 30"
Gap - length (including coils)	$\leq$ 48"	$\leq$ 60"
Gap - width	$\geq$ 40" (good field)	$\geq$ 75"(aperture, $\geq$ 40"(good field)

and do not require further explanation except for the
following points. The bending power requirement is ~ 12
kG-m per magnet in order to accommodate higher energy
experiments although we anticipate needing only 5 kG-m
bends at first. The maximum gap length of M1 is determined
by the vertical acceptance requirement. Thus, if the gap
height is > 30", the length could be correspondingly > 48".
Finally, the large horizontal acceptance requirement for
M2 allows 5 GeV particles to be detected in the first
Cerenkov counter. If new magnets are fabricated, the field
should be as uniform as reasonable cost will allow. This
would premit possible simple on-line track reconstruction.

F. Track Reconstruction Considerations and Location of

Drift Chambers

The location and orientation of the drift chambers must
meet certain goals and at the same time satisfy a number of
constraints. First, let us consider some of the constraints.

In order to take advantage of the large solid angle
provided by the two magnet system, it is necessary that the
liquid hydrogen target be placed immediately upstream of the
first magnet. Therefore, little or no field free region is
available in which to place a drift chamber. At the same
time, it is necessary to shield the first set of chambers
from the large number of highly ionizing low energy charged
particles produced in the target. These chambers must there-
fore be placed in the magnetic field of the first magnet.
On the other hand, the best momentum resolution is obtained

by placing the chambers as far upstream as possible. The
position of this set of chambers must, as a result, be a
compromise between chamber HV, current, magnetic field
uniformity, and momentum resolution. They will be located
far enough into the gap of the first magnet so that a charged
particle will have to traverse .25 kG-m before the first
chamber. Hence, no particle with $p \lesssim 5$ MeV will penetrate
to the chambers.

An additional constraint is imposed by the Cerenkov
counters. Particle identification requires that most of the
available drift space behind the second magnet be dedicated
to Cerenkov counters. Only a short distance along the beam
between C1 and C2 may be occupied.

It must be possible to make a complete measurement,
including momentum determination, on low momentum tracks
before the second magnet. To this end we place a second
set of chambers at the middle of M1. A third set is located
in the drift space between M1 and M2. In order to complete
the measurement with good resolution for high momentum tracks,
two sets of chambers are added after M2. The first is placed
between C1 and C2; the second follows C2. We have thus
arrived at a system containing five sets of chambers as
indicated in Fig. 1.

When specifying the number of planes and their wire
orientation in each set, it is necessary to keep in mind that
the system must have good multitrack capability and must
therefore have a high level of redundancy. Track coordinates

must be measured more often than geometry or resolution would require with the understanding that background tracks and coordinate degeneracies will cause the loss of some measurements. In addition, the left-right ambiguity inherent in drift chambers must be resolved. Finally, the chamber locations and wire orientations must be chosen so as to minimize computing time. This is especially pertinent to the track matching problem from one chamber module to another when it is necessary to trace rays through inhomogeneous magnetic fields.

In order to achieve the goals outlined above we have adopted the philosophy that each chamber module should simultaneously measure position as well as angles while at the same time resolving multitrack and left-right ambiguities. This philosophy allows tracking each module independently and reduces the overall spectrometer tracking problem to that of matching track segments between modules. This approach will minimize computing time and the problems of track matching in a multitrack event.

We consider now the question of left-right ambiguity resolution. For a multitrack spectrometer the best way to solve this problem is to stagger successive chambers by one-half cell. Good multitrack efficiency requires that many chambers be placed along the track to achieve a high level of redundancy. In addition the measurement of angle at each drift chamber location requires extra chambers. These three requirements are compatible and can be met by

the same set of planes. In the simplest case, that of straight tracks at normal incidence, only two chambers offset by one-half cell are required for left-right ambiguity resolution. However, when large angles of incidence are encountered, at least three chambers (four in a magnetic field) are required to establish the correct solution. Outside the magnets there will therefore be three chambers with each wire orientation in each module. These three chambers are spaced along z sufficiently far so that the angle is also determined at each module.

The chambers in the first magnet must deal with circular tracks in the horizontal plane. For tracking purposes, these circles must be over-determined. Since any three points determine a circle, we must therefore have at least four chambers with each wire orientation. It is then possible in a single view to uniquely assign hits to tracks. We consider all the chambers in M1 (D1 and D2) as a single set of chambers which are tracked together. D1 will have one chamber at each wire orientation and D2 will have three at each orientation.

There are several considerations in choosing wire orientations: 1) It must be possible to build reliable chambers. For this reason we have decided not to build chambers with horizontal wires (Y readout) which would be excessively long. The longest sense wire is therefore 2.25 m at D5 and only 1.12 m elsewhere. 2) The tracking algorithm

should be relatively simple and the chambers should allow
some flexibility in choosing the tracking philosophy.

3) Wire orientation should optimize those position measure-
ments that most affect mass resolution.

These requirements taken together lead us to three wire
orientations which provide small angle stereo in the bend
plane. These are vertical wires (x coordinate), wires
rotated clockwise about the beam by 14.04° (u), and wires
rotated counter-clockwise by 14.04° (v). The small angle
stereo gives the best possible determination of the angle
in the bend plane. The projected resolution in the non-bend
plane is worse by only a factor of ~ 4. The measurement of
θ_y is still sufficiently good so that momentum resolution
dominates the mass resolution.

D2 and D3 therefore have three x chambers, three u chambers
and three v chambers. D1 and D2 together have four chambers
at each orientation as discussed above. D5 is used for
additional tracking information in the bend plane and to
improve momentum resolution. Multitrack ambiguities and the
measurement of θ_y can be resolved with D4 so that u and v
chambers are not necessary. Therefore at D5 there are two
x planes and no u or v chambers.

G. Cell Sizes

When there is more than one track in a given cell or
strip of the drift chambers, Cerenkov counters or SLIC, there
will be some confusion in reconstructing the event. Simply

adding more cells to deal with this problem can be a very expensive matter. In order to be able to optimize cell locations and make efficient decisions on the total number of cells required per detector, we have studied predictions of particle distributions in these detectors. Two techniques were used. The $\frac{dN}{dcos\theta\ dp}$ distribution obtained by Lorentz transforming SPEAR x dependence data at 4 GeV was used to calculate the cell sizes at different locations in each detector that correspond to a given probability (f) per event that more than one track goes into any cell. As a cross check, a Monte Carlo program was run for the three different production models described earlier. There was agreement between all calculations in direct comparisons. The Monte Carlo was used mainly to study distributions and cell boundary effects in the Cerenkov counters.

For the drift chambers we have chosen cell sizes that correspond to f $\lesssim$ 10% except within 1" of the beam in D1 and D2 where f $\simeq$ 20%. This means that no more than 10% of events will have some confusion in each bank of drift chambers. This will result in a total of $\lesssim$ 2000 wires which is a financially reasonable number. The confusion for two tracks in a drift cell of a single plane results from the fact that only the track nearest the sense wire will register the proper location. However, in the forward direction one can use information from the offset twin to the drift plane to resolve this problem and determine the position of the

second track. In such cases one loses the fast timing
information for the particular cell that can normally be
obtained by summing the times from the offset planes (t_L + t_R).
The cell size calculations indicate, as one would expect,
that cell sizes can be larger further away from the beam.
We have chosen four standard cell sizes (6 mm, 1.8, 4.8, 10 cm).
The distribution of these cell sizes for each chamber location
is listed in Table VIII.

The SLIC is located so far from the target that confusion
is not a serious problem. Cell sizes of 1.25" (3.18 cm)
near the beam and 2.5" further out (as shown in Fig. 22,
Sec. VIII C) will result in f $\lesssim$ 1% everywhere. The smaller
cells near the beam are motivated by the need for better θ
resolution for small angles. As will be described later,
the shower distribution in neighboring cells is normally
used to obtain position resolution far more precise than the
cell size. The maximum cell size is chosen so that it will
not contain a whole shower. Otherwise, there would not be
shower sharing information available to get good position
resolution. Confusion results when there are two tracks in
a cell because it then becomes impossible to determine more
than the precise location of the energy weighted average of
the two tracks. The photon pair from π^o decay will go into
different cells and not be confused. Even at an energy as
high as 60 GeV the γ opening angle ($\theta > 2\frac{m_\pi}{E}$) leads to a
separation of $\gtrsim$ 9 cm.

Table VIII

Module	Dimensions Hor. Vert.	Coordinate	No. Planes	No. Wires Per Plane	Distribution				Total Wires Per Module
					6mm	1.8cm	4.8cm	10cm	
D1	70.8 x 56cm²	X	1	42	24	10	8	—	126
		U	1	42	24	10	8	—	
		V	1	42	24	10	8	—	
D2	90 x 65cm²	X	3	46	24	10	12	—	414
		U	3	46	24	10	12	—	
		V	3	46	24	10	12	—	
D3	177.2 x 120cm²	X	3	76	30	14	28	—	672
		U	3	76	30	14	28	—	
		V	3	76	30	14	28	—	
D4	229.2 x 125cm²	X	3	64	—	26	38	—	576
		U	3	64	—	26	38	—	
		V	3	64	—	26	38	—	
D5	420 x 250cm²	X	2	42	—	—	—	42	84
			32						1,872

The size of the Cerenkov light cone is an approximate lower limit on the size of Cerenkov counter cells in the central region. For this reason (as well as considerations of cost) the Cerenkov counters cannot have quite the small cell sizes of the SLIC or drift chambers. On the other hand only a fraction of charged tracks give Cerenkov signals. Furthermore, the Cerenkov cells are rectangular rather than strips. As a result, the fraction of confused events is comparable to the other detectors.

The two Cerenkov counters will each have 20 mirrors. The size of these mirrors increases with distance from the beam so that each mirror has approximately the same probability (1/20) of being hit by a secondary particle. With this design the probability of an event having two hits in the same mirror is

$$f = \sum_{i=1}^{n-1} i/20 = \frac{(n)(n-1)}{40} ,$$

where n is the number of particles which are fast enough to give Cerenkov light. For the processes simulated in our Monte Carlo studies we find $n \simeq 2\text{-}4$, so $f \simeq 0.05 - 0.30$.

A particle which is directed to one mirror may give Cerenkov light which hits another mirror. This "cross-talk" increases f, but only slightly. (See later discussion in this section.)

The particular arrangement of Cerenkov counters and magnets shown in Fig. 1 has been analyzed with a Monte Carlo

program using various particle production models which were described in subsection A. The results for the various models are similar to each other. Here we discuss in detail results from only the model which assumes a 100-GeV γ ray is diffractively excited into a $(c\bar{c})$ state. Each charmed particle decays into $K\pi\pi$ yielding a multiplicity of 6 charged particles. In Fig. 9 we present the average multiplicity (where the generated multiplicity is 6 particles) of particles that give Cerenkov light. On the average 1 of the 2 kaons and 3 of the 4 pions triggers C1 while 2.5 of the 4 pions and hardly any of the kaons triggers C2. This allows for a very clean separation of pions and kaons.

In Fig. 10 and 11 we show the x-y distribution of the particles that are above threshold for Cerenkov light for two Monte Carlo models. Superimposed are the dimensions of the individual mirrors of the Cerenkov counters C_1 and C_2.

The sizes of the individual mirrors are chosen so that the probability of any one mirror being penetrated by a particle above threshold is approximately 1/20. Thus the mirrors closest to the beam are the smallest. With the indicated mirror segmentation, the correct particle identification can be made in 90% of the events. In the remaining 10%, light from a pion going to or near a Cerenkov cell in which there is a kaon leads to the kaon being misidentified.
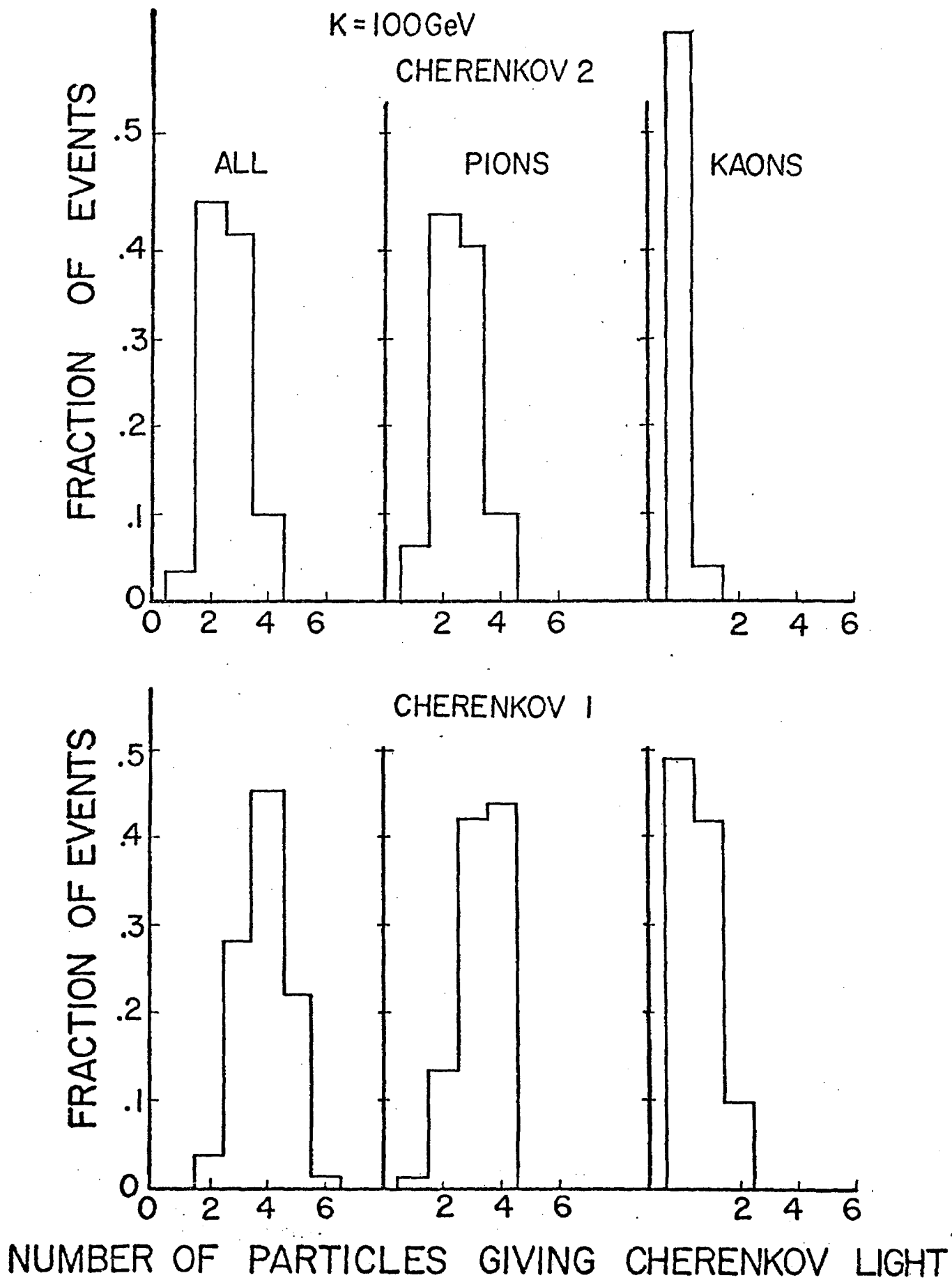
Figure 9

Fig. 10

C, Mirror Segmentation
and Monte Carlo x-y Distribution

12,000 events

Fig 11

C₂ Mirror Segmentation
and Monte Carlo x-y Distribution

y (cm) →

x-axis (cm): -200 -160 -120 -80 -40 0 40 80 120 160 200
y-axis (cm): 80 40 0

400		1900		800		300	
1000		2700	2100 1500	1800		500	

0	10	41	75	150	310	600	1000	1500	510	370	170	80	25	5	1	0
0	1	27	64	120	210	420	650	930	490	460	250	110	49	16	9	0	0
2	11	37	78	150	250	380	440	250	290	130	54	28	5	1	2	1
0	4	15	37	55	120	200	230	81	70	38	27	16	5	0	1	1
0	2	12	30	56	73	90	29	10	16	12	6	1	0			
0	4	8	19	17	8	3	6	5	1	1						
		0	19	17	1	1	1									
			0	1												
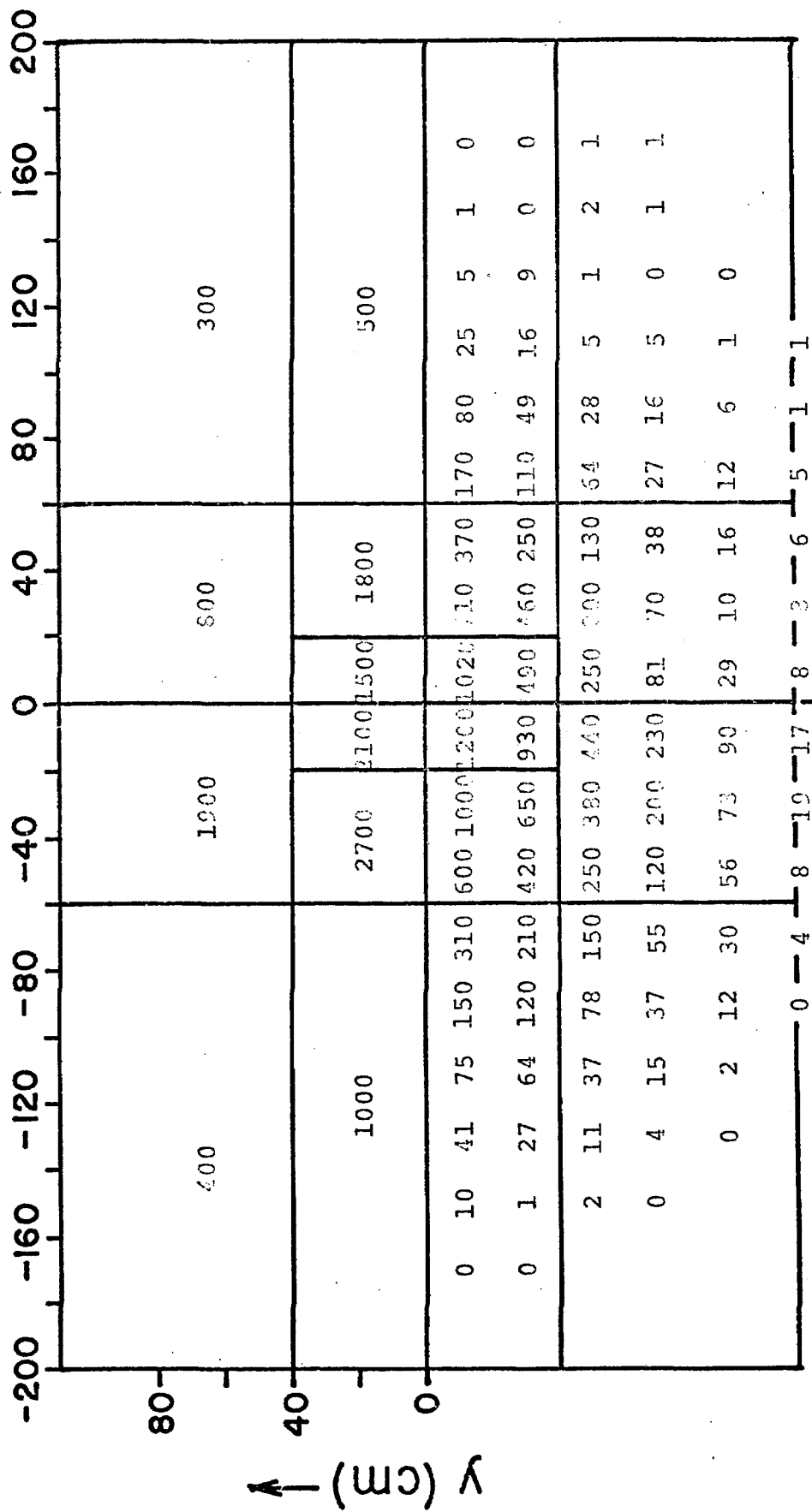
K = 100 GeV   ← DD̄ model (n_ch =6)   Lorentz transformed SPEAR model →

IV. Triggers

Triggering of photoproduction experiments can be done in a
two step process that allows very sophisticated selection. A
fast trigger using conventional logic will trigger on every
hadronic interaction and reject pair production. At the highest
luminosities being considered in this report the rate of hadronic
triggers will be ~ 6000/sec. That means that an average processing
time as long as about 10 μsec can be used to define a higher level
sophisticated trigger without causing deadtime greater than 6%.
Several higher level triggers will be described below. They will
be used initially to reduce the data taking rate from a few
thousand/second events containing all of photoproduction to 100-
200 events. The reduced data sample will be significantly enriched
with charm and hidden charm particles. This will mean that off-
line computer analysis will be simplified, thereby reducing com-
puter time and, most important, reducing the delay between data
taking and preliminary analysis results. The latter, we feel, is
crucial to being able to run experiments on this facility with
the flexibility and feedback of a small experiment. It is this
kind of closeness to the physics that is required to make this a
powerful facility. A two step trigger can also be used for exper-
iments with a hadron beam by defining a simple ~ 5K/sec fast trigger
and using a trigger processor like that discussed below to define
a selective higher level trigger.

A. Fast Trigger

The fast trigger is a coincidence of a "Tag" signal

from the tagging system and a signal indicating the presence
of a hadronic event in the spectrometer. A hadronic event
is identified by requiring a signal above threshold in either
the SLIC or hadrometer and no large signal in the pair portion
of the SLIC (horizontal strips in the beam plane) or in the
central shower counter (C) in the beam. To increase the
acceptance for this trigger (and for all γ measurements) in
the vertical direction, two lead scintillator shower counters,
above and below the beam, will be located just in front of
the downstream magnet. A large signal or a coincidence indi-
cating a minimum ionizing particle in these counters would
also give a hadronic trigger.

B. High Level Triggers

As will be seen from the discussion in the next section
on the trigger processor, the potential capability of proces-
sors based on available electronic technology is extremely
powerful. However, we feel it necessary to be cautious at
implementing this technology so that we can be sure that
the total facility system will turn on in an organized fashion
as early as summer 1978. To this end we have given clearly
defined priorities - an order of attack - to the high level
triggers we plan. The recoil system will be used in the
first high level triggers. We will select out events with
a single proton recoil and then compute the missing mass,
triggering when the mass is in a prespecified range. A
first look at a detailed processor algorithm to accomplish

this is outlined in the next section. For example, the
mass range $2.5 < M_x < 9$ GeV could be selected by the
processor. We can make an estimate of what fraction of
the total cross section this trigger will be by comparing
the relevant photoproduction channels with those measured
in the pp $\rightarrow$ pX inclusive scattering experiment of P. and
J. Franzini et al.[5] The fraction of events with a single
recoil proton will be about .35. Of these about .37 will
fall in the mass range selected and about .78 will have
$|t| \geq .04$ GeV^2. This trigger, therefore, will take about
10% of all hadronic events. Similar estimates suggest
that charm states will appear in as many as 20% of the
triggered events.

Pair production of charmed particles will lead to
multiparticle final states. The combination of the fast
hadronic trigger plus the recoil proton missing mass
processor yields a reasonably unbiased trigger for enriching
pair production of charmed particles. However, at the
highest luminosities to be expected after the spectrometer
has been brought into routine operation, the trigger rate
will be several times higher than the high data handling
capability of this facility. Thus, after exploratory studies
using the recoil trigger have been made, additional higher
level triggers must be implemented. These will probably
be biased towards some aspect of charmed particle production,
which is expected either on theoretical grounds, or empiri-
cally determined from the exploratory runs or from other

experimental results then available. In the following,
we outline considerations on various high level triggers
that involve the various forward detectors.

The purely two body decay modes of charmed states
will generally be small. Therefore, a high multiplicity of
charged and neutral particles is expected. However, the
average multiplicity of 100 GeV/c hadronic photon interac-
tions is also large, around six. Thus, multiplicity selec-
tion will only be useful in special cases such as for the
η_c discussed below. Charmed particle decays will, it is
believed, often lead to a final state involving strange
particles, such as $K^\pm$, K^O_S, K^O_L, Λ, $\bar{\Lambda}$, etc. A unique signa-
ture not yet exploited is that of a hadronic final state
which does not conserve strangeness. However, the identi-
fication of the strangeness of all of the final state
particles is difficult, and can be made only in some small
fraction of the events. This does not lend itself, per se,
to an on-line trigger, although it might be an interesting
one to pursue off-line.

Pair production of charmed baryons will lead to final
states involving a baryon-antibaryon pair. Any other process
which leads to such a pair will also be unusual and physically
interesting. Thus identification of one or more strange
particles or of a baryon (or antibaryon) in the forward
spectrometer will lead to useful, specific, although biased

triggers. These can be built into one or more trigger
processors, although in some cases they may be simple enough
to be easily implemented in standard fast logic.

The above considerations suggest that the following
particle pattern identification should be implemented in
the first high level triggers involving the forward detectors.

1. Charged particles: $K^{\pm}$ and $p^{\pm}$. Some of these are
   identifiable by the Cerenkov counters. A "not-a-
   pion" trigger in general requires some knowledge
   of the momentum of the particle.

2. Neutral particles, mostly K_L^O and n. These will
   interact in the hadrometer and be useful directly
   in the trigger.

3. "Vees", i.e., $K_S^O \to \pi^+\pi^-$ and Λ, $\bar{\Lambda} \to p^{\pm}\pi^{\pm}$, where the
   decays occur in the drift space of the spectrometer.
   (Neutral decays of vees will be seen in the SLIC
   and the hadrometer, as in 2. above.) Detection of
   vees on-line in the trigger can in principle be
   detected by a change in the multiplicity of particles,
   as seen in the various downstream detectors. In
   this spectrometer, the drift chamber modules are,
   of necessity, widely spaced out. The effective
   solid angles subtended by each module differ because
   of this spacing and because of the magnetic field

regions. Thus apparent multiplicity changes occur when none is present. However, with careful consideration, a useful change of multiplicity trigger may be realized. A 15-50 GeV K_S or $\Lambda(\bar{\Lambda})$ has mean decay length ranging from one to three meters. At 15 GeV, about 20 percent of such vees will decay in the region of the D1, D2, D3 modules, while at $\gtrsim 40$ GeV some 30 percent will decay in the D3-D4 and/or D4-D5 region. Vees can also be detected off-line by reconstructing vertices which do not occur near the interaction point in the target, e.g., vertices in the drift spaces. It is unknown whether an on-line trigger processor can be realized to perform this function. Finally, although the overall acceptance of a vee trigger may be of the order of 10 percent of all K_S^O and $\Lambda(\bar{\Lambda})$, such events are extremely useful and interesting.

Although the maximum transverse momentum of the decay products from charmed particles is large, the large average multiplicity results in an average transverse momentum per particle which is not much higher than the normal hadronic value (about 0.3-0.4 GeV). However, a selective trigger based on high transverse momentum, or a large longitudinal momentum of one or more particles might be useful. The hadrometer could provide this information for both charged and neutral particles.

The above considerations lead us to specify that the

following information be available in approximately one

microsecond for use by the next level of trigger-processors:

1. D_i cell bits

2. Cerenkov cell bits

3. SLIC large pulse height bits defined by discriminator
    thresholds (say one high, one low)

4. Hadrometer large pulse height bits.

From this information, multiplicity, change of multi-

plicity, particle identification, neutral kaon or neutron

detection, and large transverse or longitudinal momenta can,

in principle,be determined and used by a trigger processor

to enhance charmed pair production.

Although hadronic decays of charmed particles dominate

the decay process, leptonic final states need not be ignored.

Much of the above can be used to construct leptonic triggers

also, since the SLIC can detect electrons. In addition,

there will be muon counters buried in iron shielding behind

the hadrometer.

Primakoff production of the η_c is a very important

process to be found and measured. Here the cross section is

several orders of magnitude below that of charmed pairs.

The highest luminosities and a more highly selective trigger

will be required, although a preliminary search may well be

carried out with a "no-recoil" trigger. The η_c, with $I^G J^P =$

$0^+ 0^-$ and an expected mass value near 3 GeV, will have many

multiparticle decay modes. It is produced singly with all

the energy of the beam ($\gamma\gamma \rightarrow \eta_c$) and very forward, with no recoil emerging from the target. The recoil detector can be used as a veto, but no missing mass will be available.

Strict two body decays of the η_c are expected to be very small (e.g., $\gamma\gamma$, $\bar{p}p$, $\Lambda\bar{\Lambda}$..., < 1%). Decays like 2π, $2K$ are excluded by spin and parity, Decays like 3π, 5π... are suppressed by G parity (hadronic decays will dominate over electromagnetic ones). Numerous final states, like 4π, 6π,..., $K\bar{K}\pi$, $K\bar{K}2\pi$,...$\eta 2\pi$, $\eta'2\pi$... are available, and all will proceed with reasonable branching ratios. Since the cross section for η_c production is so small, one must find a trigger that accepts a significant fraction of the η_c final states. Note that a large fraction of these decay modes involve two charged particles plus several gammas (from π^o decay or direct emission). Thus it will be possible to have a crude trigger for η_c based on 2 and only 2 charged particles and an energy sum of all forward particles equal to that of the incident photons. This will require the following:

1. Charged multiplicity (available from D_i cell bits provided for in the earlier discussion)

2. Energy and angle which can be obtained from the SLIC and hadrometer if fast ADC conversion of the pulse heights can be available for the hit elements in approximately one microsecond. (Whether the high and low pulse height bits,

previously described in the discussion on charmed
pairs, can provide a reasonable η_c trigger will
have to be studied carefully.)

Fast reconstruction of forward mass can be accomplished
if item 2 listed above is available. The forward mass is:

$$M_F^2 = \sum_{ij} \frac{1}{2} P_i P_j \theta_{ij}^2$$

$$= \sum_{ij} P_i^x P_j^x (\theta_i^x - \theta_j^x)^2 + \sum_{kl} P_k^y P_l^y (\theta_k^y - \theta_l^y)^2$$

where $P_i^x \simeq P_i^y \simeq 1/2 \, P_i$ are the energy deposited by a
track in the x or y strips of the hadrometer and/or SLIC.
The mass resolution will be dominated by the hadrometer
resolution and will be $\sim .15 \, M_F$ which is adequate for
triggering purposes.

For the η_c, a narrow cut, say $2 < M_F < 4$ GeV added to the
charged multiplicity and p_T cuts would lead to a very good
η_c trigger. In addition, relaxation of the charged multi-
plicity requirement might be made, further improving the
acceptance of the trigger for η_c.

In addition, a tighter trigger for η_c could be made if
fast TDC readout of the drift modules was available. This
might allow momentum reconstruction of forward charged tracks
on-line in a trigger processor. Thus good mass resolution
on the forward mass would be available, resulting in a tighter
cut about the η_c mass.

The possibilities that are opened up by having forward track reconstruction available for the trigger are impressive. Accurate mass and $P_\perp$ triggers that are not dependent on poor resolution hadrometers will be very important. Better Cerenkov identification using momentum will be possible. Also possible will be detection of kinks in tracks indicating Λ° or hyperon decays that will be valuable as triggers. For simple final states, one or two bodies, it will not be difficult to perform fast reconstruction. On the other hand, reconstruction of multiparticle states will require the experience gained from off-line reconstruction work. For this reason we do not expect this type of information to be available for triggers for some time (1-2 years) after the facility starts up.

As higher energy photons become available, pair production of new heavy lepton states may become accessible. Many of the pieces of information made available above and the trigger processors (or modifications of them), will make triggers on heavy leptons possible.

V. Trigger Processor

The trigger processor will take advantage of the present day low prices for large amounts of memory with access times of 30 nsec or faster as well as fast arithmetic logic chips. It will be essentially a hard wired parallel processor possibly in association with a fast sequential instruction processor like that designed by T. Droege for Fermilab Experiment 400.

We will describe here a first look at a detailed conceptual design of this device by looking specifically at how the recoil missing mass trigger will be handled. We fully expect that this design will undergo extensive development as we continue to study and optimize it. For the present it will give some idea of the capabilities of and the techniques to be used in the final system.

In order to select single proton recoils the trigger must reject neutrals (from $n\pi^+$ or $p\pi^0$ states, for example) and charged pions (from $n\pi^+$). In addition the processor must reject events with several tracks at the first interaction ($p\pi^+\pi^-$, etc.) without rejecting good events in which a secondary interacts and produces additional recoil tracks. These excited proton states comprise about 2/3 of all hadronic events so that reasonably good rejection of them is necessary for a clean trigger. On the other hand, the rejection need not attain the levels possible in off-line analysis. Refer to Sections II and VI and Figures 3 and 4 for more detailed discription of the recoil system and its capabilities.

The processor will make frequent use of parallel table lookups to evaluate functions such as the missing mass function of θ, E, and k. On a smaller scale this approach was used previously in Experiment 321 by P. Franzini who suggested it to us. Table IX shows the organization of a memory made up (as an example) of 128 Fairchild 10415A 1024 x1 bit bipolar ECL RAMs.

Table IX

Memory Organization for Table Lookup Functions

Description	Function/#Bits		Organization
Neutral Veto	$NV_i \leftarrow NV\ (A_i, B_i, C_i, D_i)$ $i = 1,\ 15$		$15 - 16 \times 1$
	A_i, B_i, C_i, D_i	1 bit ea.	
	NV_i	1 bit	
	(N_v is same for all i)		
Unit conversion $z_{PWC} \rightarrow z_{timing}$	$TZ \leftarrow Z\ (Z_{PWC})$		$1 - 256 \times 4$
	Z_{PWC}	8 bits	
	TZ	4 bits	
Missing Mass Criterion	$MMC \leftarrow MMC\ (\theta,\ E,\ K)$		$64 - 1024 \times 1$
	$\theta,\ E$	6 bits ea.	
	k	4 bits	
Proton Criterion, each scintillator segment function of θ.	$PC_j \leftarrow PC\ (I_j,\ \theta)$ $j = 1,\ 4$		$16 - 1024 \times 1$
	I_j	8 bits	
	θ	4 bits	
	PC_j	1 bit	
	(PC is different for each j)		
Proton criterion selection as function of energy and θ.	$PCS \leftarrow PCS\ (PC_j,\ E,\ \theta)$ $j = 1,\ 4$		$4 - 1024 \times 1$
	PC_j	1 bit ea.	
	E	6 bits	
	θ	4 bits	

	Total			
	$84 - 1024 \times 1$		$84 - 1024 \times 1$	
	$15 - 16 \times 1$	**or**	$15 - 1024 \times 1$	
	$1 - 256 \times 4$		$4 - 1024 \times 1$	
			$103 - 1024 \times 1$	
		Spare	$25 - 1024 \times 1$	
		Total	$128 - 1024 \times 1$	

Each of these chips has a 20 nsec access time. The total cost of this memory (as of May 1, 1977) is $2330, about equal to 3 commercial coincidence modules. This memory will,in general, be used for two parameter lookup functions with the answer being a single bit. It will be possible to load the memory in a block transfer from the on-line computer and to read it back for verification and testing. This will allow flexibility in use of the trigger processor and will be essential during debugging. As can be seen from Table IX, even this relatively cheap amount of memory is not nearly filled up by the recoil missing mass trigger requirements.

We now outline an algorithm that at the very least demonstrates that this trigger can be processed easily in the 5-10 μsec that will be available. We start with two operations performed in parallel:

1. Data from the cylindrical PWC's will appear as a list of number pairs corresponding to the last wire address of a cluster and the cluster spread. These numbers will read out from upstream to downstream.

    The cluster address

    $$z_i = (Cluster)_i - (Spread)_i/2$$

    is computed by dropping the lowest order spread bit and subtracting the remaining 2 bits from the cluster last wire address. At least three such subtractions will be performed in parallel. (This operation may in fact be handled by the arithmetic unit of the PWC system

2. Identification of neutral patterns. The scintillator dynode signals will be discriminated and a bit latched for each pulse height that is above a threshold. The bits will be organized in groups of four (A_i, B_i, C_i, D_i). These groups will be used to address 15 sections of memory, each initially containing the 16 bits shown in Table X. A 1 bit is found in memory for the A, B, C, D bit patterns that correspond to a π^0 or n interaction in one of the scintillator sections. The 15 groups of $(A_i B_i C_i D_i)$ address the memory in parallel and a bit (NV) is set to 1 if any group corresponds to a neutral interaction pattern. This will in most cases be used as a veto to the recoil trigger, since the missing mass only is meaningful for single proton recoils. (There will be about a 10% loss of good triggers from secondary interactions producing neutrals in the recoil system.) The patterns stored in memory will be modified from those in Table X if experience teaches us that a different set of patterns is more appropriate. The total amount of time to cycle through the 15 sectors is ~ 15 x 20 nsec $\simeq$ 300 nsec. This veto will therefore be available ahead of the more complicated processing of tracks (described below) that will go on simultaneously. (In simpler form this operation may well be first implemented in conventional fast logic or in the matrix logic of a register logic system.)

Table X
Neutral Recoil Veto Patterns

Address	Contents of Memory
A B C D	
0 0 0 0	0
1 0 0 0	0
0 1 0 0	1
1 1 0 0	0
0 0 1 0	1
1 0 1 0	1
0 1 1 0	1
1 1 1 0	0
0 0 0 1	1
1 0 0 1	1
0 1 0 1	1
1 1 0 1	1
0 0 1 1	1
1 0 1 1	1
0 1 1 1	1
1 1 1 1	0

3. As soon as the Z_i are available from operation 1,
    the processor will start to determine PWC track parameters.
    In an ideal situation of a single proton track there will
    be 3 Z_i with $Z_3 - Z_2 = Z_2 - Z_1$. (As described in Section
    VI, the concentric wires of the three PWC's at one Z
    location are tied together into one amplifier.) In many
    cases the problem will be complicated by one or more of
    three effects: a) secondary particle interaction that
    results in recoil tracks that cross the primary recoil;
    b) multiparticle recoils at the primary vertex ($P\pi^+\pi^-$,
    for example) that are in most cases to be rejected for
    M_x calculations; c) δ rays which may add a cluster any-
    where in the inner chamber. To deal with this the processor
    will be wired to perform a three-nested do loop which we
    describe below in fractured Fortran. In this, L is the
    number of clusters and is read in from the PWC electronics.
    The δ's are parameters which may be varied from the on-line
    computer.

$$DO \quad 1 \quad I = 1, \ L-2$$

$$DO \quad 1 \quad J = I+1, \ L-1$$

$$\theta_A = Z(J) - Z(I)$$

$$DO \quad 1 \quad K = J+1, \ L$$

$$\theta_B = Z(K) - Z(J)$$

$$IF \ (|\theta_A - \theta_B| > \delta_1) \ GO \ TO \ 1 \qquad \text{(no track)}$$

STORE I,K and increment track count N

$$V(N) = Z(I) - \theta_A/2 \quad \text{Vertex, since target to}$$

inner ring $\simeq 1/2$ ring to ring distance.

IF (N = 1) STORE V(1) and GO TO 1

IF ($|V(N) - V(1)| > \delta_2$) GO TO 1

SET "more than 1 track at first vertex" bit

and exit loops.

1 Continue

IF (NO TRACK). . . .

$$\theta = \theta_A + \theta_B$$

4. The next step is to find the A,B,C,D scintillator segments that correspond to the wire chamber track. This is done by finding a ϕ sector i with end to end timing information corresponding to a location sufficiently close to Z(K), the outer chamber coordinate. The difference between pulse times at each end of the scintillators in the inner ring (A_i) will be digitized by 15 4 bit TDC's, T(I). This measures the Z location of the track in ϕ segment i to $\pm \sim 6$ cm. The outer chamber coordinate, Z(K), is converted to time units (TZ) by an 8 bit to 4 bit lookup. The memory will be loaded with data based on calibration studies of the end to end timing of the inner scintillator segments. Then the following search is performed:

DO 2 M = 1,15

IF ($|TZ - T(M)| < \delta_3$) GO TO 3

2 CONTINUE

GO TO "NO MATCH"

3 STORE M

The appropriate energy is

$$E = A(M) + B(M) + C(M) + D(M)$$

The following two operations are performed simultaneously.

5. Look up E vs θ in memory (see Table IX). If the location has a 1 then M_x is greater than a threshold or is in a range selected at the time the memory was loaded from the on-line computer. There will be up to 16 different E vs θ tables in memory corresponding to different tagging system bins of photon energy K and the appropriate table will be used. The tagging bins are latches set by the overlap of the hodoscopes in front of the tagging shower counters. This information is available immediately and is transmitted as a 16 bit word to the processor.

6. Determining whether the track is a $\pi^{\pm}$ or p is a two step process. The threshold for protons at sufficiently high energy E in each sector is a function of θ. This is determined first by four parallel lookups $I_j(M)$ vs θ (where $I_1 = A$, $I_2 = B$, etc) which set four bits (PC_j) which indicate pulses above proton threshold. Another lookup of PC_j vs E for 16 values of θ will provide a bit if the event corresponds to an acceptable proton pattern.

Typically, at the end of these operations, a NIM level will be set if the M_x criterion (above 2.5 GeV, for example) is met, the proton bit is set, and neither the neutral veto bit

nor the "greater than one track at the first vertex" bit

is set.

We can now estimate how long these operations will take:

Read in (including operation 1)
  faster than   1000 nsec

Operation 2 is parallel to
  operation 3   0 nsec

Operation 3:
  Simple case of single proton,
  no other hits, is 1 full cycle
  of do loop and will take ~ 350
  nsec. The average case of 5
  clusters with 1-2 tracks takes
  ~ 8½ short cycles (150 nsec
  each) and ~ 1½ full cycles: Average 1800 nsec
  Worst case, which may happen
  3% of the time is a $p\pi^+\pi^-$
  recoil from a secondary inter-
  action which crosses the
  primary proton recoil, needs
  about 55 short cycles and 2
  long cycles.
  Total worst case: 9000 nsec

Operation 4:
  Average of 7 cycles, 20 nsec
  each, of a sequential processor
  pulse one table lookup.   370 nsec

Operation 7: Two level lookup.   60 nsec

                                   Average total   3.2 µsec

                                   Worst case: 10.4 µsec

The average time is safely below the specified requirement

of 10 µsec.

Other triggers can be handled in a similar way. Most

of the triggers involving the forward spectrometer are,

in fact, less complicated than the recoil trigger we have

just described.

VI. Recoil System

A. *Cylindrical Wire Chambers*

The trajectory of the recoil proton will be measured by three concentric equispaced cylindrical proportional chambers (see Figures 3 and 4) with both anode and cathode readout. Their mass must be as low as possible to minimize both energy loss and multiple scattering. Rapid readout of the chambers is necessary for the fast missing mass trigger. In addition to the recoil proton, background tracks from various sources will be present, and must be properly handled. A design for the chambers within the framework of these constraints is presented below.

The readout HV cathodes, which measure the polar angle, θ, are made from foils consisting of 5 mil Al wire flattened to 1 mil and epoxied onto a mylar sheet at 1 mm spacing (such foils are available from Argonne National Lab). The foils are formed in cylinders so that each cathode wire becomes a circle in a plane perpendicular to the chamber axis. The non-readout cathodes are simply aluminized mylar foils. Two possible constructions are under consideration. The first requires that the foils be free-standing and held under tension by end rings separated by support rods (indicated in Fig. 3). Separate rings are needed for the anode wires, the inner cathode and the outer cathode in each chamber, so a complicated mechanical structure must be built at both ends. However, this type of chamber could have a low mass of .050 - .060 gm/cm^2. In the second

approach, the cathode foils are glued to ¼" NOMEX honeycomb
to form rigid cylinders. The ends of the chamber can be
much simpler, construction details in general are easier
and cheaper, but the mass is ~ .105 gm/cm^2. This is not an
intolerably high mass, so the second method seems preferable.
An additional constraint, which renders the first method less
attractive, is that the downstream end of the inner chamber
must be low mass since it intercepts part of the forward
spectrometer acceptance. However, we are presently designing
and building a 34 cm. radius prototype of the free-standing
chamber in order to understand better the mechanical problems
involved.

The gap between cathodes is ½" and the anode wire spacing
will be as large as possible, up to 5 mm (larger than this
makes the time resolution unacceptable). Any adverse effects
on the induced cathode pulse due to wide anode wire spacing
will be investigated in a small flat test chamber. Because
the anode wires are 2 m long, they must be supported at
three or four locations along their length. For this purpose,
foam rings ¼" square in cross-section will be cemented to
the inner cathode foil.

An integral part of each chamber will be two rigid beams
on either side of the 22.5° bottom access opening along the
full length. These beams will slide or roll on their own
sets of rails along the z direction so that each chamber can
easily be installed or removed for repair.

At lower values of the t acceptance the contribution to the missing mass error from angular resolution in θ is dominated by multiple scattering in the target and chambers. However, at larger t, the measurement error in the chambers is the controlling factor. In order that this not dominate the total missing mass error, θ must be measured to roughly $\pm$ 6 mr.

The measurement error is

$$\delta\theta = \frac{Wg \sin^2 \theta}{\sqrt{3} \, d}$$

where d is the radial distance between the first and third chambers, W is the cathode wire spacing and g is a factor, certainly less than $\sqrt{2}$, which accounts for the degradation in resolution due to the spatial width ($\sim$1 cm) of the induced pulse on the cathode. For the worst case, (g = 1.4, θ = 70°) we require W $\gtrsim$ 3 mm for d = 30 cm and $\delta\theta$ = 6 mr. Thus the cathode wires (1 mm spacing on the foils) can be tied together in groups of three, giving 667 channels per chamber. Since the hits in each chamber are well separated in z (θ = 70° is the largest angle of interest), independent cathode readout for three chambers would be redundant. Therefore, corresponding channels in the 3 chambers will be summed into the same amplifier. Reading out from the upstream end, the first hit then will be from the first chamber, the second hit from the second chamber and the third hit from the third chamber. In this way only 667 channels are needed for the θ measurement.

The azimuthal angle ϕ, of course, does not enter the missing mass calculation. However, for off-line reconstruction of events, and to correct for edge effects in the liquid scintillator cells, a measurement of ϕ to $\pm 1^{\circ}$ will be useful. This means anode wires can be tied together in $\sim 2^{\circ}$ bins, giving a total of 169 ϕ channels. Only one chamber's anode plane need be read out.

As discussed below, an additional 32 channels will be used to sort out background tracks. Therefore, a total of $667 + 169 + 32 = 868$ readout channels are required.

The electronics will be based on a system already built and working for cathode plane readout of a small (64 wires) chamber tested with cosmic rays. In this prototype setup it is assumed that each event has only one cluster of cathode wires to be located. Output from the amplifiers (8 channels/card) and discriminators (8 channels/unit) is fed to two 64 bit priority encoders followed by an arithmetic unit, which calculates and stores the position and width (3 - 5 channels with 3 mm wire grouping) of the cluster within 150 ns of the passage of the particle. Design of a scheme to handle several clusters is underway. It is anticipated that the positions and width of all clusters in the cathode plane can be found and stored in 0.5 - 1.0 μsec. From this information it is a straightforward task for the trigger processor to compute θ, assuming that the first three clusters belong to the recoil proton (see background discussion below).

In the system envisaged, the amplifier cards are positioned as close as possible to the chamber mother-boards in the bottom access space (recall that cathode channels at the same z from the three chambers are summed before the amplifiers - the amplifier cards therefore plug into a grandmother-board which performs the sum). Connections from amplifier to discriminator units, which sit in NIM-like bins (30 units/bin) near the chambers, are made by twisted pairs. Output from the discriminators is strobed by the scintillator trigger into the priority encoder-arithmetic box. This is also located on the experimental floor, so only cluster positions and widths are sent to the counting room; a huge bundle of cabling is thereby eliminated. The anode readout will probably be handled in a parallel, but identical, manner. Cost of the system up to the input of the trigger processor is ~ $30./channel.

Extra tracks in the chambers are possible from four sources: δ rays, low energy pair production and interactions of the secondary hadrons in the target and extra particles from the primary interactions (for example, $p\pi^+\pi^-$ target disassociation).

A crude calculation indicates that in a five prong event, ~ 2 δ rays escape the target. These typically have energy (after escape) of < 0.5 MeV and angle θ < 45°, and so will unlikely reach beyond the first chamber. Furthermore, the z distribution of escaping δ rays increases with distance from the primary interaction vertex as the secondaries spread toward the edge of the target. Thus extra clusters

in the cathode readout from δ rays are most probably down-stream of the three primary clusters from the proton recoil and cause no confusion in the trigger processor.

The background from low energy pairs is an accidentals problem. At the highest beam rates contemplated, there are ~ 5.10^6 photons/sec in the lower part of the bremsstrahlung spectrum, which yield ~ 0.1 pair in the target in the ~ 100 ns resolving time of the chambers. A very rough estimate shows that a conservative upper limit of 10% of these have an electron of low enough energy to scatter at large enough angle to enter the chambers. Thus this background is < 1% and can be ignored.

The most serious background is a second recoil particle from an interaction of one of the secondary particles in the target, which, for a five prong event, occurs with a probability of 0.5. Perhaps 20% of these overlap in z in the chambers, causing confusion in the θ calculation in the trigger processor, unless it is intelligent enough to extract two θ angles from two overlapping sets of three clusters. If we have a dumb trigger processor, ~ 10% of the events are lost. In the remaining two-recoil events there is a θ-ϕ matching ambiguity. This can be resolved for most cases by the trigger processor using end to end timing on the inner fifteen scintillation counters. Another possibility is to provide ~ 10° (to the anode wires) stereo readout on the unused cathode of one chamber. About 32 channels on the inner chamber or 60 channels on the middle

chamber would suffice. We expect to build this option into the chambers. It will be useful *for dealing with events* where the target nucleon breaks up $(p\pi^+\pi^-$, etc.)

All the above assumes noiseless chambers. In the real world the trigger processor will have to be able to recognize and ignore at least some low level of extra clusters from noise. A useful suppression criterion may be the width of the signal clusters.

B. Liquid Scintillator Range Detector

After passing through the cylindrical wire chambers, the recoil particle enters a liquid scintillator range detector. This detector has 15 separate segments in the azimuthal angle ϕ. Each segment subtends approximately 22.5°. The total coverage is over 90% of the full 360°. Every segment in ϕ has four compartments (labelled A_i, B_i, C_i, D_i in Fig. 4) which provide up to four dE/dx samples along the path of the particle. Altogether there are 60 compartments in the liquid scintillator, each having photomultiplier tubes at both ends to ensure efficient light collection. Each tube has one ADC. The innermost 30 tubes have a TDC channel as well for end to end timing which gives $\delta z \simeq \pm 3"$. The liquid scintillator detector is used for a number of on-line and off-line functions.

The total light from a stopping proton in the liquid scintillator measures its kinetic energy. The recoil detector, as seen in Figures 3 and 4, is designed to do this simply and quickly. (The kinetic energy can be

determined from a number of dE/dx measurements as well, but this is a more difficult procedure, as it depends on the recoil angle θ and may require a longer, off-line calculation.) The proton recoil energy, the angle θ and the beam energy k can be used to evaluate the missing mass in the forward arm of the spectrometer. The calculation is quite simple and will be done by the trigger processor (see Section V).

Because the recoil angle θ determines the maximum thickness of liquid scintillator, it also affects the total energy range acceptance, the energy loss per compartment and the probability of a nuclear interaction before the proton stops. These numbers are summarized in Table XI for θ angles of 90°, 45° and 30° (see also Fig. 7 in Section II). But because the signal is read out from both ends of a ϕ segment, to a first approximation the total scintillator signal will be independent of the interaction position along the z axis and the recoil angle θ. After a valid stopping particle trigger has been indicated, the 8 photo-multiplier ADC's for one segment are summed to give the total energy deposited in the liquid. This may have to be corrected slightly (<15%) for the attenuation differences to the opposite ends of the 2.4 m compartments.

The aim is a kinetic energy resolution in the neighborhood of $\frac{\Delta T}{T} \simeq \pm 8\%$ to $\pm 12\%$. As discussed in an earlier section, this range of $\Delta T/T$ provides an acceptable M_x error at masses of 2 to 6 GeV/c^2 and beam energies of 50 to 150 GeV/c.

The $\Delta T/T$ resolution of the recoil detector will be verified with tests on a prototype of one of the segments which is currently under construction.

The missing mass calculation is only valid if there is a single quasi-elastic proton recoil. There are several handles on identifying such events. These include absence of a $\pi^{\pm}$, π^{0} or neutron and counting recoil tracks from the primary vertex. Table XI shows a 0.53 probability that a photon will convert in 57 cm of liquid scintillator. A π^{0} will then have a probability of 0.72 for converting at least one of its two photons. A π^{0} signal would be indicated by one of the following no-yes combinations

$$\bar{A}_i \quad \cdot \quad B_i$$
$$\bar{A}_i \quad \cdot \quad \bar{B}_i \quad \cdot \quad C_i$$
$$\bar{A}_i \quad \cdot \quad \bar{B}_i \quad \cdot \quad \bar{C}_i \quad \cdot \quad D_i$$

This same signal may indicate a neutron interaction, in compartments B_i or C_i or D_i. The probability for a neutron interaction varies as a function of angle from 0.38 to 0.49 for $30^{0} < \theta < 90^{0}$. This signal can be used to reject most events that do not have elastic proton recoils.

For similar reasons, it is desirable to have a pion/proton identification trigger available from the dE/dx information in compartments A_i, B_i, C_i and D_i. This may be difficult in the high level trigger because it depends on the angle θ and on how good the ΔE measurement is.

Table XI

Recoil Liquid Scintillator Range Detector

		θ Recoil Angle		
		90°	45°	30°
1.	Maximum scintillator thickness (cm)	40 cm	57 cm	80 cm
2.	Acceptance from 2 m. target	100%	$\gtrsim$ 75%	$\gtrsim$ 38%
3.	Probability of nuclear interaction	.38	.49	.61
4.	Probability of photon conversion	.41	.53	.65
5.	ΔE loss for minimum ionizing particle	72 MeV	102 MeV	144 MeV
6.	ΔE loss for stopping protons	$\leq$ 250 MeV	$\leq$ 300 MeV	$\leq$ 375 MeV
7.	ΔE loss for stopping pions	$\leq$ 120 MeV	$\leq$ 160 MeV	$\leq$ 200 MeV

If more than one charged particle enters the liquid scintillator tank, it is very unlikely that more than one will enter the same ϕ segment (the probability for 2 uncorrelated particles in the same $\Delta\theta = 22.5^\circ$ is 6%). Thus the number of inner scintillator tracks (A_i) with pulses above a discriminator threshold, measures the charged multiplicity entering the liquid scintillator. This information is redundant to that available from the PWC θ readout when there is no secondary interaction.

If all of the liquid scintillator compartments A_i, B_i, C_i, D_i in one segment register a minimum ionizing particle and there is no evidence for other than single-proton recoil, the event can be interpreted as a probable high t recoil proton. For a minimum ionizing particle the signal ratios are

$$\frac{B_i}{A_i} \simeq 2, \quad \frac{C_i}{A_i} \simeq 3, \quad \frac{B_i}{D_i} \simeq 3$$

for thickness A_i, B_i, C_i, D_i = 6, 12, 18, 4 cm respectively. These ratios are a test for high t recoil which is independent of the recoil angle θ. Higher mass diffractive states are apparently produced with a flatter t slope. Therefore a signal indicating a high $|t|$ recoil may be a useful additional way of enhancing higher mass states in the trigger.

Off-line it will be possible to use careful calibration

and mapping to increase the level of sophistication in the use of the recoil information. For example, a careful off-line analysis of the four dE/dx samples for an exiting (high $|t|$) proton should enable one to extend the measurement of the energy range. This will be determined by the precise $\Delta T/T$ values of the resolution function. If a stopping proton interacts with and transfers energy to a neutron in the liquid scintillator, the dE/dx measurement is not valid. Furthermore, if the proton stops but a neutron carries some kinetic energy out of the liquid scintillator, the proton range measurement E is not valid. The added check for a consistent set of dE/dx in A_i, B_i, C_i, D_i for a stopping proton hypothesis will help identify a "clean" data sample in the off-line analysis.

The large cylindrical container enclosing the cylindrical proportional chambers will have an inside radius of 57 cm, outside radius 97 cm and a length of 240 cm. The volume enclosed is about $4.52 \, m^3$ (1000 gallons) and the weight of this volume of liquid NE 235 A scintillator is 3900 kg (4.3 Tons). The construction material for the container will be steel, which will be coated with teflon and/or NE #561 scotchlight white epoxy paint on all the inside walls in contact with the liquid scintillator. The large cylindrical container will come in three separate sections (labelled I, II and III in Fig. 3). The three sections will bolt rigidly together when in place on the experimental floor and a set

of wheels on rails will provide movement for the whole
unit along and perpendicular to the beam axis. As seen in
Figure 3 a missing wedge on the underside provides access,
support and readout space for the cylindrical chambers.

The inside (r = 57 cm.) surface of the container must
have a minimum amount of material to maximize the acceptance
for the low end of the proton energy spectrum. The present
thought is to use a 1/16" stainless steel plate, but if this
proves unacceptable from a structural standpoint, an alter-
nate solution is to place thick acrylic scintillator slabs
in the space between the third PWC and the inside steel
surface. This would improve the acceptance for low energy
protons, and allow for a thicker container wall. The hydro-
static pressure on the inside surface of Sections I or II
has the maximum value of 1.4 lbs./sq. in.

The 60 compartments will be separated from each other
by thin walls designed only for light isolation. These
inner walls will only support themselves and not provide
any structural rigidity for the container. They will be
thin so that a stopping particle can scatter across and
leave energy in the adjoining compartments. Appropriate
small holes will allow for the scintillator to flow between
the compartments when the containers are being filled or
emptied.

The end faces of the cylindrical vessel will have
plexiglass windows, to contain the fluid and transmit the
light to green wavelength shifter bars (as shown in Figure

13). The shifter bars will be viewed by light guides and 2" photomultiplier tubes. The plexiglass ports will have to be individually cut and then glued to an opaque barrier between the compartments. Considerable care will be taken to seal these ends so that they do not leak. The purpose of the green shifter bars is twofold. First they are used to ensure a reasonably uniform light collection efficiency over the whole end face of each compartment. If the output pulse is to be used in the trigger, there will be time to evaluate only the most simple types of corrections. Secondly, on the downstream end of the range detector there is a maximum of 40 cm. between the scintillator and the first magnet face. The shifter bars bend the output light signal through 90° and the photomultiplier tubes can be kept away from the magnet and its fringe field.

The dynamic range of signals from the various compartments is shown in Table XII. The attenuation length of NE 235 A is about 1.7 m. Thus equal signals at 0.1 meter from one end and 2.3 meters from the other end will have a pulse height ratio of about 4 for the two phototubes. Combining the dynamic range requirements with the attenuation factor of 4 suggests that we use ADC's with a range of 1 : 1000, or 10 bits. At present this range of 10^3 seems a rather conservative estimate. Resolution studies with the scale model later this year may reduce it.

LIQUID SCINTILLATOR LIGHT COLLECTION
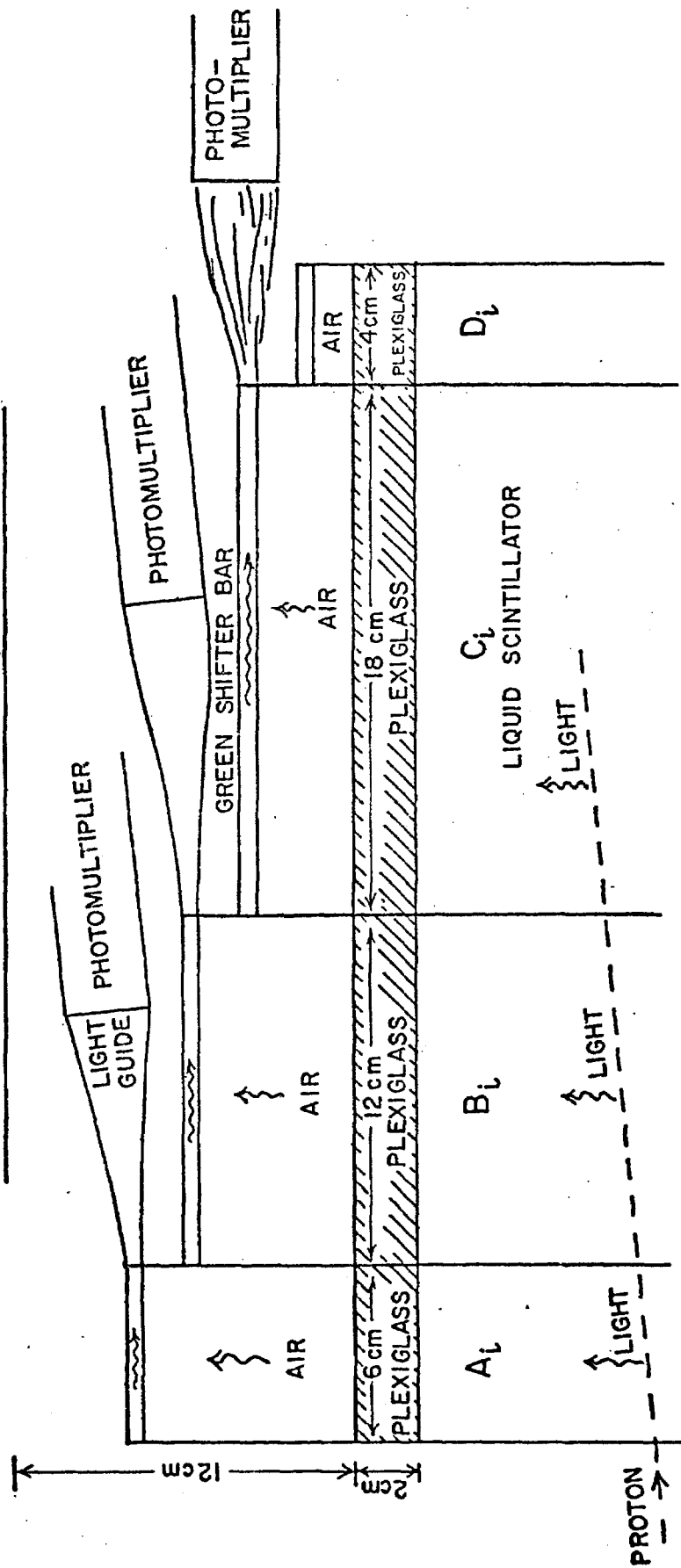
Figure 13

Table XII

Dynamic Range Requirements of Recoil Liquid Scintillator Compartments

Compartment	Thickness	$\theta = 90°$		$\theta = 30°$	Sensitivity	Dynamic
		Min. Ioniz.	Max.	Maximum	Required	Range
A	6 cm	12 MeV	80 MeV	125 MeV	1/2 MeV	250
B	12	24	120	175	1	200
C	18	36	150	230	2	100
D	4	8	46	100	1/2	200

The absolute calibration of the phototubes will be done with real experimental data during the run. Compartment A tubes can be calibrated with protons that traverse it and just barely enter into the next compartment B. Knowing the θ angle from the PWC's one can calculate the exact range of the proton traversing A (to ± 2 mm). The range then specifies the energy, which then calibrates the photomultiplier tubes. Compartments B and C will be calibrated in a similar fashion. Compartment D will be calibrated using minimum ionizing particles passing through A, B, C and D.

VII. Liquid Hydrogen Target

The liquid hydrogen target system will accommodate target flasks of various lengths. It will be possible to exchange these in a few days turn around time. This will allow experiments to optimize the length for the particular physics being pursued. For example, to maximize rates a 2 m target will be used. To reduce the interaction of secondaries a short 1/2 meter flask would be possible. The flasks will be of thin wall construction to offer the minimum possible mass to low energy recoil protons and will be supported from only one end. Initially, the target flask will have a diameter of 2 inches and a length of 2 meters. Figure 14 shows a cross section of the target with the various dimensions. A breakdown of the material comprising the target is as follows:

	Thickness	Mass

A) Flask (Mylar)
   $\rho = 1.39$ g/cm^3 0.005"   .0177 g/cm^2

B) Foam Vacuum Jacket (Rohacell)
   $= 0.053$ g/cm^3 0.5"   .0673 gm/cm^2

C) Outer Vacuum Jacket Skin
   (Mylar)
   $\rho = 1.39$ g/cm^3 0.005"   .0177 gm/cm^2

                                     Total   .103 gm/cm^2

This compares with .36 gm/cm^2 for 2" liquid H_2.

The volume of the 2m flask is about 4 liters. The hydrogen gas will be condensed and refrigerated by a 10 watt Air Products helium refrigerator. The time required for filling from warm will be about 25 hours. The time to empty the target into the reservoir is about 12 minutes while the refill is about 60 minutes.

The target system will be mounted on a rail system to allow it to be withdrawn from the recoil detector. Pump cart compressor and controls will be located on top of the shielding adjacent to the rails with flexible tubes connected to the refrigerator.

HYDROGEN TARGET FLASK

OUTSIDE MYLAR
SKIN (0.005")

FOAM VACUUM
JACKET (0.5")

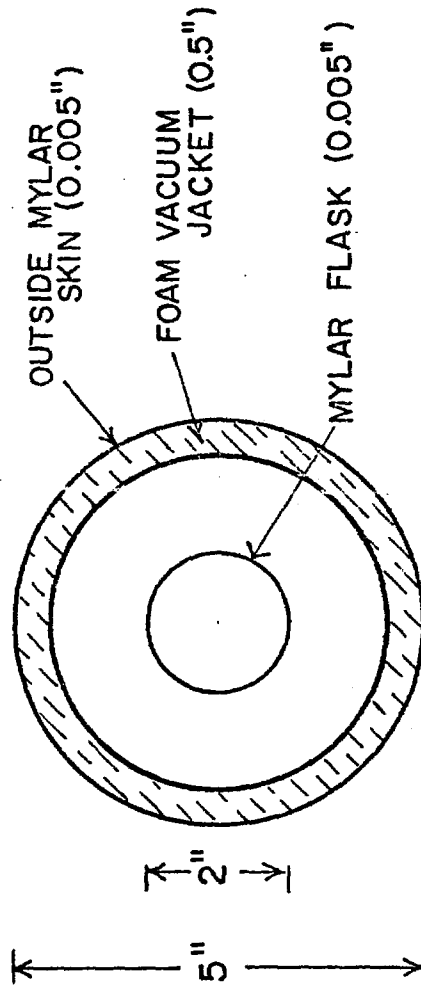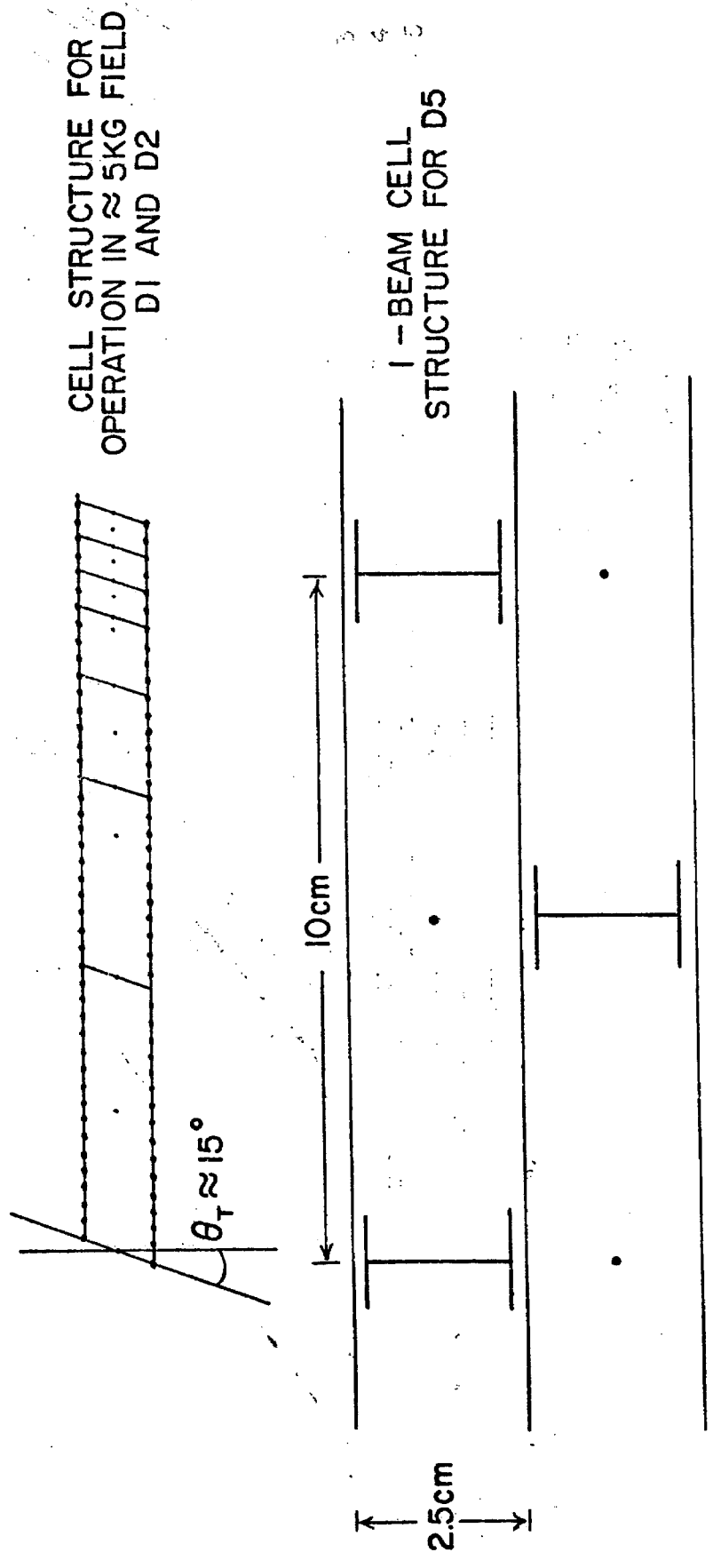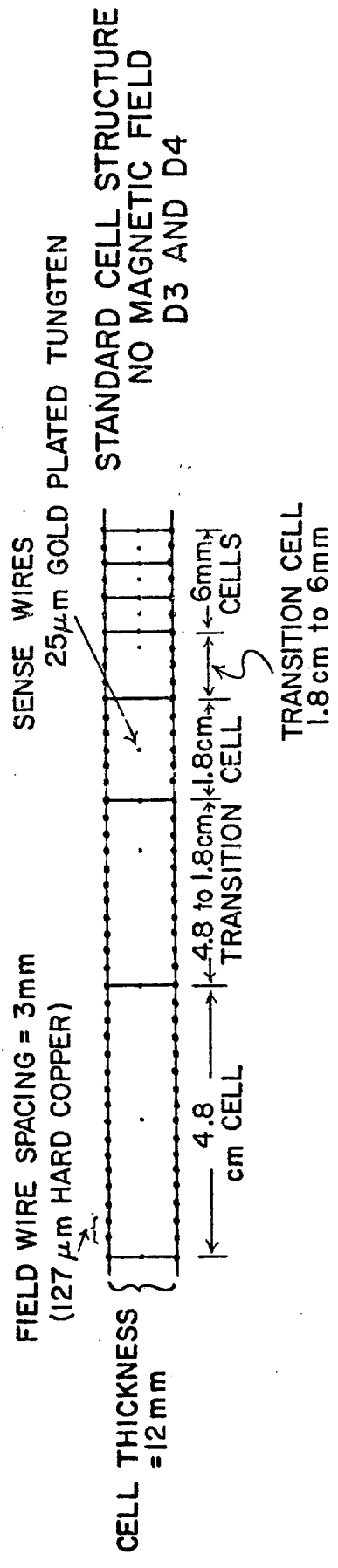MYLAR FLASK (0.005")

2"

5"

Figure 14

VIII. Forward Detectors

    A.   Drift Chambers

        Charged particles will be tracked in the forward spectrometer by 32 planes of drift chambers. The general characteristics of these chambers are summarized in Table VIII (Sec. II F). The motivation for our choice of wire orientation and chamber location was discussed in earlier sections of this report. We will now discuss some of the mechanical and electrical details of the chambers.
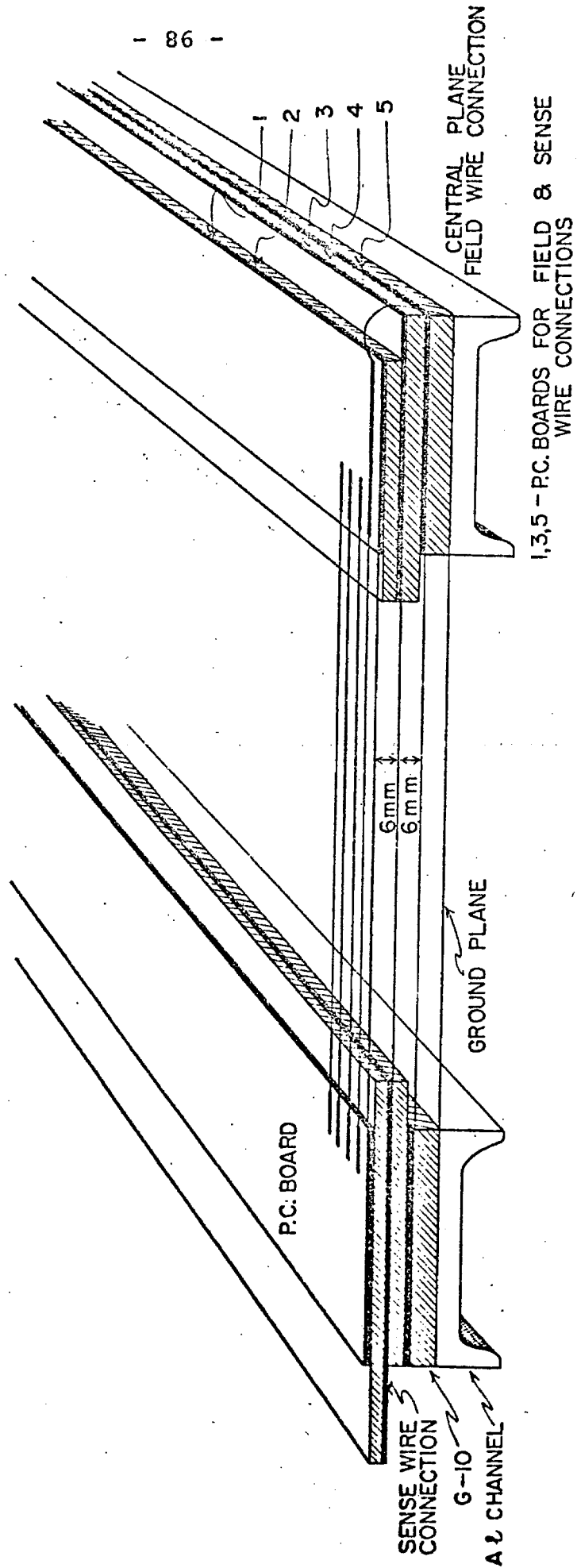
        The chamber construction will be guided by the results of a prototype and testing program which will begin soon. We envisage a technique similar to that of R. Thun et al.[6] Field shaping wires will be 127 μm diameter hard copper wire and sense wires will be 25 μm diameter gold plated tungsten. Figure 15 shows the structure planned for the cells.

        Sense (anode) wires will be at ground potential and nearby field wire potentials chosen at negative voltages which give nearly cylindrical equipotential patterns around each sense wire. All wires will be mounted on G-10 frames which will be mounted in groups inside a gas tight aluminum box. This box simultaneously provides a rigid surveyable mounting structure and shields against noise. In addition, each chamber will be isolated from its neighbor by a ground plane which will be a plane of aluminum wires in order to minimize material in the spectrometer. Figure 16 indicates the preliminary design for construction of a single plane.

CELL STRUCTURE

Figure 1.5

1,3,5 – P.C. BOARDS FOR FIELD & SENSE WIRE CONNECTIONS

1,2,3 – LAMINATED WITH EPOXY

4,5 – LAMINATED WITH EPOXY

ENTIRE ASSEMBLY BOLTED TOGETHER

CROSS SECTION
OF SINGLE DRIFT PLANE

Figure 1(

The guiding principles for this design have been service-ability (it should be possible to easily access all wires should it be necessary to replace a wire for any reason) and the ability to mass produce the final design.

We have seen earlier that the physics we want to do places rather severe requirements on our ability to resolve closely spaced tracks inthe chambers. There are two possible competing philosophies which may be adopted to meet these requirements: 1) Large cells may be used which then have multiple track readout capability, and 2) Smaller cells may be chosen with the capability to read only one coordinate. In the first instance the pulse width which may be obtained in a drift chamber limits the inherent pulse pair resolution to 50-100 ns (2.5 mm - 5 mm). In addition, the electronics is complicated by either having more than one TDC per wire or by a multiplexing scheme to route pulses to a smaller number of TDC's. In the second case one has more wires to deal with but the electronics is much simpler. The smallest drift space which is practical is 2-3 mm which matches the pulse pair resolution described above. Our choice is to simplify the electronics and keep cell sizes relatively smaller.

As described earlier four cell sizes (.6 cm, 1.8 cm, 4.8 cm, and 10 cm) will be used with the size increasing away from the beam. The distribution of cells is shown in Table VIII.

It should be noted that the overall cost of the system is dominated by the cost of the readout electronics. It may be that the most cost effective technique is to minimize the cell size. For example, we are considering the possibility that it may be less expensive to make chambers with only 6 mm cells (3 mm drift spaces) and thereby have only TDC's with a smaller number of bits. There are also advantages involving the field shaping wires in the magnet (M1) for small drift spaces since compensation for the B field will probably not be necessary.

Our experience has been that Argon (90%) - CO_2 (10%) is a satisfactory gas for drift chamber use. However, the drift velocity in Ar - CO_2 is more strongly dependent on electric field than in some other hydrocarbon mixtures. This may be a disadvantage in an experiment where most of the cell sizes are small and one is more often than not in the region close to the sense wire where fields vary rapidly. For this reason we will investigate this variable during the prototype and test stage.

It is now well known that it is possible to operate large drift chambers in high, uniform magnetic fields by skewing the $\vec{E}$ field to compensate for the average Lorentz force on the drifting electrons. For small drift spaces this compensation is not necessary. For larger drift spaces (1.8 cm and 4.8 cm cells) it is our intention to arrange the voltage divider networks for the field shaping wires so that the

$\vec{E}$ field skew angle ($\theta_T \approx \sin^{-1} (\frac{vB}{E})$) = 14° for E = 1000v/cm and B = 5 Kg) is easily variable within limits so that there is some flexibility in choosing the magnetic field in M1. This option may be most important as the Energy Doubler/Saver becomes operational.

It is desirable from the standpoint of avoiding noise problems to have the amplifier-discriminator shielded well and as close to the chamber as possible. Therefore, small packaging is necessary so that even for 6 mm cell sizes it is possible to place the amplifier-discriminator directly on the chamber. In addition, little space is available for electronics on the chambers inside the magnet before reduction of solid angle becomes an important question.

However, placing the amplifier-discriminator directly on the chamber may not be desirable from the serviceability point of view for the chambers in the first magnet. An additional requirement for the amplifier-discriminator is set by the desire that the discriminator output be available to a preprocessor. For example, such information may be used in a multiplicity trigger.

Electronics for drift chambers is a continously developing field. We outline here the requirements that the electronics for this system of drift chambers will have to meet. Average drift velocities on the order of 5.0 cm/µs are expected. Thus, the drift times for .6 mm, 1.8 cm, and 4.8 cm

cells are expected to be 60 ns, 180 ns, and 480 ns. We are
striving to reach a spatial resolution of from ± 100 μm to
± 150 μm which implies measuring drift times to an accuracy
of ± 2 ns. We therefore, desire a digitizing system with a
least bit accuracy of ~ 2 ns. For a strictly digital system
this requires a 500 MHz clock. Analogue systems readily ob-
tain this accuracy but there is an additional burden to cali-
brate and monitor independently each TDC channel. A hybrid
technique like that of T. Droege eliminates this problem.
We note that for the drift times mentioned above we require
TDC's with 5 bits, 7 bits, and 8 bits, respectively in order
to achieve the desired accuracy.

We will use Droege high voltage power supplies like those
presently in common use for MWPCs and drift chambers else-
where at Fermilab. Each chamber will be provided with a sep-
arate voltage divider for each cell size in order to provide
field shaping. Because there are only four separate cell
sizes, we need only 4 distinct voltages. However, it is ex-
tremely desirable when debugging chamber problems to have a
limited number of chambers sharing one supply. Chamber pro-
blems are then localized more efficiently. For these reasons
we will use 18 dual modules. There are then nine supplies at
each of 4 voltages. With 32 chambers we then have at most 4
chambers on any one supply.

B.   Cerenkov Counters

We will use two segmented Cerenkov counters for particle identification. The first one will be a 3.25 meter long nitrogen gas filled counter and the second will be a 7 meter long nitrogen helium mixed gas counter. The basic properties of these counters are shown in Table XIII. Also Figs. 17 and 18 show the excitation characteristics of these counters. In addition we will be able to use other gases like CO_2, C_8H_8 (propane), and Fr_{12}, as the experimental situation requires it.

In order to handle the large multiplicity expected in the final states that will be studied, each of these Cerenkov counters will have a 20 mirror segmentation arrangement. These spherical mirrors will be slump-molded out of thin Plexiglas in order to reduce the amount of material in the path of the particles. The focused Cerenkov light will be reflected into Winston cones whose dimensions are shown in Fig. 19. Finally, the light is detected by RCA 8854 5" phototubes which have a high photoelectron efficiency (~18%). An ADC will be attached to every phototube in order to measure pulse height. This procedure may help extend the range of separation of pions and kaons.

Using threshold information alone, the counter will separate pions from either kaons or protons for momenta between 5.5 and 36 GeV. All three particles can be separated from each other for the more restricted range of 21-36 GeV.

TABLE XIII

Upstream Cerenkov Counter (C_1)

Gas	100% N_2
Length of Counter	3.25 m
Transverse Dimensions Upstream	1.4 x 0.64 m
Transverse Dimensions Downstream	2.5 x 1.14 m
Index of Refraction (n-1) at STP ($\lambda \approx 3500 \overset{o}{A}$)	3.089×10^{-4}
Cerenkov Angle ($\gamma \to \infty$)	25 mrad
Threshold for Pions	5.5 GeV/c
Threshold for Kaons	20 GeV/c
Threshold for Protons	38 GeV/c
Number of Reflections (N_R)	2
Total Number of Photoelectrons ($\gamma \to \infty$) N_{pe} per cm = 170 $\sin^2\theta_c \times (.70)^{N_R}$	16

Downstream Cerenkov Counter (C_2)

Gas	21.8% N_2 & 78.2% He by volume
Length of Counter	7 m
Transverse Dimension Upstream	2.1 x 1.25 m
Transverse Dimension Downstream	4.3 x 2.5 m
Index of Refraction (n-1) at STP ($\lambda - 3500 \overset{o}{A}$)	0.950×10^{-4}
Cerenkov Angle ($\gamma \to \infty$)	14 mrad
Threshold for Pions	11 GeV/c
Threshold for Kaons	36 GeV/c
Threshold for Protons	69 GeV/c
Number of Reflections (N_R)	1
Total Number of Photoelectrons ($\gamma \to \infty$) N_{pe} per cm = 170 $\sin^2\theta_c \times (.70)^{N_R}$	.15

PROPERTIES OF THE
UPSTREAM CERENKOV COUNTERS (C₁)
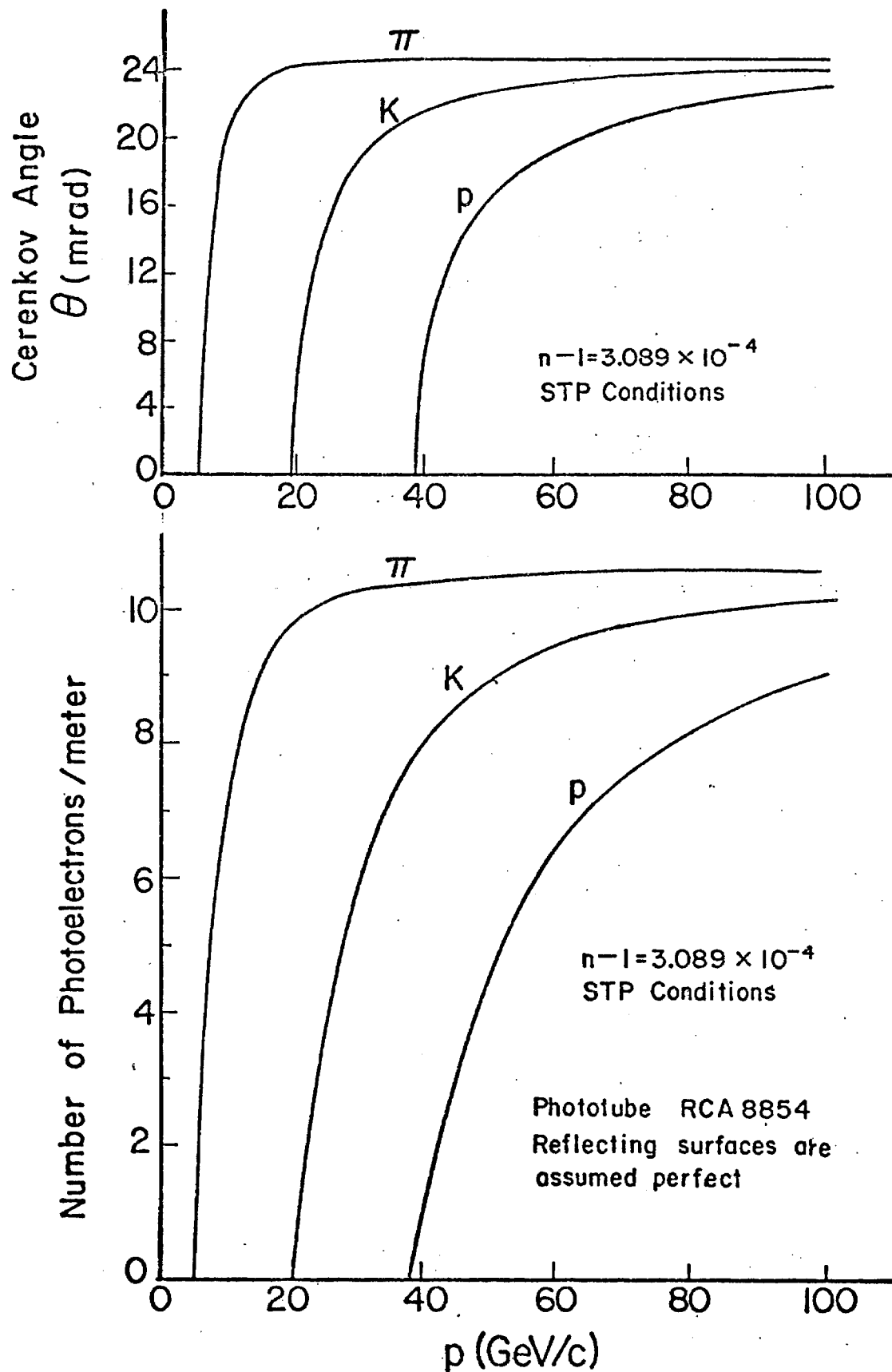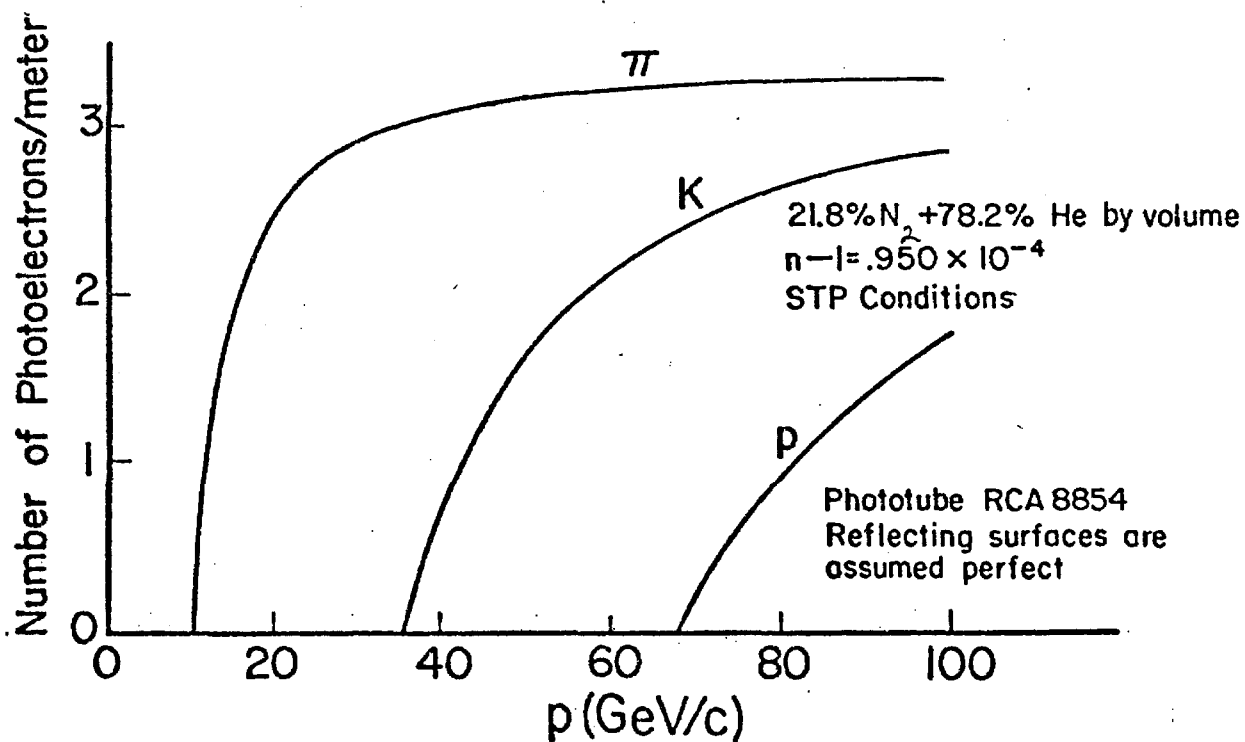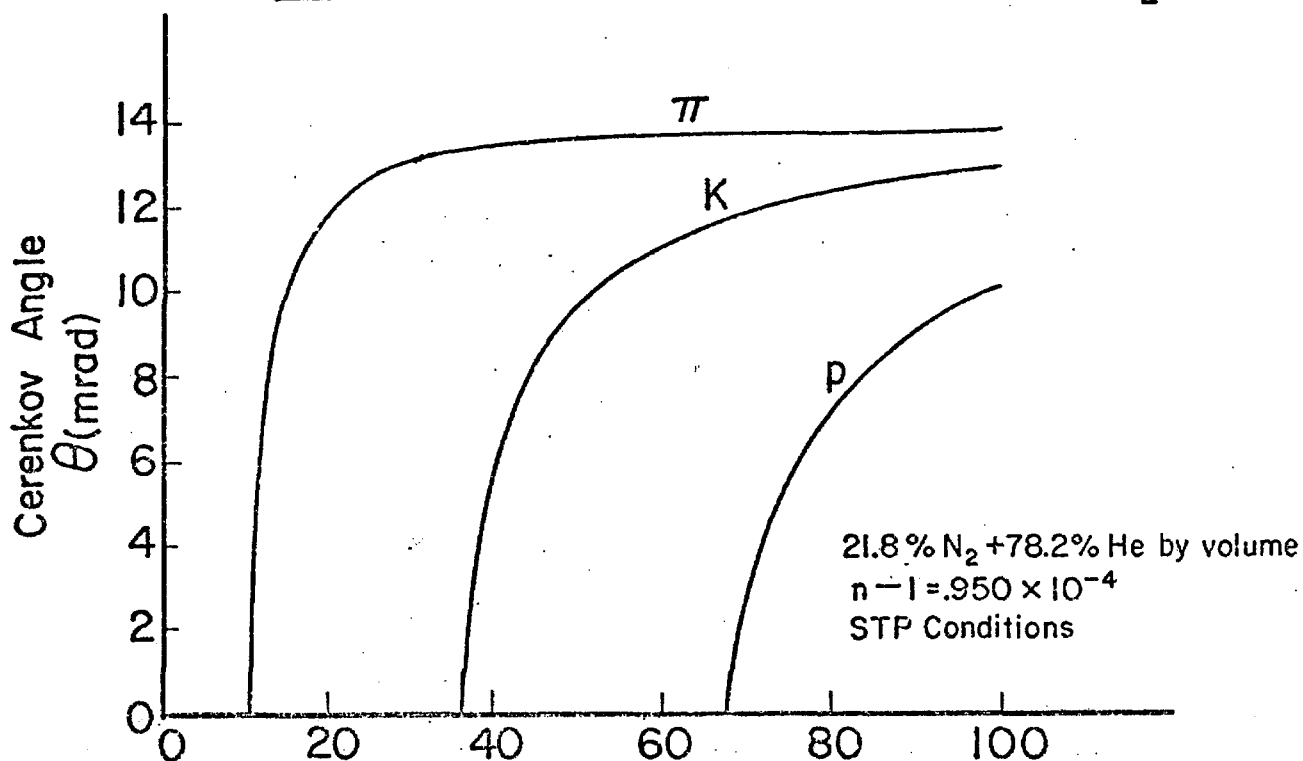

Figure 17
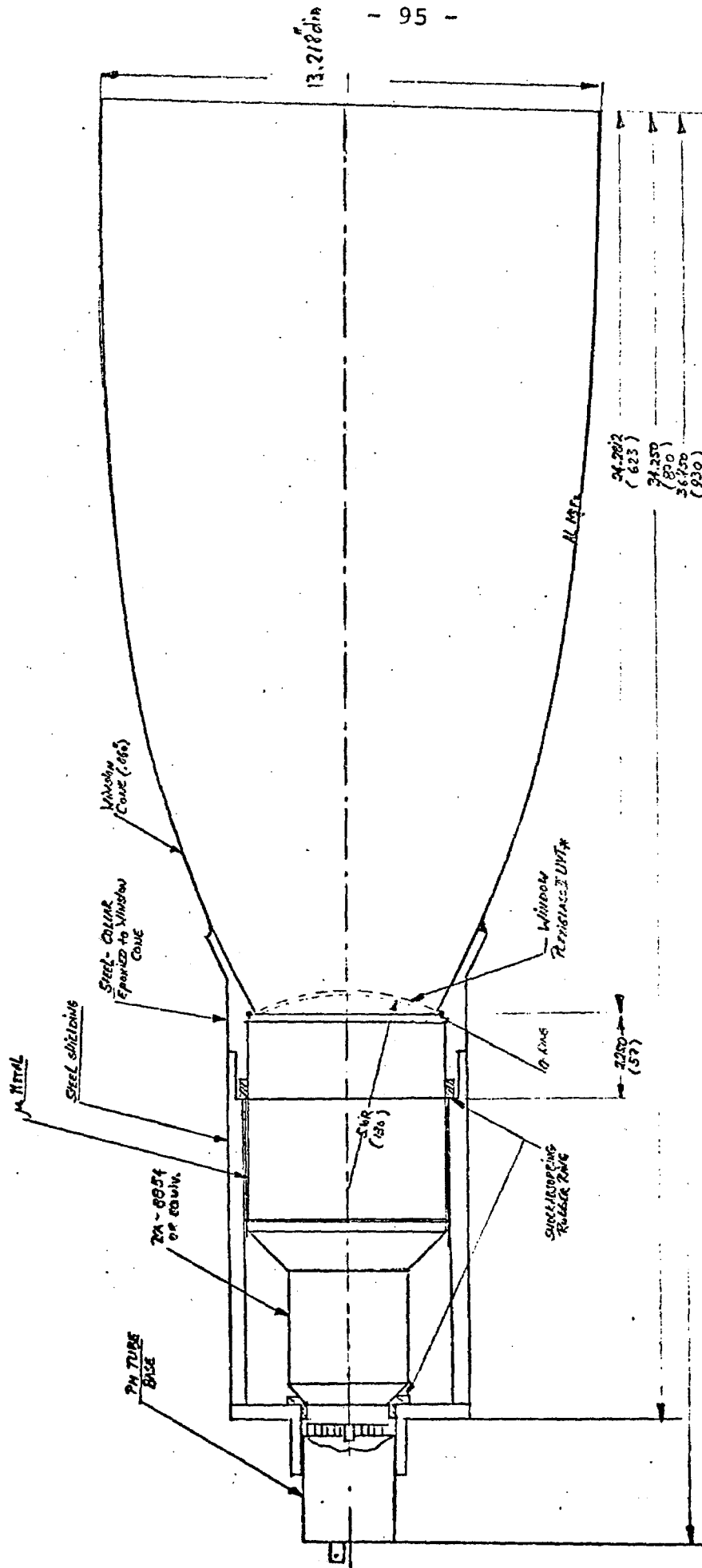
PROPERTIES OF THE
DOWNSTREAM CERENKOV COUNTERS (C$_2$)

Figure 18

Figure 19

The counters, however, are sufficiently long that about 15 photoelectrons can be recorded from the passage of a single particle. By recording the number of photoelectrons the upper limits on the range of particle distributions can be increased by 50%.

Both Cerenkov counter vessels are manufactured from 1/4" thick 6061 T6 aluminum plate welded into frustum-shaped containers, reinforced with externally welded ribs. Both ends of each vessel will have a full sized flanged opening, to allow the use of thinner material along the path of the beam. Two access ports in each vessel (24 x 48") are provided to permit entry for mirror alignment. The small vessel (C_1) will be manufactured in two sections joined together with flanges. The large vessel C_2 will be in three sections. After manufacture, both vessels will be purged with helium and tested for leaks. Each vessel will be equipped with its own support and leveling device to permit alignment. Estimated net weight for the large counter is 4500 lbs. and for the small counter, 1800 lbs.

After closing the counters, they will be purged with dry nitrogen. The nitrogen-helium mixture for the large vessel and nitrogen for the small vessel will be introduced into the top of the counter. Displaced gas is vented through the bottom until the desired purity or mixture is obtained (Fig. 20). A low range differential switch will provide regulation.
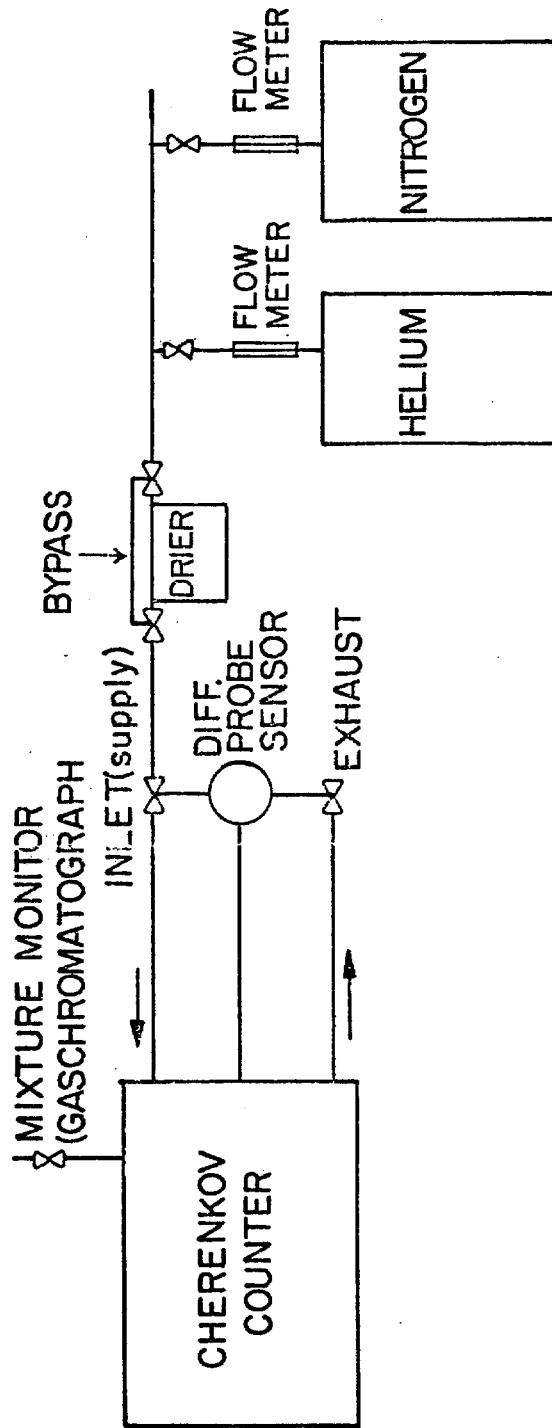
Figure 20

The mirror planes in both counters will have 20 segments of various sizes but constant focal length (78"). To minimize labor costs and material expenses 1/4" block acrylic sheet is being considered. The surfaces of acrylic are already of sufficient optical quality; the exiting light ray should deviate from its expected direction by no more than 5 milliradians.[7] The construction of the mirrors will proceed as follows: oversized sheets will be slumped into a female aluminum mold to produce a spherical shape.[7] A cover will prevent deposition of dust and permits uniform heating of mold and acrylic sheet. The cover also will prevent local deviations in the plastic sheet. A fluorocarbon release agent will be applied to the mold prior to shaping to prevent sticking of the plastic to the mold surface. Acceptable mirrors then will be attached to their mounts and aluminized. If necessary the mirrors will be reinforced with a hexcell structure.

The collection cones will be fabricated in one of two ways: A) Spinning aluminum sheet over a steel mandrel of desired shape; and B) By blowing acrylic tubing inside a heated mandrel of correct size.[8] While option A entails a minimal expense in manufacturing aluminum cones, the polishing process is very time consuming and laborious. Option B on the other hand, presents a greater expense for both material and mandrel. If metal cones are used, prior to aluminizing, cones will be dipped and baked with a lacquer

coating to increase reflectivity. If acrylic cones are used, the aluminizing will be the same process as for the spherical reflectors.

To prevent leaking of helium-gas into the photomulti-plier tube (RCA 8854) we plan to install a 3/16" thick UV-transmitting window slumped to an inside spherical radius which will mate with the spherical face of the tube. The separation of about 1/16" between tube-face and plastic window can be continuously flushed with nitrogen gas to keep helium away from the phototube window. (Nitrogen gas is essentially transparent over the wavelength range $1875\overset{\text{o}}{\text{A}}$ to $8000\overset{\text{o}}{\text{A}}$.[9]) To increase sensitivity to UV photons the plastic window will be coated with an organic wavelength shifter, P-terphenyl (PTP) or diphenyl stilbene. This process converts photons in the 1700 to $3600\overset{\text{o}}{\text{A}}$ range to a range centered around $3805\overset{\text{o}}{\text{A}}$.[10]

C.   Segmented Liquid Scintillator Shower Counter (SLIC)

As shown in Fig. 21, the SLIC is a multilayered lead-liquid scintillator shower counter. Position resolution is obtained by segmenting the liquid layers into a number of teflon coated light pipe channels. Every third channel, pro-gressing longitudinally through the detector, will be oriented in the same direction.

The periphery of the detector is composed of Lucite windows and thin wave bar strips optically coupled to photo-tubes. The strips are oriented longitudinally and have a

WAVE BARS
(ONLY TWO SHOWN)

39 Layers
Pb 22X°
Scintill.

210 cm

19 NARROW VERTICAL STRIPS
24 WIDE VERTICAL STRIPS
(EACH HALF)

20 NARROW STEREO STRIPS
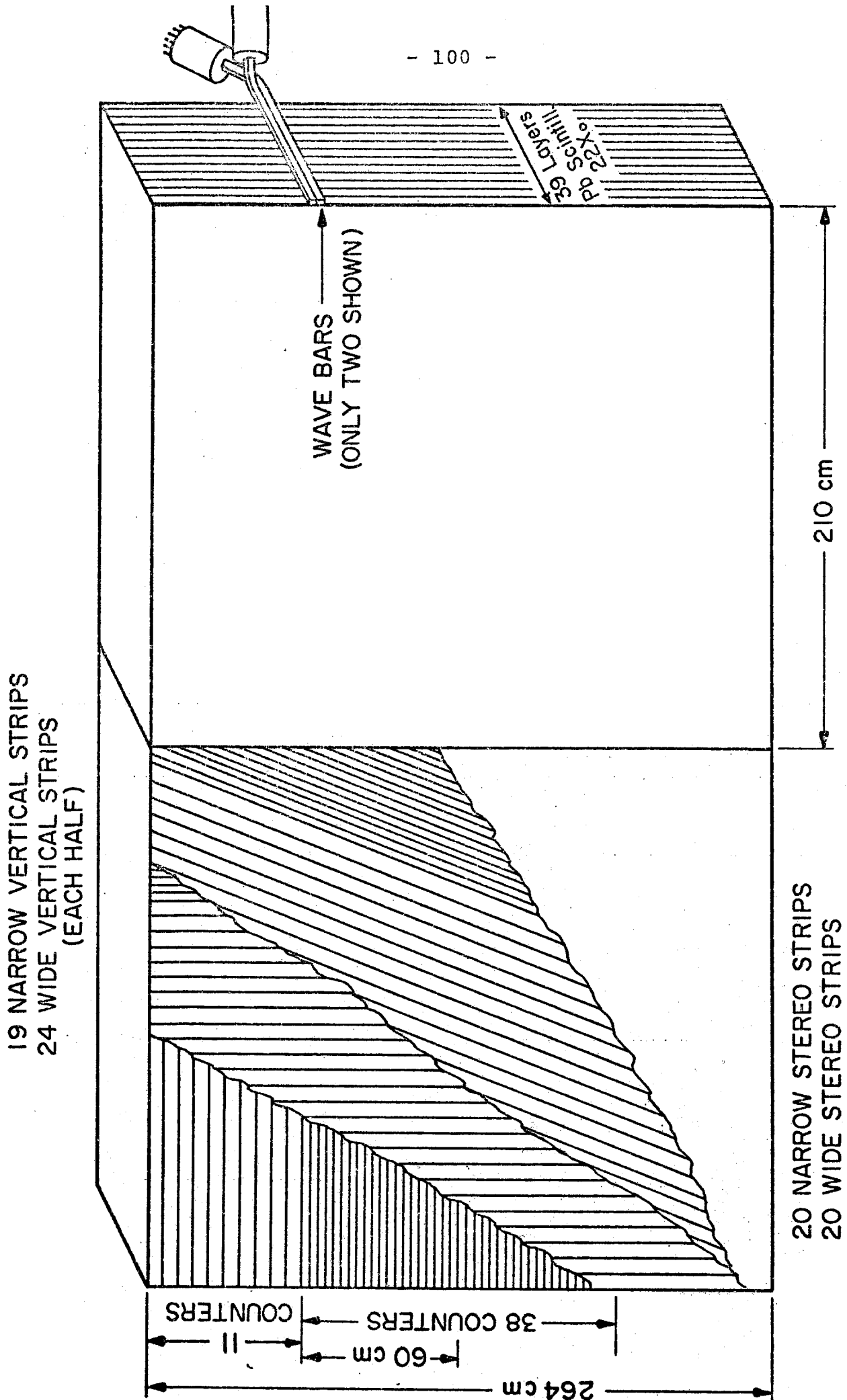20 WIDE STEREO STRIPS

11 COUNTERS

38 COUNTERS

60 cm

264 cm

Figure 21

width which is a multiple of the light channel widths. For a single shower, the position of the shower is determined from the location of the photomultipliers which view light from the top, giving the x coordinate, and from the side, giving the y coordinate. In fact, from the distribution of pulse heights on the neighboring counters, the position can be determined much better than the width of the channels. Our experience with lead glass indicates that with 2.5" channels one can always do better than $\pm$ .6" and will usually have a resolution of $\pm$ 0.2". This corresponds to $\delta\theta \approx .3$ mrad.

The third view, at 20° with respect to the vertical and taken from the bottom of the detector, is to remove ambiguities for cases of multiple showers. These ambiguities are not as serious as for the case of wire chambers since they only arise in the case of showers of nearly equal energy. We believe, however, that this degree of redundancy will be very useful for resolving complex patterns. In addition, at least at lower beam intensities, this may enable us to eliminate separate lead glass pair counters for the fast trigger (see Section IV A). This in turn will improve our ability to have a running calibration of the SLIC using the high rate of pairs.

We plan to have segmentation of 1.25" (3.18 cm) in the region near the beam and 2.5" toward the periphery. The regions are shown in Fig. 21. The total number of counters is 278.

A nice feature of this type of counter is the great variety of possible configurations which are economically feasible. The scintillator and segmenting materials are relatively cheap so thatthe counter can be made with many layers improving resolution.

The wave bar light collection scheme also allows for great flexibility in design. One has the choice of taking one or more views of the shower light between each lead layer. This choice involves compromises between various desirable counter performance characteristics. For example, taking three views between each lead layer would improve the ability to separate complicated patterns since each view would have the full energy resolution. But then either the counter would need to be deeper resulting in more overlap of close showers, or the liquid layers would have to be thin leading to worse light attenuation, or one would have fewer layers of lead leading to worse overall resolution.

Another example of flexibility results from the fact that the wave bars are not glued to the scintillator channels. This means that if in the future it is desirable to change the readout cell size of the SLIC, it will be possible to move wave bars of differing widths (always multiples of scintillator channels) to different regions of the SLIC. This change could be made without changing the basic liquid scintillator and lead structure.

Since this detector is a new development, some of the

important input design information is not yet available.
In particular, we can only estimate the total amount of
light, the number of photoelectrons which will actually be
produced per GeV, and the effective attenuation properties
of easily fabricated liquid channels. Experimental studies
of these quantities are underway using a prototype but are
not yet complete. The design presented here is therefore
based on estimates of these properties obtained from the
literature combined with our limited experience.

We believe that we can achieve attenuation lengths of
greater than the 2.4 meters length of the longest channels
of the detector. Mirrors at the far ends of each channel
will improve this further. Combined with the self-calibrating
properties of this detector this should be quite adequate.
The main disadvantage of the long channels is the somewhat
sloppy threshold for triggering on pulse height that will
result.

A total length of 22 radiation lengths should be
adequate since this is longer than the lead glass blocks used
at similar energies in Experiment 25A where $\frac{\delta E}{E} \approx \pm \frac{13\%}{\sqrt{E}}$ was
obtained. But we note that the light attenuation effect of
the glass in that case tended to cancel the effect of fluc-
tuations in shower loss out the back of the counters. The
same will be true in this case with the wave bars if the
tubes are downstream. If the tubes are placed upstream,
which is advantageous for geometrical reasons, the counter

may need to be somewhat deeper. The 22 radiation lengths are divided into 39 layers of .56 radiation lengths each. If the light collection is adequate, this will lead to a resolution which is improved by $\sqrt{.56}$ compared with standard $1X_O$ detectors and might be as good as $\frac{\delta E}{E} \approx \pm \frac{8}{\sqrt{E}}$%. Finer sampling could be achieved at the cost of either worse attenuation (thinner layers) or a longer detector. The latter case would lead to more overlap of close showers. We believe that the 39 layer choice with 1/2" liquid layers is a good compromise.

The detector will contain about 16 tons of lead. To make manageable modules we will build it in two roughly square modules. The lead will be in sheets laminated between .040" layers of aluminum. This ensures that the surfaces are flat and provides mechanical support for the lead. While the lamination adds to the cost of the lead, it will make possible a very simple mechanical construction.

D. Hadrometer

The hadrometer is a steel/scintillator hadron calor-
imeter segmented both vertically and horizontally. It is
designed for use with the segmented electromagnetic shower
counter (SLIC) for measurement of hadron energy and angle.
In particular, it will provide the only information on the
energy and angle of neutral hadron components in the dis-
integration of charmed states. It also provides the capa-
bility of a fast trigger based on a rough mass calculation
from angles and energies of several hadrons. Calorimeters
of this type have also been effective in resolving ambigu-
ities in the off-line pattern recognition.

A sketch of the hadrometer is shown in Figure 22a and
a summary of the specifications are shown in Table XIV. The
hadrometer consists of inter-spaced layers of steel and
acrylic scintillator. The counter is divided into four sections,
two located right and two left of the beam line. Each part
consists of a stack of 32 steel plates each one inch thick.
The modules composing the scintillator segments are made up
of 16 strips of acrylic scintillator each 0.5 inch thick and
four inches wide. Acrylic wave shifter bars collect the light
from the scintillator strips and connect to the RCA 6342A
phototubes by means of a folded lucite light pipe. (See
scintillator module details in Figure 22b.) Some tests will
be performed to acertain the exact combination of scintillator
thickness, wrapping, gluing and light filtering techniques to
insure that the response across the module is uniform. On

Table XIV

Hadrometer Specifications

| Total Thickness: | Fe | 8 collision length |
| | Scintillator | 1 collision length |

Sample Interval: 1" Fe, 0.5" Scintillator

Total Samples: 32

Phototubes: RCA 6342A

Energy Resolution: $\frac{\delta E}{E} \simeq \pm \frac{.65}{\sqrt{E}}$

Position Resolution: ± 2 inches

	Vertical	Horizontal
Size:	295 cm	490 cm
Angular Acceptance:		
Magnets at same polarity		
P = 5 GeV (charged)	± 81 mr	± 87 mr
P = 20 GeV (charged)	± 81 mr	± 123 mr
Magnets at opposite polarity and neutrals	± 81 mr	± 135 mr
Segmentation:	56 modules	56 modules

HADROMETER

WAVE BAR

PMT

16 Vertical Scintillator Strips
2.95×.10×.012m

SIDE

2.95m
(28 Strips)

FLOOR

4.9 m (56 Strips)

FRONT

1.65m

PMT

32 Steel Plates
2.45m × 2.95 ×.025m

16 Horizontal Scintillator Strips
2.45 × 0.1 ×.012 m

TOP
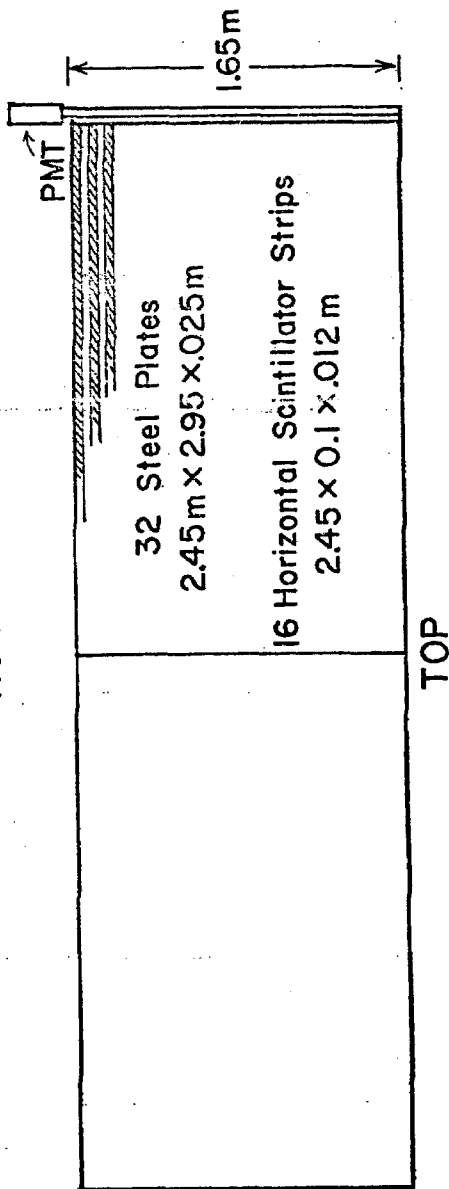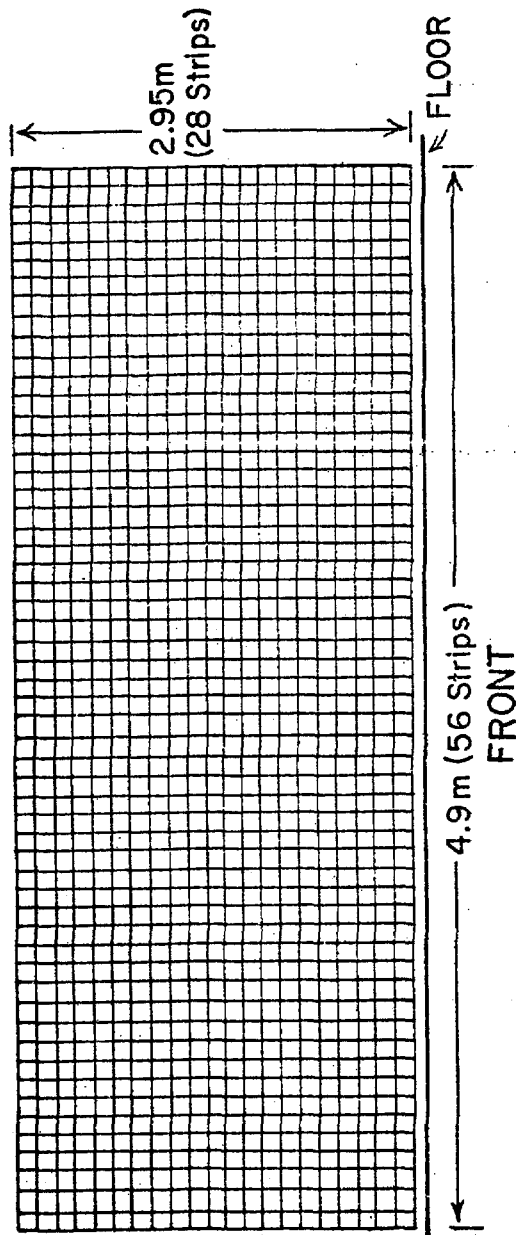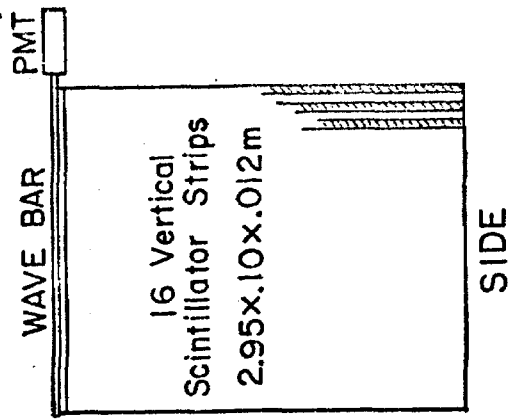
Figure 22a

TYPICAL VERTICAL SCINTILLATOR MODULE

WAVESHIFTER BAR (0.5" THICK)

20 STRIPS SCINTILLATOR (0.5")

(Doped Acrylic)

PM | BASE

2.2m

FOLDED LIGHT PIPE

PM | BASE

10cm
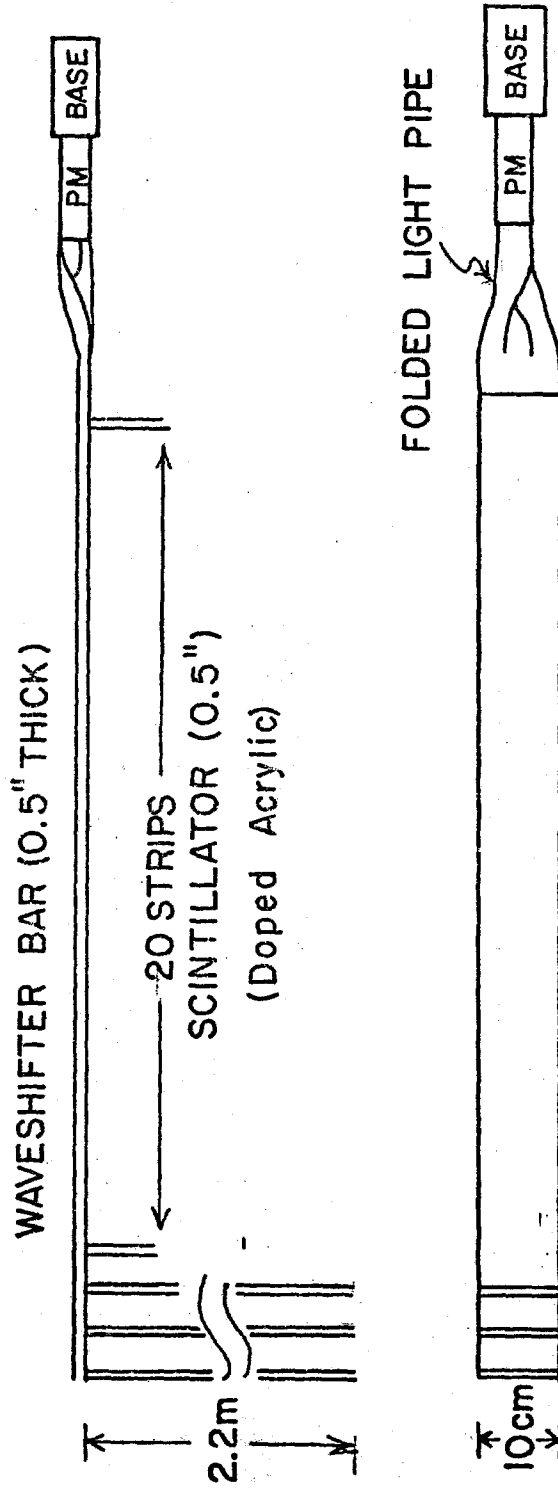
Figure 22b

the basis of previous work,[11] it is likely that the uniformity
can be maintained within a few percent.

The dynode signals of all 112 tubes are routed to ADC's
for transfer to storage. Signals are also used as input
to processors capable of making event selections on the basis
of kinematics.

The gains of the modules are balanced using pulse
heights from muons through all parts of the counter. Energy
calibration is determined from low energy beams transported
down the tagged photon line. The calibration will be moni-
tored and maintained by a laser/fiber optics system like that
used on the E-25 lead glass.

The hadron energy resolution of the hadrometer in con-
junction with the SLIC is expected to be:

$$\frac{\delta E}{E} \simeq \pm \frac{.65}{\sqrt{E}}$$

The position of the incident hadron is determined from energy
shared by adjacent strips that cover the shower. Although
the counter width could in principle give a position of $\pm$ 1 inch,
the position resolution is dominated by the jitter in transverse
deposition of energy. The final position resolution will be
about $\pm$ 2 inches. At 15 meters this gives an angular resolu-
tion of about $\pm$ 4 mrad.

Following a meter of steel behind the hadrometer sixteen
12 inch wide by 1/4 inch thick counters with high gain tubes
will identify spectrometer tracks that are muons.

IX. Online Computer Configuration

A. Hardware Requirements

Our choice of computer hardware is motivated by the particular experimental data acquisition problems. The event rate contemplated, assuming the fast trigger logic, is 100 to 200 events per beam-second. Our estimate of the number of 16 bit words per event is 400 words (average). We plan for 1 or 2 beam-seconds every 7 clock seconds.

To handle this data rate, we need to buffer to disk and to core. The best buffering rate to disk actually achieved is 40,000 words/beam-second with disks currently in use on the PDP/11. This will handle the low rate limit. To handle the high rate limit, which will more likely be the average, we will need 32K of core buffers for the one second spill case. We will require 64K of core buffers for the two second spill case. These core requirements are over and above that required for the monitor and data acquisition program.

This core buffer will require CAMAC transfers into the region above 32K. Thus a Jorway 411 branch driver which handles memory addresses greater than 32K will be required. Manipulation of this data by the CPU will be necessary, and a KT-11 memory management unit will be required to access the data above 32K.

At even 1 beam-second per 7 clock-seconds, one 2400 foot tape will be filled in 68 minutes at the 100 event per second rate, assuming a 1600 BPI tape drive. A two second spill is anticipated and an average rate nearer the 200 per second figure is also more likely. Two 1600 BPI tape drives will be required to handle this efficiently if the time due to tape

changing is not to be a significant fraction of the running
time.

The offline analysis of large volumes of taped data
is costly. Thus it is important to analyze, compress, and
filter the data as much as possible before writing it to
tape. This sort of processing should be done in a high-level
language and as fast as possible. The high-level language is
required to maintain flexibility and ease of understanding of
the processing programs by facility users. The speed is re-
quired to reduce the number of data tapes to as few as possible.
These considerations dictate the use of the fast in-line
Fortran available under RSX-11M, the use of an 11/55 CPU
with its faster processing capability, and the use of the
hardware floating point option.

Complete analysis of a portion of the data is required to
be certain that the physics goals are being met. The results
are needed quickly in order to respond to current problems.
We require a BISON-NET link to the central computing facility for
this purpose.

The RSX-11M software provides much of what typical large
experiments eventually build into less advanced monitor softwares,
such as sophisticated overlay schemes, checkpoint capability,
and multi-tasking features. To start with these features
already developed will speed up the programming for the facility
considerably. This system will require 2 RK05 disks to handle
the monitor, the buffering, and the fast Fortran disk storage
requirements.

Our estimate for the core requirements for the monitor and

data acquisition programs, exclusive of the core buffering
is obtained by simply adding the size of the on-line programs
under RT-11 to the size of the RSX-11M monitor. The first
size is 26K (28K total size for program and monitor less 2K
for size of the monitor). The second size is between 12K and
16K, depending on various capabilities included in the monitor.
The core estimate is thus 38K to 42K.

The total core requirements are 70K to 74K for the one
second spill case and 102K to 106K for the two second spill
case.

In addition to the above general hardware requirements,
we require certain peripherals. The standard ones are:
a Versatec Printer/Plotter, 2 Floppy Disks, a Bison Interrupt/
Gate Control Box, and a 613 Tektronix Storage Scope with hard-
copy interface.

Also we will require a second 613 storage scope and two
"dumb" CRT terminals. Note that we will not need a DECwriter.
We plan to rely on the Versatec line printer for hardcopy
printed output. We plan to set up two separate console stations.
Each will have a graphics channel (the 613) and a totally
separate command channel (the CRT terminal). We plan to use
one console station for the immediate monitoring and control
of the experiment. The second console station will be used
for the review of past experimental status using the data-
base continually generated by the data runs being taken.
Our further use of these separate console stations is discussed
in the software plans stated below.

We need to monitor the beam line controls for such informa-

tion as target parameters, magnet settings, etc. We also need to monitor the experiment's high voltages. To accomplish these things, we will need a set of 036 modules for interfacing with the beam line controls system and a Peripheral Node Module for transfer of graphics information from the control system. For the voltage monitoring, we need a computer-controlled digital voltmeter.

The online computer configuration is summarized in Table XV.

TABLE XV

Online Computer Requirements

1. PDP 11/55 CPU

2. Floating Point Processor Hardware

3. Memory Management Unit (KT-11)

4. MOS Memory, 74K for 1 second spill, 106K for 2 second spill

5. Two 1600 BPI 9 track Magnetic Tape Drives

6. Jorway 411 CAMAC branch driver

7. Versatec Line Printer

8. Two Floppy Disk Drives

9. Two RK05 Cartridge Disk Drives

10. Bison Interrupt Gate/Control Module and DR-11C

11. Two 613 Storage Scopes with Hardcopy Unit

12. Two "Dumb" CRT Terminals

13. BISON-NET Link

14. Two Beam Line Interface 035 Modules and 1 Peripheral Node Module

15. A Computer-Controlled Digital Voltmeter

B.   Online Software

Within the RSX-11M framework, we plan to develop a set of data acquisition routines. These will be tailored to the special needs of the facility for handling high data rates. This set of routines will use software currently being developed within the Computer Department for fast CAMAC data acquisition and disk buffering under RSX-11M.

To solve the experimental control and data monitoring needs, we will use the package called "MULTI". It has already been quite successfully used by a number of Fermilab experiments (E-110, E-379, etc.). The experimenter will use MULTI to do such things as begin and end runs, to monitor high voltages, positions of centroids on pulse height histograms, etc. This sort of monitoring, control, and alarms typeout will be done at the first graphics/command console.

MULTI gives the experimenter the capability to set up from the keyboard various histogramming and display processes for data items. These may be set to be done conditionally depending on the value of other data items. For example, a pulse height in one scintillator may be histogrammed whenever a bit in a latch has fired.

MULTI further gives the experimenter convenient places to attach special subroutines. In these subroutines, one can process the data in ways difficult or inefficient to do via the general keyboard capability. The output from these special subroutines is then available to the general keyboard processor for histogramming and display.

In addition to data acquisition and monitoring of current data, we require a capability to review past runs to compare rates and other characteristics with the present run. We plan to use the second graphics/command console for this review. The advantage of a second console is that the review activity may proceed, even while the experimenter is handling an alarm or equipment problem that may have arisen at the other console. Further, when two experimenters are present, both may easily conduct investigations of the data. It will also be used for the preparation of configuration files, specifying the run parameters for subsequent runs. The data acquisition, control, and monitoring system will continually generate files in the style of a data-base. The information in these files will characterize the last several events, the last several beam spills, and the last several runs. The experimenter will use this second console to compare and look for problems and trends.

At present, our plan is to implement a dual console version of MULTI. At the second console, the experimenter can examine the data-base through the use of the same commands that are used at the first console to control and monitor the experiment.

The data acquisition routines are already being developed for RSX-11M by members of the Computing Department in connection with other projects. The adaption of MULTI to RSX-11M is also currently being developed for similar reasons. Completion of the MULTI in RSX project is predicted for June, 1977. Thus, much of the software is well along towards implementation for this facility.

X. Track Reconstruction

It has been indicated in previous discussions of the drift
chambers that a great deal of thought has been given to the problems
of tracking multiparticle events in the forward spectrometer and that
the chamber number, positions, and wire orientations have been
chosen to ease the pains of tracking.

We will not reiterate here all the reasons for our choice of
geometry. Instead, we will discuss approaches to tracking the pro-
posed chamber system that will be developed for the Central Lab-
oratory Computing Facility programs.

The forward chamber system is pictured schematically in
Figure 23. For tracking purposes D1 and D2 are considered together
as a single module (D1-2) with four chambers having each wire
orientation (x, u, and v). D3 and D4 both have three chambers with
each wire orientation. D5 has only two planes of x chambers.
Note that except for the two D5 chambers, the system is identical
in the x, u, and v planes.

We now describe a tracking algorithm which demonstrates the flex-
ibility of the system. Common to any tracking technique is the
necessity to convert TDC counts to position coordinates, each wire
hit generates two such coordinates equidistant to but on opposite
sides of the hit wire. The techniques for performing this conversion
are straight forward and need not be elaborated here.

The algorithm begins by independently finding track segments in
the three modules (D1-2, D3, D4). We believe that it is very im-
portant for computing speed that the coordinate data be presented
to the tracking program in an ordered form. Increasing address
should correspond to increasing coordinate. This may be accomplished
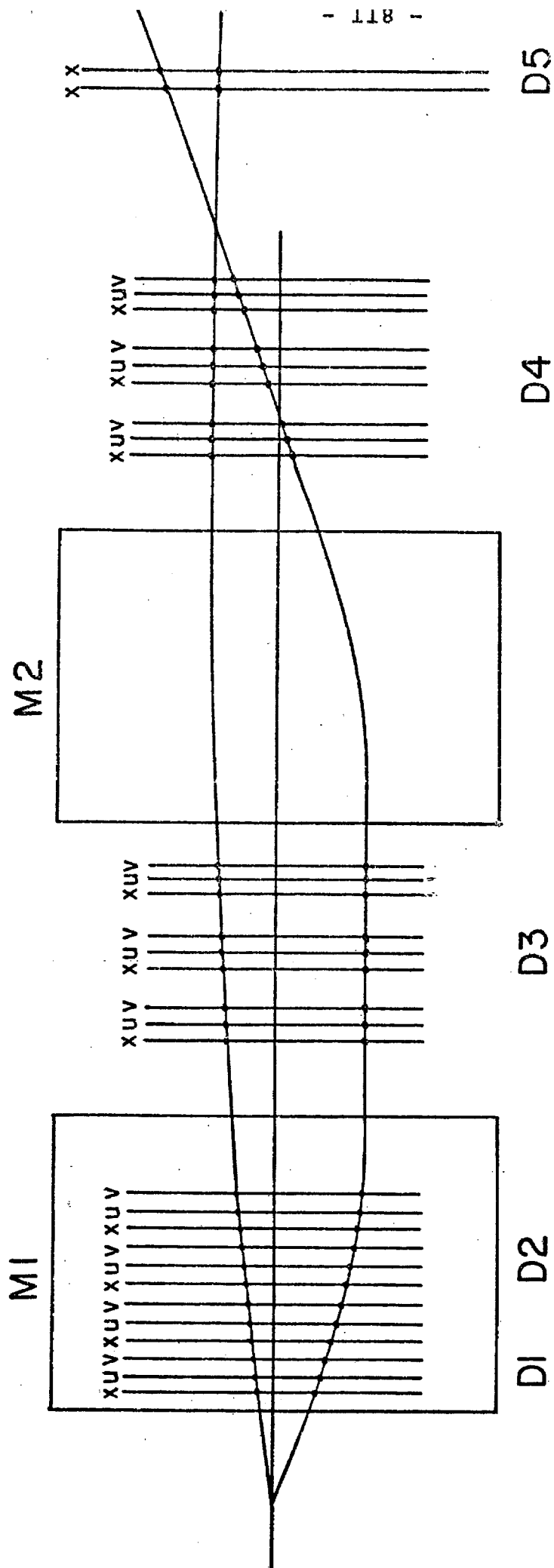in the hardware or (less desireably) at some earlier point in the

Figure 23

analysis programs.

Tracking Algorithm:

1.   Find all 3 hit lines in D3 and D4 in each view. Let ξ_i be one of x, u, or v. A line is found when: $\frac{1}{2}(\xi_1 + \xi_3) - \xi_2 < \delta\xi$, where $\delta\xi$ is a cut whose size is related to the spatial resolution and which is determined experimentally. As soon as a coordinate is used in a line, eliminate that co-ordinate and its left-right ambiguous pair from the search. Note that the ordering of the data will speed up this process considerably. Reasonable tracks will have a specified range of angles relative to the beam line. This fact will be used to limit the number of ξ_3 coordinates which are paired with a given ξ_1. The outer limits for this pairing can be established and the data ordering insures that only those coordinates within these limits will be searched. Similarly in checking ξ_2 for the third hit on a line one searches until a match is found or until a coordinate is found which exceeds the predicted value. Again the data ordering insured that the correct coordinate has not been missed. All these techniques limit the combinatorial growth of computing time expected with a straight forward brute force approach.

2.   After all three point lines are found, define all two point lines possible from unused hits in each view of D3 and D4. The set of two point lines can be limited by considering only reasonable angles.

3.   Correlate the three views eliminating "ghost" lines. Consider only lines which have three hits in at least one view.

4.   Project x view of "real" lines in D4 into D5. Use D5 information to refine x slope if at least one out of two D5

chambers gives a match.

5.   Proceed to tracking D1-2. Each view has four chambers which are equally spaced. We may use the property that the two line segments defined by ξ_1, ξ_2, and ξ_3, ξ_4 must meet within a calculable distance on a line halfway between the second and third chamber. Given the bend angle implied by the two line segments, one can calculate how the lines should intersect if they indeed form a single track. A lower momentum cut will limit the set of line segments for which this test is attempted. Also, a proximity requirement can be imposed for the two line segments. After 4 point circles are found the corresponding coordinates are eliminated from the search. Finally, all three point circles which can be formed from unused hits and which have reasonable momenta are tabulated.

6.   Correlate the three views in D1-2. This can be done by requiring that the same momentum can be obtained in each view or from purely geometrical considerations. Ghost tracks are, thereby, eliminated. A track candidate should have a four point circle in at least one view.

7.   At this point we have established track segments inside M1 and in the drift space before and after M2. It is possible to calculate intercepts and slopes in any plane, and it should, therefore, now be an easy task to match track segments. This can be done by seeking common slopes and intercepts in the vertical plane. It can also be accomplished in the horizontal plane by looking for a match at the magnet centers.

8.   After at least two tracks are found, a vertex can be established. This vertex can be used to relax the hit requireme   ;

in the first magnet. For example, if a track projects to the vertex properly it need not be required to have four hits in any view.

9.   Similarly, we can use the information from one module to track another. For example, two point line segments are perfectly acceptable if they intersect track segments from other modules properly at the magnet centers.

Finally, it should be noted that the above discussion can not possibly do justice to the hundreds of man hours of programming effort which will ultimately go into tracking. We have tried to make the point that the system is sufficiently redundant that efficient multiparticle tracking is possible. Further, we think that the system is designed so that computing time is efficiently used and that the combinational problems encountered in tracking events are well under control.

XI.   Beam

To a large degree the range of photon physics that will be feasible
is determined by the fluxes available in the beam. Here we look
at the question of how much tagged photon flux can be reliably
anticipated in the next generation of experiments based on present
experience with the beam. The real limit on flux is the rate at
which one can tag photons. Using techniques based on some developed
during summer 1975 we will be able to tag as many as 6×10^6 γ/
second. Modest improvements to the electron beam and reasonable
assumptions about 1978 proton beam parameters (6×10^{12}, 450 GeV,
480 seconds/hour) will make it possible for us to obtain this photon
flux with 150 GeV e^-. Figure 24 shows the photon spectrum expected.
Also shown is the e^- spectrum. Details of how we will obtain these
fluxes are given below. Figure 25 is a schematic drawing of the
Tagged Photon Beam and may be helpful as a road map in the discussion
that follows.

During August of 1975, the beam was operated at $\sim$ 100 GeV
with 3×10^{12} 400 GeV protons on target and produced about 2.2 x
10^7 electrons. With 450 GeV protons and 6×10^{12} p/sec, we can
expect 6×10^7 electrons/sec. at 100 GeV. This flux is more than
adequate for much of the physics to be done on this spectrometer.
However, experiments dealing with low cross section states (η_c,
heavy leptons) will need all the flux they can get. The electron
flux is presently limited by the relatively smaller vertical acceptance.
This vertical acceptance can be recovered in one of two ways.
In a Technical Memo, TM-633, Morrison and Murphy suggested increasing
the vertical acceptance by installing the lead convertor (that
converts photons from the primary target to electrons) inside a

ANTICIPATED ELECTRON &
TAGGED γ FLUXES

scale
N(k) dk
Untagged γ
100 GeV e⁻
6×10^{12} 450 GeV p

N_e electrons
6×10^{12} 450 GeV p
scale

Tagged γ N(k) dk
140 GeV e⁻ 6×10^{12} 450 GeV p
or 100 GeV e⁻ 2×10^{12} 450 GeV p
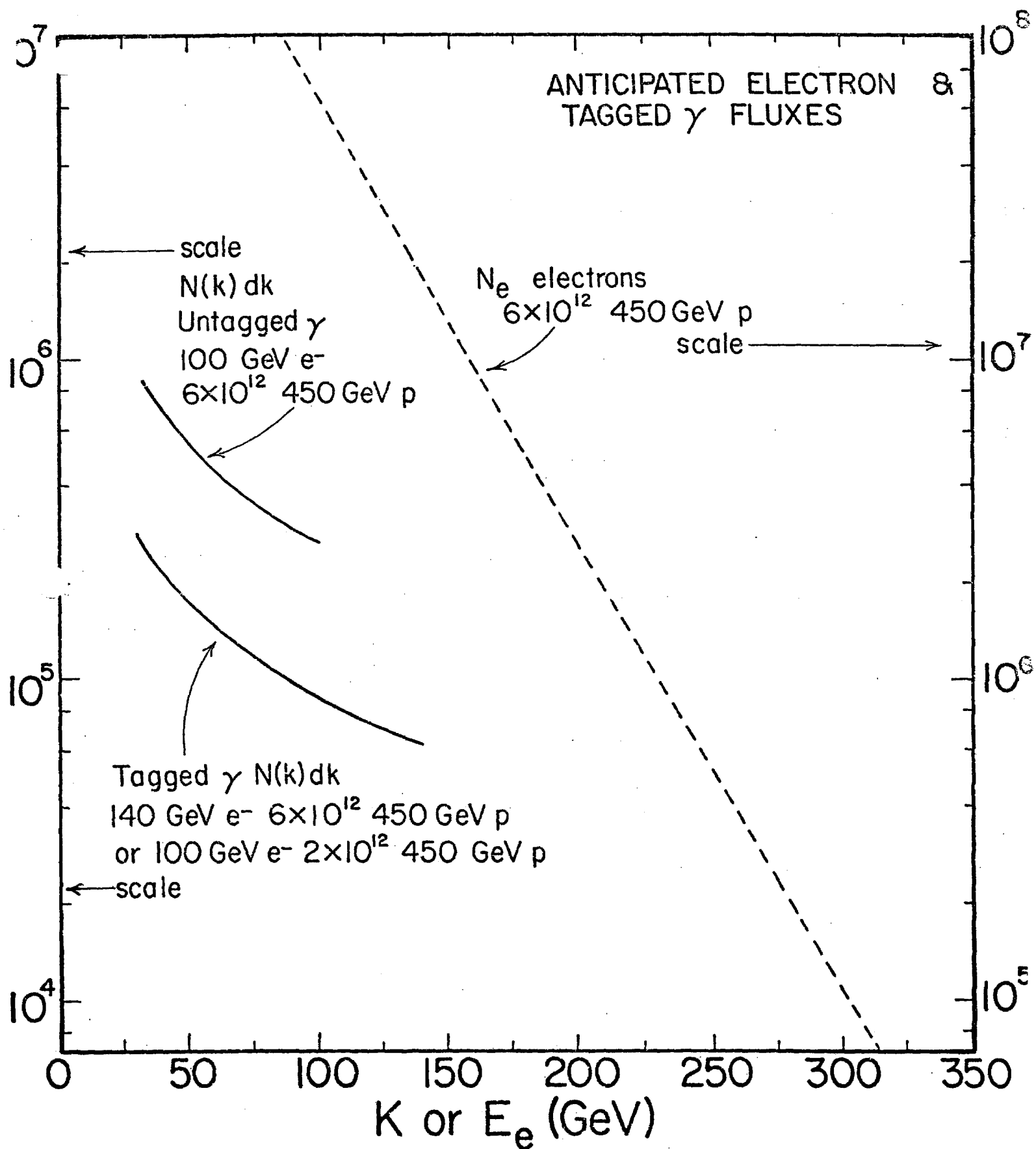scale

K or E_e (GeV)

Figure 24

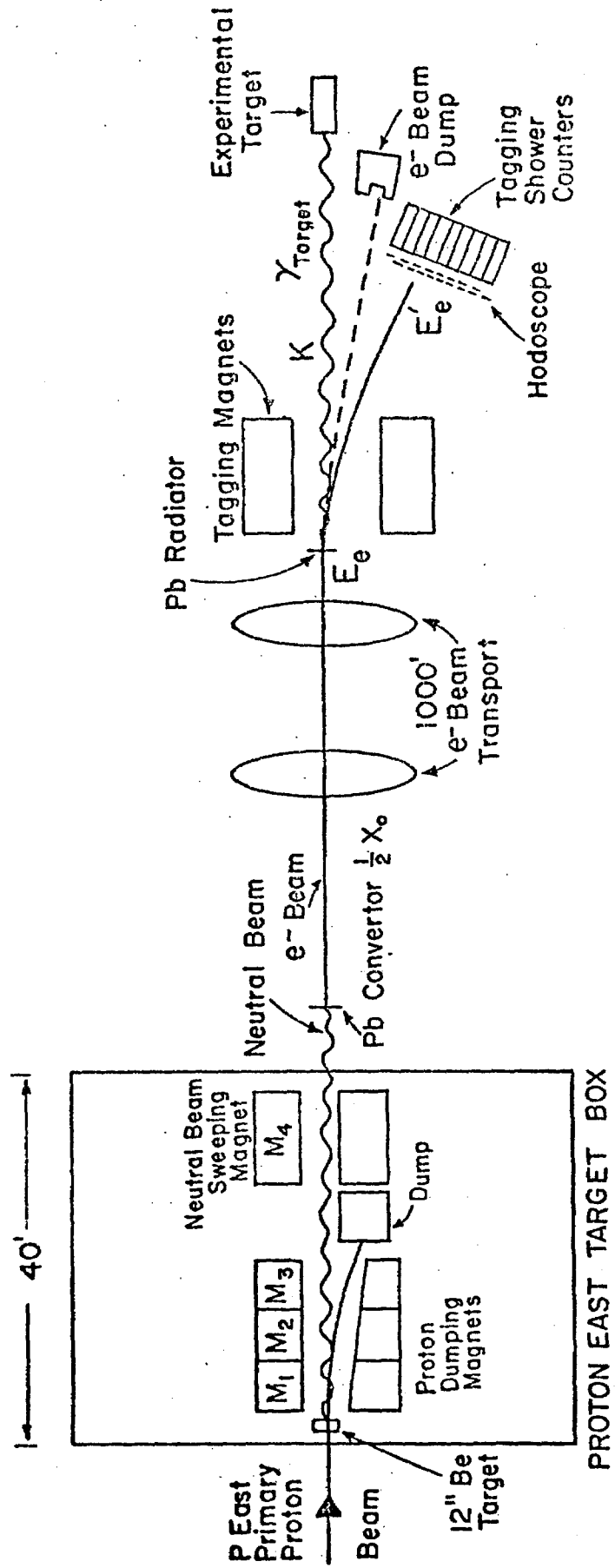SCHEMATIC DRAWING OF TAGGED PHOTON BEAM

Figure 25

dipole. As can be seen in Figure 26, the lead is at a shallow angle (α) relative to the beam axis. Thus the more positive the photon production angle the more magnetic field will be traversed by the resulting electron. The net effect is a vertical focussing of the electrons plus a small mean bend which is corrected by a following magnet. There is no horizontal defocussing. To get the most significant increase in vertical acceptance using this approach the lead convertor would be placed in the third dumping magnet (M3) inside the target box with the sweeping magnet (M4) acting as the correction magnet. This would increase the vertical acceptance from ~1 mr to ~5mr with negligible effect on other beam parameters. Using measurements of the electron beam flux as a function of production angle, we estimate this larger vertical acceptance will increase the flux at 100 - 150 GeV by ~ 3.5. This would give ~ 2×10^8 100 GeV or 6×10^7 140 GeV electrons (see Figure 25). Another approach (suggested by B. Cox) is to add a third quadrupole to the first doublet and thereby achieve a more symmetric acceptance. A careful transport study of using a triplet will have to be made before deciding whether to use a Morrison element or a triplet to increase the beam acceptance.

Using a 20% radiator and ignoring tagging for the moment

$$N_\gamma(k) dk > N_e \times .2 \times f(k) \times \frac{1}{k} dk =$$

$$\frac{2.6 \ 10^7}{k} dk \quad 100 \ \text{GeV}$$

$$\frac{8.7 \ 10^6}{k} dk \quad 140 \ \text{GeV}$$

The factor $f(k) = .65$ comes from thick target and QED corrections to the simple $\frac{dk}{k}$ form. Integrating from 20 GeV to k_{max} we will get 4.2×10^7 photons for the 100 GeV setting and 1.8×10^7 with 150 GeV electrons, untagged. This high rate is useful for physics

SCHEMATIC DRAWING OF VERTICAL FOCUSING

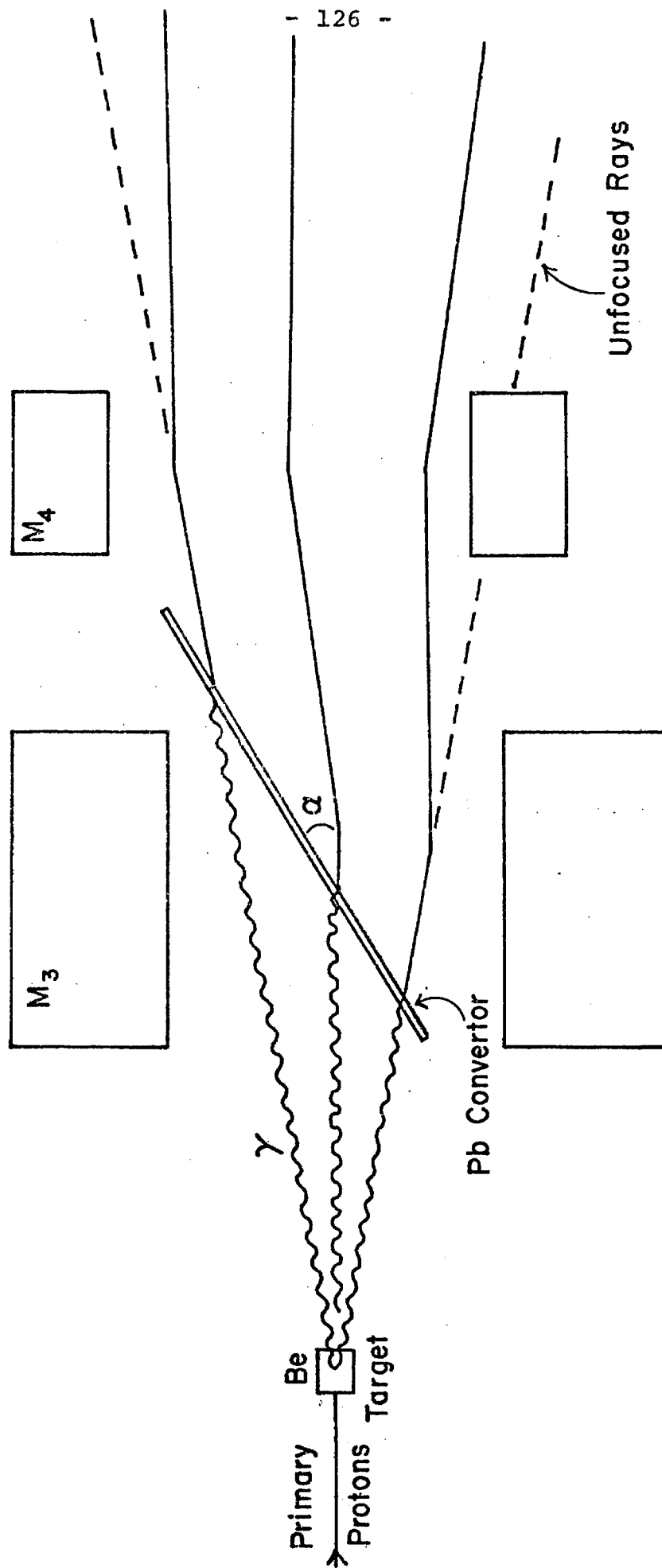OF ELECTRON BEAM IN TARGET BOX

Figure 26

when one chooses not to take advantage of the energy constraint and missing mass capability allowed by the tagging system.

If tagging is required, the real limit on flux is the rate at which one can tag the photons. With electron fluxes approaching those noted above, a large fraction of RF buckets will be populated with more than one electron. The likelihood of more than one radiated photon of significant energy per electron is also high when using a thick radiator. Thus, it is necessary to cope with more than one electron and more than one photon to tag the energy of the interacting photon. The saving grace is the very low interaction probability of photons which means that it is extremely unlikely ($< 10^{-3}$) for more than one γ to interact hadronically per bucket. The energy of all non-hadronically interacting photons in the beam ($\Sigma \, k_{NI}$) will be measured by a central counter (C) which will measure photons that have not converted and by the central horizontal strip of the SLIC which will measure $e^+ e^-$ pairs with $p > 1.5$ GeV that have been swept out of 0° in the bend plane.

Extra scintillation counters near the beam in the tagging array will pick up higher energy electrons that radiated lower energy photons. Combined with the shower counters of the tagging system, these will determine the number of electrons (N) in the bucket and their total energy after radiating ($\Sigma E'$). Thus, one can determine the interacted photon's energy:

$$k_I = N E_{beam} - \Sigma E' - \Sigma k_{NI}.$$

A specific scheme has been worked out along these lines which allows tagging radiated photons with a resolution of $\dfrac{\delta k_I}{k_I} \sim 5\%$

from up to 6×10^7 100 GeV e^- in a 20% radiator (6×10^6 tagged photons). The only changes to the tagging system are eleven scintillation counters which would be added to the present tagging hodoscopes on the high e^- energy end. The tagging magnets would be run at maximum current (the present 300 GeV setting) in order a: to spread out the electrons so that there is a sufficient spatial resolution to measure E' of the higher energy electron well enough to get $\delta k_I \sim 5.5$ GeV; and b: to keep the counting rate < 2MHz in the hodoscopes and < 0.3 MHz in the shower tagging counters.

The C counter will require special consideration. The pulse height of this counter, like the tagging counters, will be digitized for any RF bucket with an interaction that satisfies the experimental trigger. The problem is to get the pulse height information from only the relevant bucket without contamination from the preceding or following buckets. The pulse can be clipped to 15 ns and the ADC gate set short enough to ignore the following bucket. The energy at the preceding bucket can also be digitized (with appropriate delaying). Using calibration data one will then be able to subtract the energy that leaked from the previous bucket. The problem is by no means trivial, but techniques like these are similar to those used in correcting for shower leakage from a neighboring shower counter.

We have described above what might be called a second generation tagging system which, with minor modifications based on previous experience, will push the tagging rate a factor of ~ 6 beyond that already attained. When 1,000 GeV protons are available in P-East, the choice will be whether to use the extra energy to do physics in the 200 - 300 GeV range or to continue in the 100 - 150 GeV range with substantially increased intensity. If the latter choice

is made, the tagging system will have to be modified to cope with the higher rates. Perhaps this will be done by adding more magnets which will spread the electrons and photons out vertically and horizontally to keep rates manageable in each of a greater number of counters.

The electron beam can also be used to transport pions into the Tagged Photon Laboratory[12]. R. Rubinstein notes that although spot sizes will be somewhat larger the intensities are potentially only a factor of $\sim$ 3 below the P-West pion beam.

XII. Schedule

Rough time estimates for various components in the facility have been made (Table XVI). The primary purpose of these estimates is to detect the critical time elements in the assembly of the facility. Work has already begun on prototype components. This work puts the whole program in an excellent starting position. These efforts are being made in good faith and with the conviction that the facility is too important not to proceed as indicated. Nevertheless, formal approval of the facility will be required to permit component acquisition in sufficient quantity to mount an experiment. The importance of this approval for those groups seeking extraordinary funding for their contributions can not be overemphasized.

One other most critical element is the final specification of the exact magnet apertures to be used. If existing magnets are to be made available, this task is easier. It is directly related to the formal approval. If new magnets are to be built, an added constraint arises. Unless existing copper coil supplies can be utilized, coil winding will be hindered. One possibility is to do design work now and begin copper procurement before the new fiscal year.

Many of the major final component commitments can be delayed until next fiscal year, but only if bid packages and decisions have been made in advance of October 1, 1977. For example, if an ADC system of the type now being discussed in PREP is ordered for other purposes and debugged earlier, our time estimates remain reasonable. Similarly, most photomultipliers, metals, and plastics can be purchased after October 1, 1977.

The net effect of the schedule is to suggest that the facility could begin set up in the Tagged Photon Laboratory in April. First

beam testing of the assembled apparatus would be useful as early
as June, 1978.

Table XVI   Time Schedule

TAGGED PHOTON FACILITY

	MAY	JUNE	JULY	AUGUST	SEPT	OCT	NOV	DEC	JAN	FEB	MARCH	APRIL	MAY	JUNE
TARGET Design Construction Testing														
RECOIL - PWC Prototype Tests 3 Unit Assembly Electronics			PROTOTYPE											
RECOIL - LIQ. SCINT Test Module Design Assembly	CONST.	ARGONNE												
MAGNETS Fix Aperture Design Bids Copper Order Winding Yoke		WAIT FOR GO AHEAD	*		BIDS	BIDS	WAIT FOR Cu							
DRAFT CHAMBERS Prototype Design & Assembly Prototype Tests Final Design Full Construction Electronics & Cham.		DESIGN		ASSEMBLY										
SLIC Prototype Tests Design Pb/Al, PM Orders Light Guides Assembly				FOIL		Pb/Al	PM's & LG's							
HADROMETER Design Scint/Acrylic Light Guides PM's and Bases Mechanical Assembly							PARTS DELIVERED			ASSEMBLY				

Tab XVI (continued)

TAGGED PHOTON FACILITY

	MAY	JUNE	JULY	AUGUST	SEPT	OCT	NOV	DEC	JAN	FEB	MARCH	APRIL	MAY	JUNE
MUON I.D. Steel Scint/Acrylic														
Pb GLASS Support Design Support Assembly														
MID-MAGNET SHOWER DET. Design Box Assembly Scint/Light Guides PM's and Bases														
CERENKOV CTR's Design Mirror Tests Mirror Assembly Winston Cones Box Assemblies PM's & Bases				PROTOTYPE		BID	TUBES							
CABLES Order Testing														
ELECTRONICS ADC's TDC's PWC C/R's Drift Ch Read/Out Trigger Proc. DC Logic		DESIGN			DESIGN		CONSTRUCTION	CONSTRUCTION	DEBUG	DEBUG	DEBUG			
COMPUTER - ON LINE Hardware Spec. Software Spec. Software Development Hardware Assembly														
ANALYSIS - OFF LINE Reconstruction Data Format Spec. Compaction														

XIII. Cost Estimates

The new equipment costs of the Tagged Photon Facility will be borne approximately equally by Fermilab and the out-of-laboratory collaborators of P-516. A detailed breakdown is given in Table XVII. In the table, the items with an asterisk might well be delayed until after the startup of the facility. This would delay a portion of the Fermilab expenditure. However, such an action would be severe from the point of view of starting with a complete facility.

XIV. Acknowledgements

Table XVII
Tagged Photon Facility
Estimated Costs of New Facility
May 1, 1977

	Fermilab Exist'g	Fermilab New	Other
A. Beam Improvements*			
1. Slanted Target in Magnet \} either one	20K	20K*	
2. New Quadrupoles in Target Box \}			
B. Tagging System Improvements*			
1. 20 Scintillation Counter Hodoscope		5K*	
C. Hydrogen Target			
1. Mechanical Assembly: flask, vacuum, transfer lines, etc.		15K	
2. 10-12 watt, ½ ℓ/hr refrigerator, dewars	35K		
D. Recoil System (Canadian Collaborators, P-516)			
1. Cylindrical PWC (1,200 wires)			
a. Fabrication of Mechanical Assembly			60K
b. Electronics at Chamber			36K
2. Range Liquid Scintillation System			
a. Fabrication of Mechanical Assembly			20K
b. 120 Photomultipliers, bases, guides			30K
c. Liquid Scintillator			10K
d. Laser Calibration System			6K
E. Magnets			
1. Moving 2 SCM105's from Argonne and Assembly		14K	
2. Power Supplies (2 ½-MW Transrexes or equivalent)	32K		
3. Additional LCW Cooling		20K	
F. Calorimeters			
1. Segmented Liquid Ionization Counter (UC, SB)			
a. Fabrication (including Pb plates, teflon foil, liquid).			90K
b. Phototubes, Light Guides (278 elements)			35K
2. Hadrometer*			
a. Steel Plates		50K*	
b. Fabrication of Mechanical Assembly		5K*	
c. Acrylic Detectors with Phototube Assemblies		69K*	
3. Muon Identifier			
a. Steel Absorber	20K		
b. Acrylic Detectors with Phototube Assemblies (16 elements)		7K	

*These items might be delayed or simplified at the beginning of the facility (164K total).

TAGGED PHOTON FACILITY

page two of two

	Fermilab		Others
	Exist'g	New	
4. Shower Counters (Univ. of California, Santa Barbara)			
a. Between Magnets		18K	
b. Pb Glass			2⊦
G. Gas Cerenkov Counters (U of Colorado)			
1. Metal Enclosures (C1, C2)			25⊦
2. Photomultiplier Assemblies (40 elements)			58⊦
3. Winston Light Funnels			15⊦
4. Spherical Mirrors and Mounts			15⊦
H. Trigger Counters (33 elements)			
1. Scintillators and Guides		4K	
2. Photomultiplier Assemblies		8K	
3. Supports		1K	
I. Forward Spectrometer Drift Chambers			
1. Mechanical Assemblies (32 planes)		48K	
2. Electrical Circuits (including TDC's)		108K	
J. Cables			
1. Drift Chamber and PWC Cables		16K	
2. Analog Signal Cables	6K	15K	
3. High Voltage Cables	6K	16K	
K. Electronics			
1. ADC's (550 channels)		33K	
2. TDC's	4K		
3. Discriminators and Logic Modules	30K		
4. Crates, Bins, Racks for above units	20K		
5. PWC Specialized Units and DC Logic		10K	
6. Trigger Processor (Recoil)		20K	
7. Trigger Processor (Forward Spectrometer)*		15K*	
8. Miscellaneous Spectrometer Electronics		5K	
L. Computer			
1. Bison System (standard)	96K		
2. Additional Facility Equipment	38K		
TOTALS	307K	522K	402⊦

*These items might be delayed or simplified at the
 beginning of the facility (164K total).

REFERENCES

1. J. Appel, P. Mantsch, T. Nash, R. J. Morrison and G. Luste, Proposal to Study Photoproduction of Final States of Mass Above 2.5 GeV with a Magnetic Spectrometer in the Tagged Photon Lab, Fermilab Proposal 516·

2. R. F. Schwitters, Proc. 1975 Intern. Symp. on Lepton and Photon Interactions at High Energy, Stanford (1975).

3. A. De Rújula, Howard Georgi, and S. L. Glashow, Phys. Rev. D 12, 147 (1975), A. D. Sukharov, JETP Lett. 21, 258 (1975).

4. Mary K. Gaillard, Benjamin W. Lee, Jonathan L. Rosner, Rev. Mod. Phys 47, 277 (1975).

5. J. Franzini, P. Franzini, et al., (Private Communication).

6. R. Thun et al, Nuclear Instruments and Methods 138, (1976) 437-444.

7. G. B. Bowderr, R. C. Field, R. A. Lewis, C. T. Howard, K. Skarpaas, and P. Baker Nuclear Instruments and Methods 138 (1976)·

8. G. Grayer et al, Max Planck Institut fur Physik und Astropysik (Exp. El 40, June 1974).

9. E. L. Garwin and T. Rodes, Nuclear Inst. and Methods 93 (1971).

10. Y. Tomkiewicz and E. L. Garwin, Nuclear Inst. and Methods 114 (1974).

11. P. Mantsch, et al. "A Segmented Hadron Calorimeter for Use as a High Transverse Momentum 'Jet' Trigger", Fermilab Technical Memo TM-721, April 5, 1977.

12. R. Rubinstein, "Use of the NAL Electron Beam for Pion Experiments", NAL TM-476.